ABSTRACT

RONG, GUO. High Efficiency Charge Pump Based DC-DC Converter for Wide Input/ Output Range Applications. (Under the direction of Dr. Alex Q. Huang.)

Portable electronic devices are taking an indispensable part in people's everyday life. To meet the growing needs of people, the number of function blocks inside the portable devices keeps on increasing but the portable devices tend to be small and exquisite. As a result, the power supply must be very compact and also very efficient during battery lifetime. Charge pump regulators are considered as an ideal solution in low power portable applications for their compact sizes and low cost. However, traditional charge pumps are not very efficient for battery powered applications because of the input voltage variations and the requirement for output regulation. The power rating of charge pumps is also very limited. A Multi-modes regulated charge pump with improved efficiency over wide input and load range is proposed. It can realize 2x, 1.5x, and 1.33x conversion modes. During each mode, the output voltage is regulated by a controlled current source. A hybrid control scheme is proposed. By using device segmentation control and pulse skipping modulation according to the load condition, the efficiency can be improved over a wide load range. Simulation and test results are provided to verify the control scheme.

For automotive system and telecommunication systems, the input voltage varies much wider than in portable applications. For industry applications, the front-end bus voltage is relatively stable, but can be selected from 12V, 24V, and 48V. However, customers prefer

a high performance one-fits-all power supply to avoid additional time and cost for re-design. Therefore, a power supply that can operate under a very wide input voltage range is a must for these applications. The most popular non-isolated step-down DC-DC converter, Buck regulator, usually shows a low efficiency at high input voltage. In addition, a high step-down ratio creates significant challenges for the PWM controller design because it has to control very narrow PWM pulses. A high efficiency charge-pump based wide input range Buck converter is proposed. The first stage is a multi-modes charge-pump and the second stage is a synchronous buck converter. The charge-pump is unregulated and adaptively switches between 1x, 0.5x, and 0.33x modes according to the input voltage. It does the rough voltage conversion while the Buck converter does the fine voltage regulation. Theoretical analysis proves that the total efficiency will be improved, especially at the high input voltage. It also simplifies the compensator design and benefits the transient performance. Experiment results show the highest efficiency improvement is 7% at heavy load and 16% at light load.

Similar merits can be found when combining a Multi-modes Charge Pump with a Boost converter for high gain applications, such as driving a long LED string from a single lithium battery. A high gain Transformerless LED driver is proposed and verified by the experiment. The efficiency improvement is 10% when driving 11-12 LEDs from 2.7V input voltage.

High Efficiency Charge Pump Based DC-DC Converter for Wide Input/Output Range Applications

by
Rong Guo

A thesis submitted to the Graduate Faculty of
North Carolina State University
in partial fulfillment of the
requirements for the degree of
Doctor of Philosophy

Electrical Engineering

Raleigh, North Carolina

2010

APPROVED BY:

_____	_____
Dr. Alex Q. Huang Committee Chair	Dr. William Davis
_____	_____
Dr. Subhashish Bhattacharya	Dr. Srdjan Lukic

DEDICATION

TO MY PARENTS
AIZHU GUO AND LAHUA DENG

AND MY HUSBAND
ZHIGANG LIANG

BIOGRAPHY

The author, Rong Guo, was born in Hunan, China. She received B.S. in Electrical Engineering from Xi'an Jiaotong University, Xi'an, China, in 2003, and M.S. in Electrical Engineering from Zhejiang University, Hangzhou, China, in 2006. She started to pursue the Ph.D. degree in North Carolina State University in 2006. She was a Co-op of Marvell Semiconductor in 2007. She joined International Rectifier as an application engineer in June 2010.

ACKNOWLEDGMENTS

I would like to express my sincere appreciation to my advisor, Dr. Alex Huang, for his continued guidance, encouragement and support. Dr. Huang's extensive vision, great intuition and accurate judgment have been the source of inspiration for my study and research in North Carolina State University in the past several years. It was an invaluable learning experience to be one of his students. The most precious things I have learned from him are the ability of independent research and also a careful research attitude.

I am grateful to my committee members, Dr. William Davis, Dr. Subhashish Bhattacharya, Dr. Srdjan Lukic for their valuable suggestions and help. Also I would like to thank Dr. Eunkyoung Shim for her service as the Graduate School Representative of my defense.

The research work in this dissertation is supported by the Power Management Consortium of SPEC and also part of the research work is supported by RF Micro Device. I would like to give my special thanks to Mr. John Endredy in RF Micro Device who gave very valuable suggestions to this research work.

It has been a great pleasure to work in the Semiconductor Power Electronics Center (SPEC) as well as in the newly NSF funded Future Renewable Electric Energy Delivery and Management (FREEDM) Systems Center. I would like to thank my colleagues in the Power Management Micro-systems (PMM) group and all members of SPEC and FREEDM Systems Center, including Dr. Jinseok Park, Dr. Xiaojun Xu, Dr. Jiwei Fan, Dr. Liyu Yang, Dr. Xin Zhou, Dr. Sungkeun Lim, Dr. Xiaopeng Wang, Dr. Jingzhen Hu, Mr. Ning Zhu, Mr. Zhaoning Yang, Mr. Pochih Lin, Mr. Gaurav Bawa, Mr. Anand Ramamurthy, Dr. Chong

Han, Dr. Bin Chen, Dr. Jun Wang, Dr. Yu Liu, Dr. Jeesung Jung, Dr. Yan Gao, Dr. Wenchao Song, Dr. Tiefu Zhao, Dr. Jun Li, Ms. Juming Lai, Ms. Zhengping Xi, Mr. Jifeng Qin, Mr. Xiaohu Zhou, Mr. Gangyao Wang, Mr. Qian Chen, Mr. Woongje Sung, Ms. Zhan Shen, Mr. Zhuoning Liu, Mr. Sanzhong Bai and Mr. Edward van Brunt.

I appreciate the assistance from the staff members of the SPEC and FREEDM Systems Center, especially Mr. Anousone Sibounheuang, Ms. Colleen Reid and Ms. Karen Autry.

I also would like to give my special thanks to Mr. Wenkang Huang and Mr. Richard Fitzpatrick in International Rectifier for their support and help during my preparation of this dissertation.

My heartfelt appreciation goes toward my parents, Aizhu Guo and Lahua Deng, who have always support and encourage me to pursue higher education.

Finally, with deepest love, I would like to thank my husband, Zhigang Liang, who has always been there with his love and encouragement, and also gave valuable suggestions to my research work.

TABLE OF CONTENTS

LIST OF TABLES

LIST OF FIGURES

Chapter 1. Introduction

1.1 Research Background

In people's everyday lives, portable electronic devices are taking an indispensable part. Most consumers own at least one mobile phone, and at least one other portable device, such like digital camera, MP3 player, notebook, etc. As the name suggests, portable devices need to be small in size and light in weight. In addition, as they are powered form batteries, it requires that their voltage converter has high efficiency and low quiescent current so the devices can be powered for a long time before needing to be recharged. Moreover, consumers' demands of multi-function portable devices become more and more intensive nowadays. In stead of carrying three single-function portable devices, consumers tend to buy a single device which integrates multiple functions. As a result, it brings great challenges to the design of portable devices. A large number of function blocks inside a portable device greatly increase the occupied space and the power consumption goes up as well. However, the size of portable devices should be limited to maintain a fashionable outline. As a result, the power supply must be very compact and also very efficient during the battery lifetime.

Fig.1.1 A Ultra Slim Multi-Function Portable Device: IPad [1]

Inductor-based converters, usually with one or more inductors, and inductor-less converters, also known as charge pumps [2], are two sorts of DC-DC converters that are widely used for today's portable power supplies.

Inductor-based converters can have very high efficiency over the entire battery voltage but the cost and volume often make the engineers think twice. Charge pump regulators are considered as an ideal solution due to their well-known compact sizes [3]. It first began with unregulated ICs and then to regulated ICs with regulated output voltages. It eliminates the use of inductor, thus reduces the cost and size. However, traditional charge pump, such as the voltage doubler, is not very efficient for battery powered applications. The battery voltage varies widely but the output voltage needs to be regulated to a fixed value [4]. The topology of a charge pump sets a limit to the maximum efficiency it can achieve at one given input voltage. Meanwhile, the regulation of charge pump converters is more lossy compared with inductor-based converters [5~14].

On the other hand, the power rating of charge pump converters is limited due to huge conduction loss at high output current. In today's market, there are hundreds of charge pump ICs. Table 1.1 shows a statistics of commercial charge pump ICs from different Vendors. Most of them can support power below 1W, but very few of them can support power above 2W. Conduction loss is a big concern when it is designed to be used in high power rating because the charge pump has more transistors. If it is intentionally designed for high power rating, big devices with low on-resistance must be used. However, light load efficiency will suffer due to increasing switching loss.

Therefore, increasing the power rating and optimizing the efficiency of charge pump converters over the entire battery life becomes a significant topic for designing the future power supplies for portable devices.

Table 1.1 Commercial Charge Pump Products [15]

Vendor	**# of ICs**	**Step-up ICs**	**LED driver IC**	**V_{in} range**	**V_{out} values**	**$I_{out,max}$**	**$P_{out,max}$**
TI	70	44		1.8-3.6V, 2.7-5.4V, 0.9-1.8V.	5V, 3.3V	0.3A	1.5W
Linear Tech	73	30	21	1.8-4.4V 2.7-5.5V	5V, 3.3V	0.5A	2.5W
Maxim	50	17		1.8-5.5V 2.7-5.5V	5V, 3.3V	0.25A	1.25W
Fairchild	5	2		2.7-5.5V	3.3V, 4.5V, 5V	0.2A	1W
National	21	2	19	2.7-5.5	3.3V, 4.5V, 5V	0.18A	0.9W

In automotive and telecommunication systems, which use backup batteries, the input voltage variation is much wider than of portable applications, for example, 18-58V in an automotive system [16]. In industry applications, the front-end bus voltage is relatively stable, but can be selected from 12V, 24V, and 48V. Instead of redesigning the converter each time when the bus voltage changes, customers may prefer a high performance one-fits-all power supply to avoid additional development time and cost. Therefore, a power supply that can operate under a wide input voltage range is a must for these applications. In addition to wide input voltage range, the conversion ratio is another challenge when converting the highest input voltage to the given low voltage bus. A high input-to-output step-down ratio creates significant challenges for the PWM controller design because it has to control very narrow PWM pulses. Meanwhile the converter switching frequency keeps on increasing to reduce the size of inductors and capacitors. Therefore, the PWM pulses can become even shorter and very difficult to control. For example, a Buck regulator with an input voltage of 66V and an output voltage of 3.3V will require a duty cycle of approximately 5%. At a typical switching frequency of 300 kHz, the required PWM on-time of the Buck switch is a mere 166 ns [17]. However, if the switching frequency increases to 2MHz, the on-time will be reduced to 25ns. It is extremely demanding as it requires the switches have a very fast turn-on and turn-off speed which limits the maximum frequency.

In addition, efficiency is always a target and needs to be as high as possible over the wide input range. Since most of the converters are optimized at one operation point, the performance at other operation points can be very bad. Fig.1.2 shows the efficiency

variations of two commercial products with input, output voltage and load. It shows that the efficiency difference can be 20%-30% at the same load when input or output voltage varies. It is the switching loss that usually dominates the total loss when the input or output voltage becomes high. Advanced devices can help reduce the switching loss, but the cost will go up.

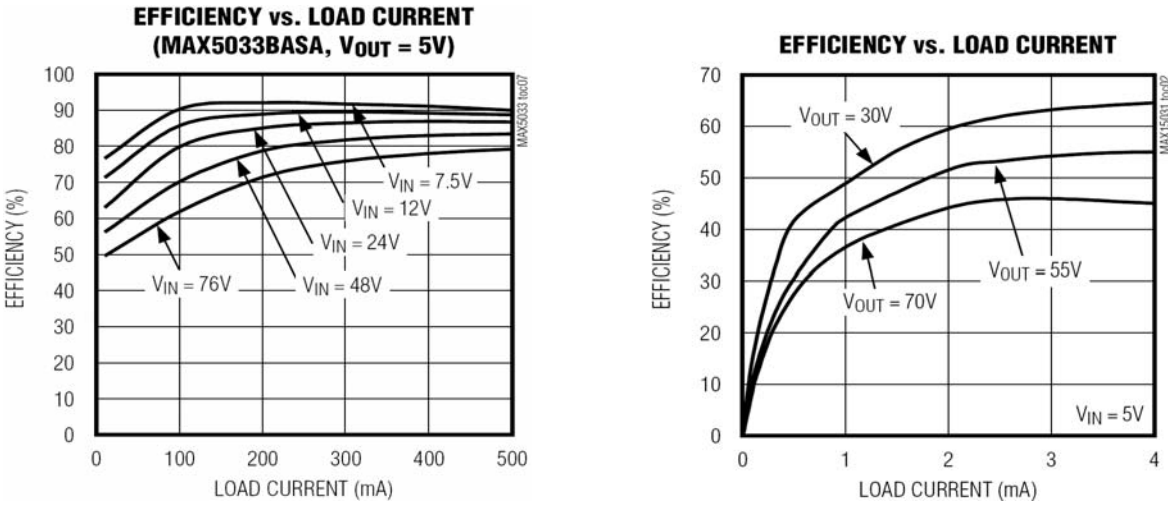

(a) Buck Regulator (MAX5033) (b) Boost Regulator (MAX15031)

Fig.1.2 Efficiency Curves over Wide Input/Output Voltage Range and Load Range [18, 19]

A transformer based converter is a better choice to solve the above two issues. By utilizing the turn-ratio of a transformer, extremely narrow duty cycles can be avoided. However transformers are usually bulky and expensive if isolation is not required. Besides, core loss at high frequency cannot be neglected.

As a result, it becomes very significant to research possible advanced topologies and control methods to improve the performance and efficiency of wide input/output range

DC-DC converters.

1.2. Dissertation Outline

The dissertation consists of six chapters. They are organized as follows.

Chapter I. The background information and motivations of research are introduced.

Chapter II reviews the characteristics of existing charge pump converters. It starts with a comparison between inductor-based converters and charge pump based converters, mainly focusing on cost, size, efficiency, pin number, and output Noise. Then existing topologies of charge pump circuits are reviewed. Although the topology differs, the basic cell is a voltage doubler. A gain that equals to two is usually enough for portable applications; therefore the voltage doubler becomes the base design of power supplies. Finally, the regulation methods of charge pump converters are categorized and reviewed to provide references for designing a regulated charge pump.

Chapter III proposes a high efficiency regulated charge pump over wide input (2.7-4.5V) and load range (10mA-500mA) for battery powered applications. It adaptively changes the conversion mode at different input voltage ranges. It also applies different control schemes to different load conditions. A hybrid control scheme is proposed: When load decreases to light condition, device segmentation control is used; When load further decreases, pulse skipping modulation (PSM) is used in addition to the device segmentation control. Due to the

complexity of control schemes, it is important to know if the system can remain stable over the entire input range and load range. The small signal model and stability analysis for the multi-modes charge pump are also derived to provide references for designing the compensator. Key function blocks are explained in detail, including Mode Change Control Logic, Universal Current Sensor, Device Segmentation and PSM Selector, and Soft Start. Finally, a prototype is built to verify proposed control scheme. The experiment results show that the total loss at light load can be reduced by 56% to 83%.

Chapter IV proposes a high efficiency multi-modes charge pump based Buck converter for wide input range applications. An unregulated multi-modes charge pump is used as a pre-regulator of a standard buck converter and does the rough voltage conversion. According to the input voltage, the charge pump can adaptively select the best mode to step down the input voltage. The input voltage range of Buck converter is greatly reduced and therefore low cost device can be used. Since the Buck converter and the charge pump converter exhibit different efficiency tendencies within the same input range, it is proved that the total efficiency can be improved by combining them, especially at high input voltage. Theoretical efficiency analysis and comparisons between multi-modes charge pump and synchronous Buck are given. On the other side, the fine regulation of output voltage is achieved by the Buck converter. Now the duty cycle will not become extremely low because the input voltage range of Buck converter becomes more centralized after the charge pump. It also directly benefits the compensator and output LC filter design of Buck converter. A 10W prototype is built to verify the benefits of proposed solution. Experiment results show that the highest

efficiency improvement is 7% at heavy load and 16% at light load.

Chapter V proposes a high efficiency transformerless Step-up DC-DC Converter with high voltage gain for LED Backlighting applications. To overcome the shortage of low efficiency when increasing the number of LEDs that a single Boost converter is driving, a multi-modes charge pump is cascaded with the Boost converter. Using the similar concept shown in chapter IV, the efficiency can be improved by changing the mode of charge pump according to the number of LEDs in series.

Chapter VI summarizes the present work and proposes the future work regarding the application of multi-modes charge pump converters.

Chapter 2. Characteristics of Existing Charge Pump Converters

2.1 Inductor based vs. Charge Pump based DC-DC converter

Nowadays, the most widely used approach to perform DC to DC conversions is inductor-based DC-DC converters, which includes at least one inductor. For low-power and highly integrated electronic systems, inductor-based converters usually have the switches integrated with the controller. Fig.2.1 shows the typical configuration of inductor-based DC-DC converter. The way how the inductor is connected can result in different topologies. Buck, Boost, and Buck-Boost Converter are three general DC-DC converters that are used in portable applications.

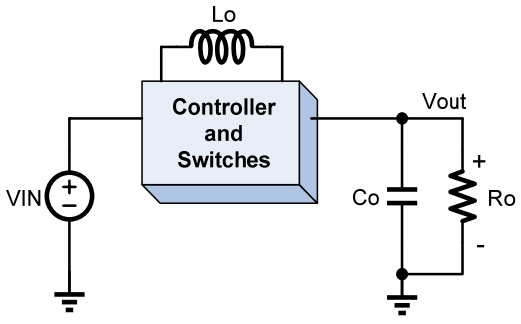

Fig.2.1 Inductor Based DC-DC Converter

As an alternative of inductor based converters, charge pump based converters can also perform DC-DC conversion, but with only switches and capacitors. Compared with an inductor-based converter, it stores energy in capacitors instead of inductors. Different arrangement of capacitors and switches can result in different voltage gains, such as voltage doubler, divider, inverter, and etc. Basically, charge pump circuits utilize flying capacitors with their bottom plates connected to a voltage pulse signal. The flying capacitor can be seen as a voltage source with a constant voltage V_{Cf} if it is sufficiently large. As a result, the voltage of top plate will change with the bottom plate but one V_{Cf} higher or lower. From this point of view, the maximum voltage we can get from a voltage doubler will be only two times the battery voltage. Depending on the power rating, charge pump converter can be partially integrated or fully integrated. Fig.2.2 (a) is the configuration of a charge pump converter without integrating the flying capacitors while Fig.2.2 (b) shows a fully integrated charge pump converter.

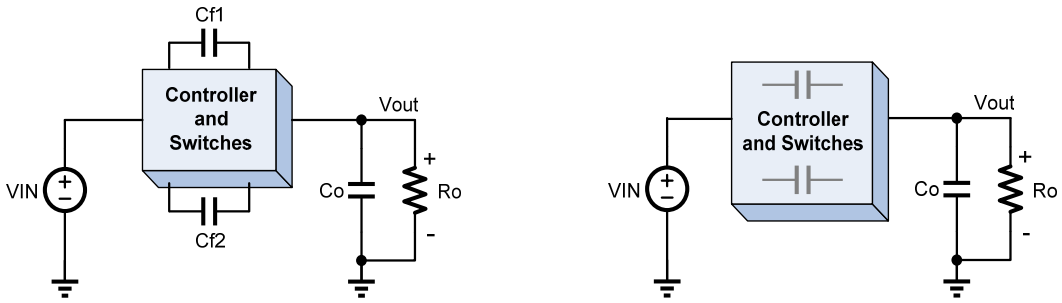

Fig.2.2 Typical Charge Pump Converters (a) Flying Capacitors OFF Chip (b) Flying Capacitors ON Chip

It is often controversial in selecting either inductor-based topology or Charge Pump-Based topology before designing the power supply for portable devices. Therefore, it is very important to know the advantages and disadvantages of both.

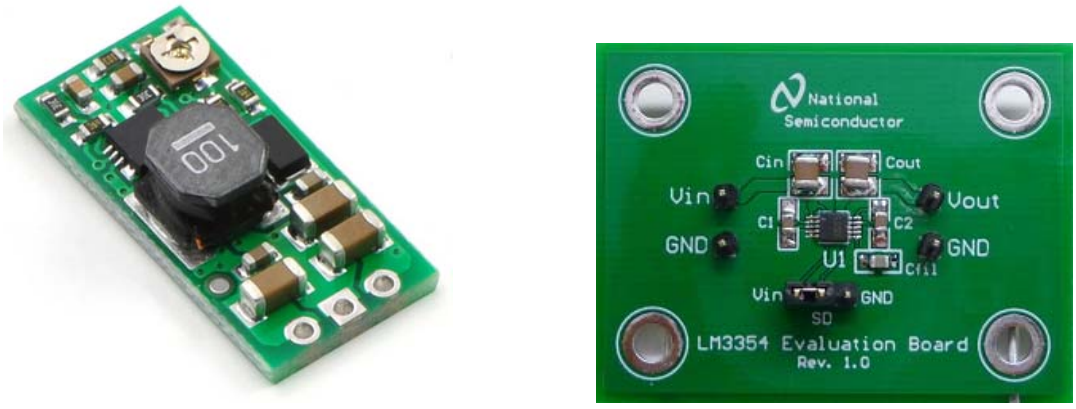

Fig.2.3 Demo Boards of a Boost Regulator and a Charge Pump Regulator [20]

1) Cost and Size

In inductor-based DC-DC converter, it is the inductor that usually dominates the cost and size. In portable applications, the inductor used in a DC-DC converter usually can take 2-5 times more area than that of the regulator IC. Moreover, it is usually at least 2 times thicker than the regulator IC. Although the switching frequency has been greatly increased in today's power supplies and more compact designs of SMT inductors become available, it is still not easy for the inductors to be integrated on chip or even packaged within chip. Fig.2.4 shows the dimension of compact SMT inductors from CoilCraft. In addition, the cost of high performance inductor with low DCR usually is not cheap. Engineers tend to use cheaper inductors that dissipate more power, thus the power efficiency will be degraded.

Fig.2.4 SMT Inductors with Slim Outline [21]

On the other hand, the availability of high value multi layer ceramic capacitors makes the charge pump converter a strong competitor of the inductor-based DC-DC converter. The charge pump converter only includes several ceramic capacitors besides of the regulator IC. Compared with inductor based converters, for a given output capacity, the flying capacitors in charge pump converters are roughly 5 to 10 times less expensive than the inductor, and also 5 to 10 times smaller [3].

Fig.2.5 Charge Pump ICs [22]

With output power below 100mW, fully monolithic charge pump converters with flying capacitors on chip are already commercialized. Packaging the flying capacitors with the silicon chip is an alternative way of integration. Fig.2.5 shows the profile of charge pump ICs for mobile applications from National Semiconductor. Both ways form an ultra integrated solution for the voltage conversion in portable devices. The regulator then only needs one external output capacitor.

2) Efficiency

Inductor-based converters are usually considered more efficient for voltage conversion than charge pump converters. For example, a Boost converter only needs two switches, but a voltage doubler needs four switches, two at each side of the flying capacitor. Therefore, within limited chip area, the current paths in a charge pump converter are much more resistive than that in an inductor-based converter. When load current increases, the conduction loss goes up quickly and efficiency decreases. However, with advanced process technology, the charge pump can almost compete with inductor-based converters. The innovations in process technology make MOSFETs available with very low resistance per given chip area, as shown in Fig.2.6.

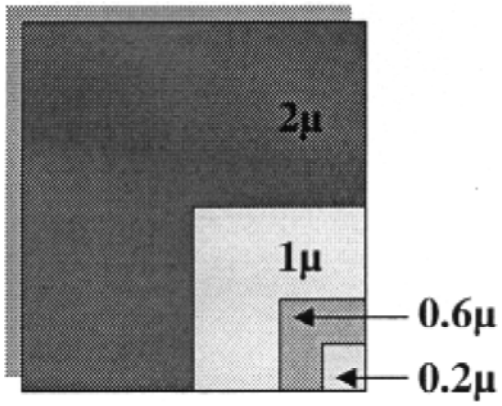

Fig.2.6 Transistor Size with Equal Current Driving Capability [23]

On the other hand, unlike inductor-based converters, the maximum efficiency of charge pump converters highly depends on their structures and input voltages. For example, a voltage doubler can have a 95% efficiency when the input voltage is around half of the output voltage, but the efficiency can decrease to less than 50% when the input voltage is equal to the output voltage. This is very bad because the voltage of a typical battery changes during its discharging cycle, as shown in Fig.2.7. However, multi-modes charge pump products are now available and can provide an average efficiency similar to inductor-based converters over a typical battery voltage range. It can adaptively select the proper conversion mode to achieve the best efficiency according to the ratio of output voltage to input voltage, as shown in Fig.2.8. In today's market, charge pump ICs with two conversion ratios are very popular. Very few ICs that use three flying capacitors to achieve four conversion ratios are available.

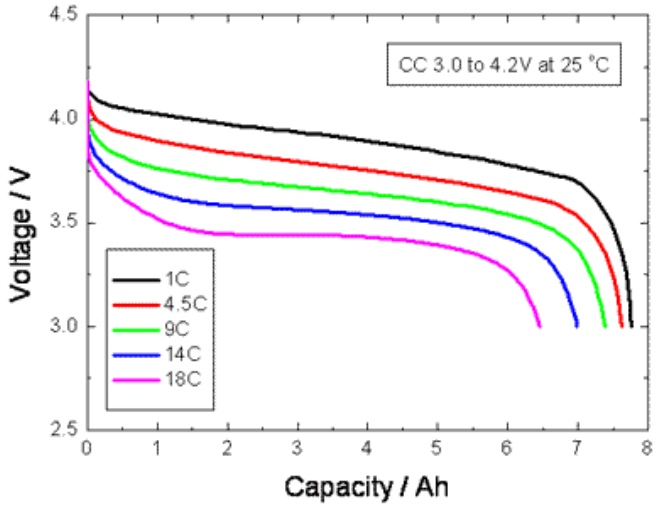

Fig.2.7 Discharging Curve of a single Li-ion Battery [24]

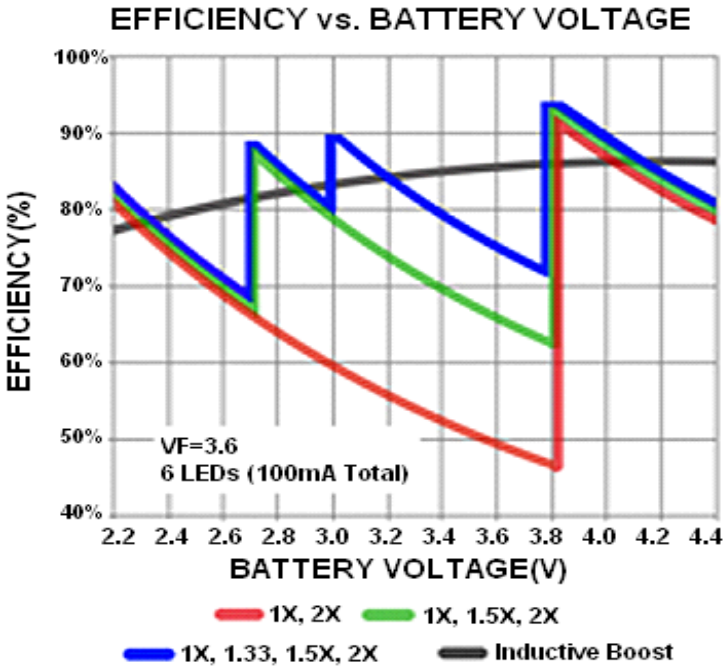

Fig.2.8 Efficiency vs. Battery Voltage using Charge pump and Boost Converter [25]

3) Pin Number

For inductor based converters, it generally requires at least four pins: Input voltage, Inductor connection, Feedback Voltage, and ground, which can be seen from Fig.2.1. In practical, an Enable pin is often added. For charge pump converter, the pin numbers can vary a lot. It can be seen from Fig.2.2: if it is a fully integrated charge pump or with flying capacitors packaged inside, it only requires three pins: Input voltage, Output Voltage, and ground, which is less than inductor based converter; if flying capacitors are out of package, then it needs four more pins in addition to the original three pins for flying capacitor connections. However, pin numbers can be even more depending on the current capacity, conversion ratio and additional features. Therefore, it is obvious that low current charge pump converters have less pin numbers while high current charge pump converters have more pin numbers than inductor based DC-DC converter.

4) Output Noise

Theoretically, there are plenty of noise sources in a switching power supply. However, intrinsic noise which is generated by the regulator itself is considered dominant compared to any other noise sources [3]. The switching nature of inductor-based and charge pump converters are different. One uses inductors to store energy while the other uses capacitors to store energy. Fig.2.9 shows the noise profiles of the inductor-based and charge pump converters. It can be seen that both converters show output noise around switching frequency and its harmonics. However, for inductor-based converters, additional noise is introduced by the LC filter around its resonance frequency, and it is usually located within the audio or

video frequency range in portable applications. Reducing the amplitude of switching intrinsic noise can be done by increasing the output capacitor value, but this will also shift more deeply the LC filter resonance frequency into the sensitive audio band [3].

On the other hand, the inductor on a PCB board can be considered as an antenna and emit electromagnetic waves when the converter is switching. The Electro-magnetic interference (EMI) may cause other sensitive circuits nearby to fail to work correctly. Therefore, the EMI issue is a big limitation for an inductor-based converter to be used in RF and audio applications. Shielded inductors are often used to reduce the EMI; however it definitely further increases the cost and weight.

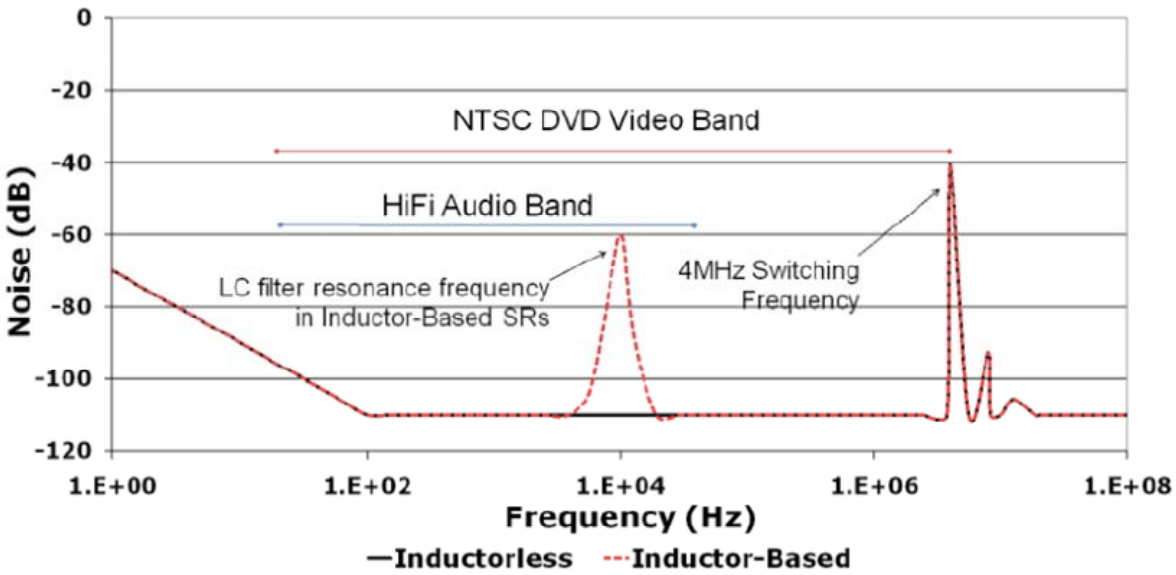

Fig.2.9 Noise profiles of inductor-based and charge pump converters [3]

From all of the comparisons above, it can be concluded that the charge pump DC-DC

converters are equally able to meet all the requirements of portable devices. It has low weight, low cost, small size, and comparable efficiency over variable input voltage range with the inductor-based converter. Moreover, it generates less noise, which is good for noise sensitive circuits in portable devices.

2.2 Topology of Existing Charge Pumps

A number of charge pump circuit topologies exist in the literature [2][7][10][12][26-28], such as Dickson charge pump, Ladder, Makowski charge pump, Series-Parallel Charge pump, Voltage doubler, and so on. Fig.2.10 shows the topologies of five step-up charge pump circuits. Each of them uses three flying capacitors, but the switch number and the maximum gain may be different. The merits of each topology are given in [9]. It seems that there are lots of topologies to select, but it actually highly depends on the respective application. For a charge pump that targets portable applications, it mostly needs to step up the battery voltage (2.7-4.5V) to 5V. Therefore, a maximum gain of 2 is already enough. It can be seen from Fig.2.10 that the basic cell of the five charge pump topologies is the same, which is a voltage doubler, as shown in the red block. Therefore, a voltage doubler becomes the base design for the power supply in portable applications.

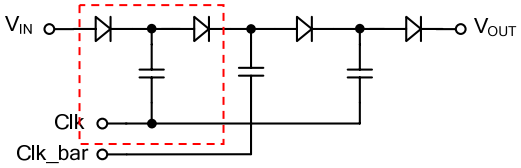

(a) Dickson Charge Pump

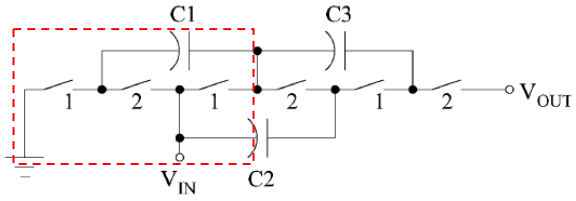

(b) 1:4 Ladder

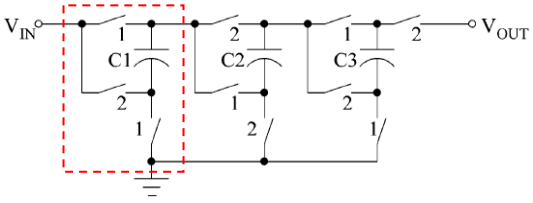

(c) 1:5 Fibonacci (Makowski)

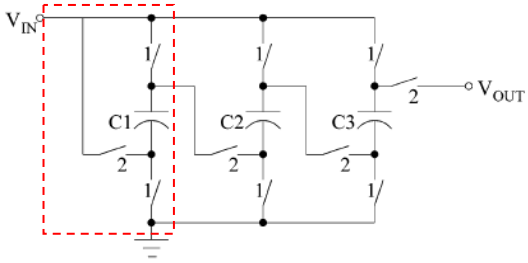

(d) 1:4 Series-Parallel

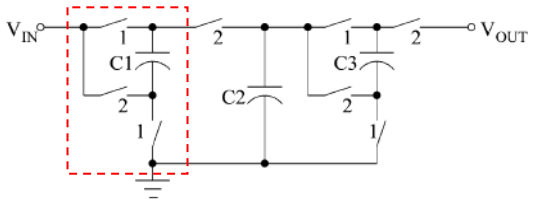

(e) 1:4 Doubler

Fig.2.10 Five Step-up SC Converter Topologies. (a) Dickson Charge Pump (b) Ladder. (c) Fibonacci (Makowski) (d) Series-Parallel. (e) Doubler. [9]

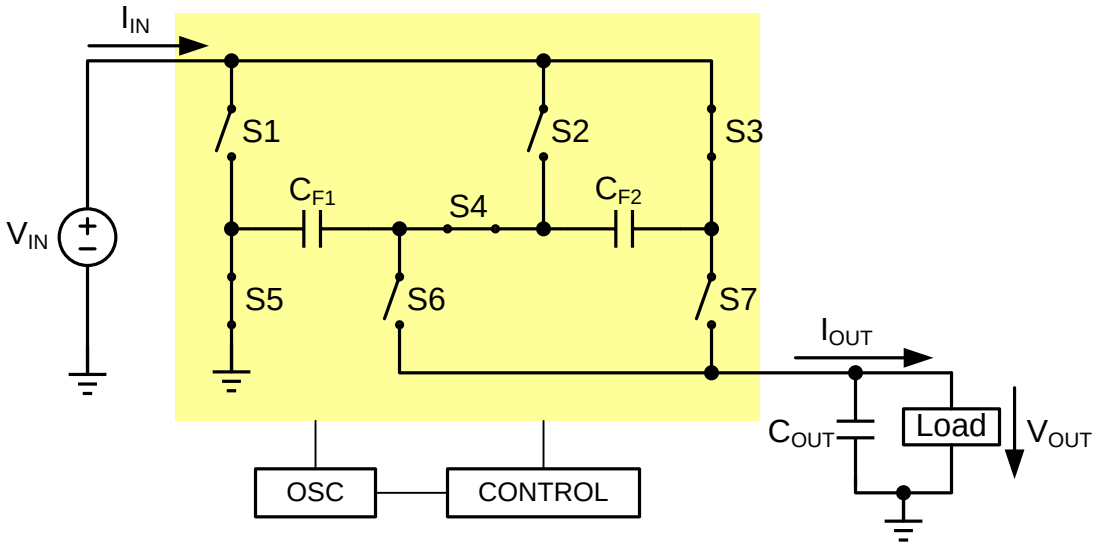

Fig.2.11 1.5-times charge pump [13]

Based on the principal of a voltage doubler, several other charge pump topologies can be derived, such as 1.5-times charge pump, 1.33-times charge pump, multi-phase voltage doubler, and so on. Fig.2.11 shows the topology of a 1.5-times charge pump. Similar to a voltage doubler in structure, but the flying capacitors are charged in series to 0.5 times the input voltage in a 1.5-times charge pump. Fig.2.12 shows an interleaving two-phase voltage doubler. In this topology, two charge pumps are connected in parallel but operate with 180° phase shift angle. When the duty cycle is set to 50% for both charge pumps, the output current is therefore continuously supplied from the input, thus reducing the ripple to a minimum.

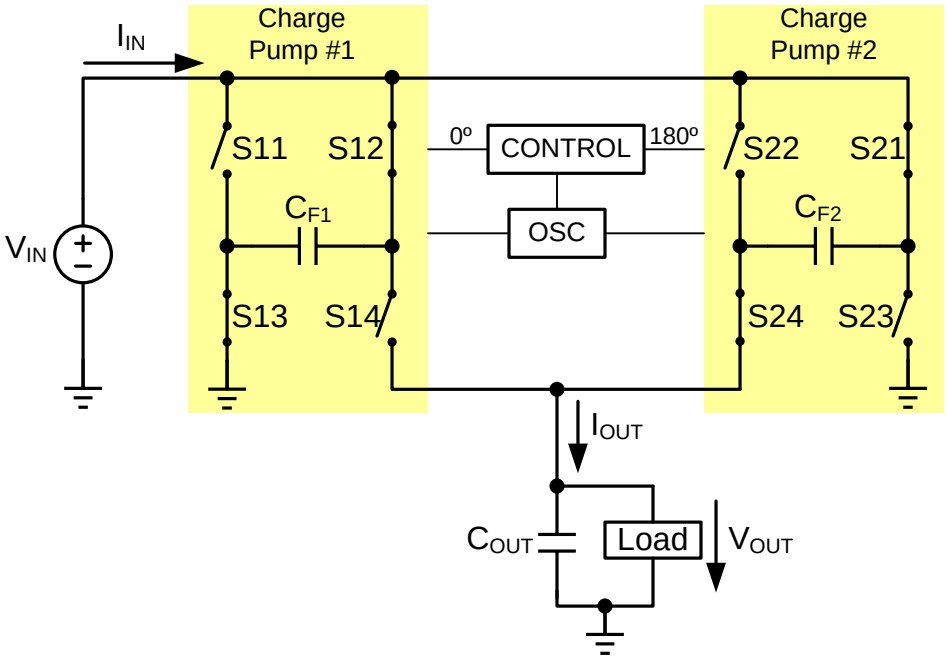

Fig.2.12 Two-phase Voltage Doubler [13]

2.3 Unregulated or Regulated Charge Pump

Depending on the application, a charge pump converter can be regulated or unregulated. When it is unregulated, the output varies with input and delivers a multiple of the input voltage. In portable applications, it often requires charge pump to transform the decreasing voltage of a discharging battery into a stable supply. Therefore, regulation is required for charge pump converters. Generally, the regulation schemes can be summarized to two categories according to the switching frequency: constant frequency regulation and variable frequency regulation.

2.3.1 Constant Frequency Regulation

1) Voltage Mode Control

The regulation scheme using voltage Mode Control is usually achieved by controlling the on-resistance of a single or multiple switches in either the charging or discharging path. As the on-resistance of switch is regulated, the voltage drop across the switch is controlled. An error amplifier compares the output voltage against a reference voltage, and feeds back an error signal to the on-resistance control block, as shown in Fig.2.13 [5]. For low load current or high input voltage, the on-resistance will be increased and consume the excessive voltage; for high load current or low input voltage, the on-resistance gets smaller. The duty cycle of charging and discharging phase is fixed to 50%. The biggest advantage of this method is fixed frequency operation with a very low output voltage ripple that makes filtering easier.

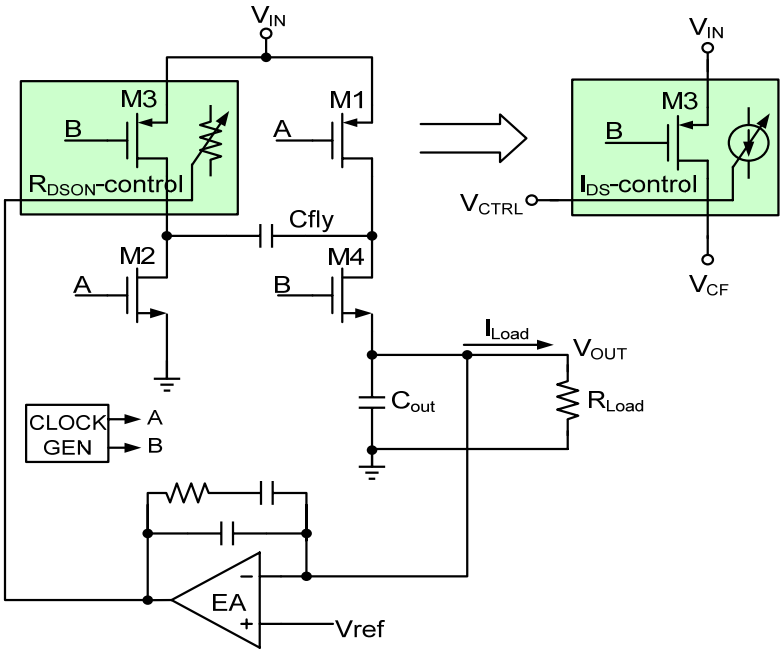

Fig.2.13 Voltage Mode vs. Current Mode Charge Pump

2) Current Mode Control

Instead of regulating the on-resistance, the current mode regulation controls the current flowing through the switch. Therefore, the regulated switch operates as a controlled current source instead of a variable resistor, as shown in Fig.2.13. The current source can be either located in the charging path [14] or discharging path [5]. When the current source is placed in the charging path, the charging current of flying capacitor is controlled thus the voltage across the capacitor is regulated. It is easier to regulate M2 since its source is connected to the ground instead of floating. Similar to this, when the current source is located in discharging path, M3 is usually easier to be regulated than M4. Same with voltage mode control, the duty cycle of charging and discharging phase is also fixed to 50%.

3) Pulse Width Modulation (PWM) [11, 29]

Another regulation scheme of charge pump with constant frequency is PWM control. Instead of fixing the duty cycle to 50% in current and voltage mode, the duty cycle will change with the input voltage and load current. Fig.2.14 shows a regulated step-down charge pump using PWM control. The output voltage Vo is fed back to the error amplifier and compensation circuit. Then the output of compensator will be compared with a sawtooth waveform and generates desired duty cycle. Finally, the logic circuit will convert the duty cycle signal to gate driving signals for the four switches in the charge pump. By controlling the duty cycle, the average energy that charge pump delivers to the load is controlled and thus the output voltage can be regulated. The biggest drawback of PWM regulation is that it will be difficult to generate extremely narrow duty cycle at light load.

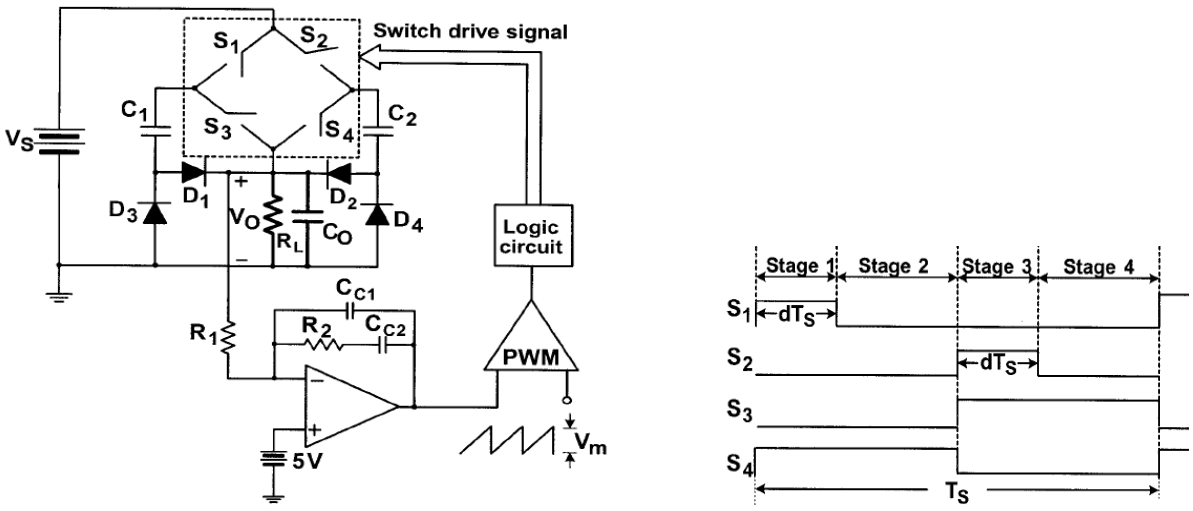

Fig.2.14 Step-down Charge Pump (a) Schematic (b) Switch drive signals.[11]

2.3.2 Variable Frequency Regulation

1) Pulse-Skip Regulation

In pulse-skip regulation, the output voltage is regulated by skipping unneeded pulses. If output voltage is lower than the reference voltage, the charge-pump continuously switches and charges the output capacitor. If the output voltage exceeds the reference voltage, the charge pump stops and no energy will be provided through the charge pump. The regulation scheme is shown in Fig.2.15. The advantage of this regulation is the low average control current, especially at light load condition since the charge pump stops operation most of the time. The disadvantages are wide frequency variations and higher output voltage ripple compared to Constant-Frequency regulation [13].

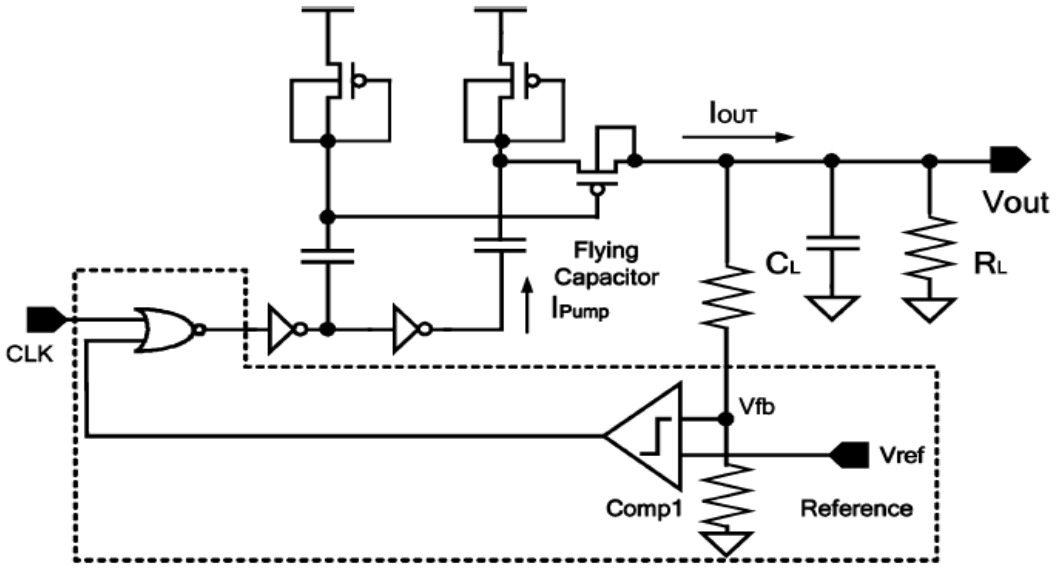

(a) Schematic of Charge Pump with Pulse-Skip Modulation [8]

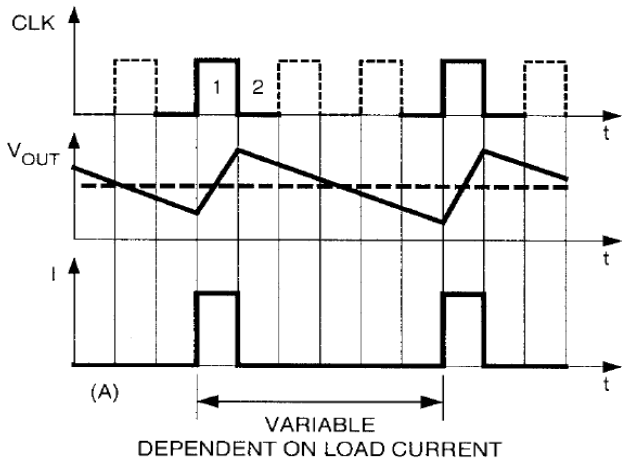

(b) Typical scheme of Pulse-Skipping Regulation [13]

Fig.2.15 Schematic and Scheme of Pulse-Skip Regulation

2) Linear Skip Regulation

To improve the output voltage ripple at pulse skip modulation, an improved control 'Linear Skip Regulation' (Fig.2. 16) is proposed by [29]. LinSkip regulation uses 3 phases, charge phase, transfer phase and wait phase. During the wait phase, the charge pump stops operation and the load current is only supplied by the output capacitor. In addition to pulse skipping, this scheme also regulates the current transferred to the output. If load current is high, there will be no wait phase and the frequency is fixed. Only the current transferred per cycle is regulated. If load current is low, the current is fixed but the duration of wait phases is regulated, similar to pulse skip modulation.

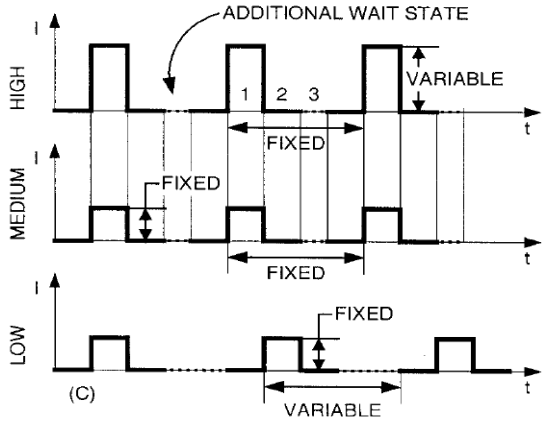

Fig.2.16 Scheme of Linear-Skip Regulation [29]

2.4. Summary

In order to know the strength and weakness of charge pump converters and see how they can compete with inductor-based converter, an overall comparison between inductor-based

DC-DC converters and charge pump converters was presented in this chapter. For portable application, charge pump DC-DC converters beat the inductor-based converter with lower weight, lower cost, smaller size, and comparable efficiency. Popular topologies and control schemes of charge pump converters were also briefly reviewed to make the basis for the design in the following chapters.

Chapter 3. Design of A High Efficiency Regulated Charge Pump over Wide Input and Load Range for Portable Applications

3.1 Research Motivation

In DC-DC converters, charge pump regulators are well known for their compact sizes since they do not have large and expensive magnetic components. Unlike LDO regulators, which can only step-down the input voltage, charge pump regulators can either boost or buck the input voltage by using different topologies. As a result, charge pump regulators are usually considered as an ideal solution in low power portable applications.

However, the traditional charge pump, like a voltage doubler, is not a good solution for applications where the input (Battery) voltage varies a lot, and the output voltage needs to remain regulated. It only has high efficiency when desired output voltage is close to two times input voltage. The power loss will be particularly high when the input voltage is close to the output voltage. Multi-Modes Charge Pumps were proposed by researchers to improve the efficiency over wide input range. By alternating the connections between switches and flying capacitors during charging and discharging period, multiple conversion ratios can be obtained [34]. Once the optimum mode is selected for one input voltage, the output voltage

can be regulated using on-resistance regulation, duty cycle modulation, etc [13].

On the other side, when a charge pump needs to operate over a wide load range, the light load efficiency is important, especially for applications, such like cell phones, which mostly work in standby mode. Normally, the devices' sizes are optimized to reduce conduction loss and maintain regulation at maximum load; therefore, they are big devices with small on-resistance. However, small on-resistance will not contribute to the light load efficiency because the conduction loss is not dominant anymore. On the contrary, those big devices still need a lot of power to drive them since the gate driver loss does not scale down with the load current. In order to improve the light load efficiency, the driving loss needs to be as low as possible. This is also true for inductor-based DC-DC converters. Many solutions have already been proposed, by using either advanced control or improved power stage, such as pulse frequency modulation, pulse skipping modulation, device segmentation, etc [35-49].

A high efficiency regulated Multi-Modes Charge Pump over wide input and load range is proposed. The input is a single Li-ion battery with voltage between 2.7V and 4.5V, while the output voltage needs to be regulated to 5V. The charge pump can automatically adjust the conversion modes: 2x, 1.5x, and 1.33x according to different input voltages, therefore enhance the average efficiency over the entire battery life. The maximum load current is 500mA, but can go as low as 10mA. When the load current decreases to light load condition, device segmentation control is used; and when the load further decreases, pulse skipping modulation will be used in addition to the device segmentation. By using proposed hybrid control scheme, the gate driver loss and switching loss at light load can be greatly reduced, and finally improves light load efficiency.

3.2 Regulation Scheme of Multi-Modes Charge Pump

Ideally the efficiency of a charge pump can be approximated by (3.1) if the gate driving loss, switching loss and quiescent loss are neglected. N is the mode conversion ratio. It can be seen that the maximum efficiency it can achieve is limited by its topology. If it is a voltage doubler, N=2 and the maximum efficiency at any input voltage will be equal to $V_{out}/2V_{in}$.

$$\eta = \frac{V_{out}}{V_{in} * N} \tag{3.1}$$

When V_{in} gets close to 0.5 V_{out}, the maximum efficiency is close to 1; When V_{in} is much higher than $0.5V_{out}$, the efficiency will become very low; When V_{in} is lower than $0.5V_{out}$, the output will be out of regulation. Therefore, the efficiency varies with input voltage when the topology is fixed. To achieve a high efficiency over wide input range, a simple voltage doubler certainly cannot meet the requirement. Instead, Multi-Modes Charge Pump which can adaptively change the mode according to the input voltage will be a good solution. Fig.3.1 shows the topology of a Multi-Modes Charge Pump.

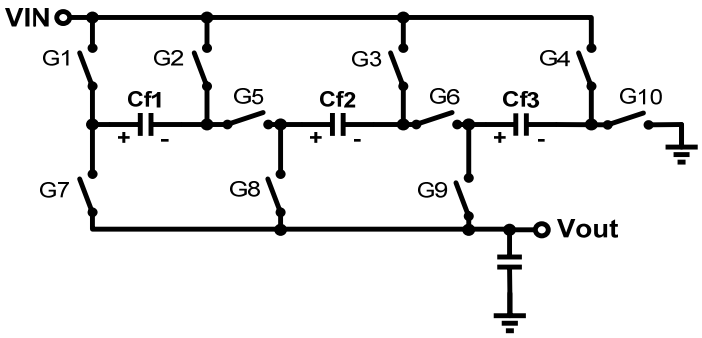

Fig.3.1 Topology of Multi-Modes Charge Pump

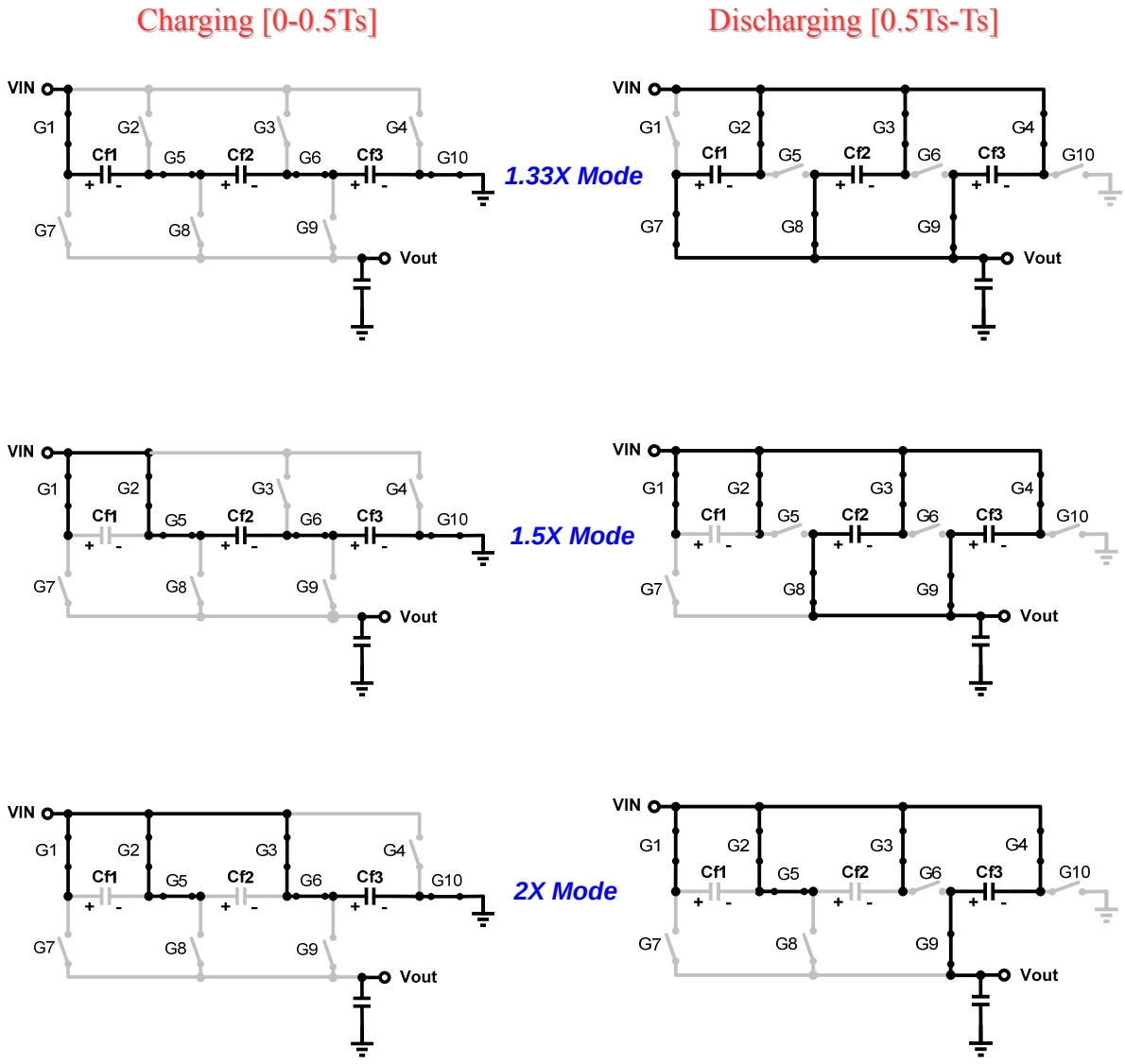

Fig.3.2 Topology transformation of the Multi-Modes Charge Pump

Three different conversion ratios can be realized by alternating the arrangement of switches and capacitors. Take Mode 1.33x as the example. During [0-0.5Ts], G1, G5, G6, and G10 are ON while G2, G3, G4, G7, G8, and G9 are OFF. Flying capacitor Cf1, Cf2, Cf3 are

in series connection and being charged by the input source V_{in}; during [0.5Ts-Ts], G1, G5, G6, and G10 are OFF while G2, G3, G4, G7, G8, and G9 are ON. The branch circuits of Cf1, Cf2 and Cf3 are in parallel connection and discharge energy to the output. The output voltage therefore is the sum of V_{in} and the voltage across the flying capacitor. The topology transformation of Mode 1.33x, Mode 1.5x and Mode 2x in one cycle are shown in Fig.3.2.

Fig.3.3 shows a simplified DC model of charge pump without considering gate driver loss, switching loss and leakage loss. R_{out} is the output impedance of charge pump. When V_{out} is not regulated, R_{out} is fixed. Therefore, V_{out} is close to $N*V_{in}$ and changes with V_{in}. When output needs to be regulated, R_{out} will vary with V_{in}, load current I_{out}, and mode conversion ratio N, as shown in (3.2).

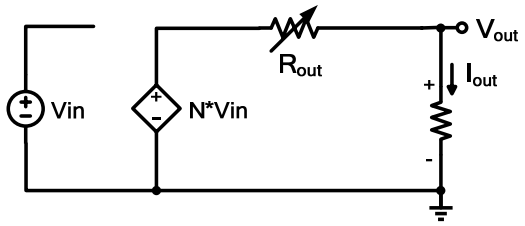

Fig.3.3 Simplified DC model of Charge Pump

$$V_{out} = N * V_{in} - I_{out} * R_{out} \tag{3.2}$$

There are two ways to regulate the output of charge pump. One is Constant Frequency Mode Regulation. The output voltage is regulated using error amplifier by controlling either the on-resistance of transistors or duty cycle. Since switching frequency is fixed, the output voltage ripple and the size of output capacitor can be reduced. The main drawback is high quiescent current and thus low efficiency at light load condition. The other way is Skip Mode

Regulation. A hysteresis comparator is used to control the on and off of switches according to the output voltage variation. It does not need any amplifier or compensator and it can have high bandwidth and fast transient response. It also has low quiescent current which is good for light load efficiency. However, it has high output ripple and variable ripple frequency which is not easy for the following filter design.

A good compromise is to combine the two regulation technique so that a trade off the ripple and efficiency can be achieved.

Comparing the methods of constant frequency regulation, regulating the on-resistance of switches while the duty cycle is fixed to 50% is preferred than regulating the duty cycle while the on-resistance is fixed. It will be difficult to control narrow duty cycle when $N*V_{in}$ is much higher than desired V_{out}. The maximum frequency is therefore limited.

Generally, there are two options when selecting the transistors that will be regulated. One is regulating the transistors in charging path and the other is regulating the transistors in discharging path.

For Option I, only the on-resistance of transistor G10 in the charging path is regulated. Transistors G1-G9 will have fixed on-resistance. Assume G1-G9 have equal on-resistance $R_{sw,}$ while the impedance of regulated transistor G10 is R_t. All capacitors have the same ESR. The DC output impedance of charge pump can be derived according to its loss dissipation. Taking Mode 2x as the example. The charging and discharging paths of the Multi-Modes Charge Pump in 2x mode are shown in Fig.3.4. In order to maintain the charging balance, the integration of the current through Cf3 in one cycle should be: $<I_{Cf3}>_{Ts}=0$. Since duty cycle is fixed to 0.5, the average value of charging and discharging current through Cf3 should be

equal, as: $I_{Charge}=I_{Discharge}$. Similarly, the average value of charging and discharging current through output capacitor C_{out} should also be equal, as: $I_{out}=I_{Discharge}-I_{out}$. Therefore, $I_{Charge}=2I_{out}$. The transistor conduction loss P_{Con}, flying capacitor loss P_{Cf}, and ESR loss P_{ESR} can be derived using (3.3), (3.4), and (3.5). The total loss is the sum of conduction loss of transistors, flying capacitors and ESR, gate driver loss and leakage loss, as shown in (3.6). Ultimately, the DC impedance of Charge pump can be obtained, as shown in (3.7).

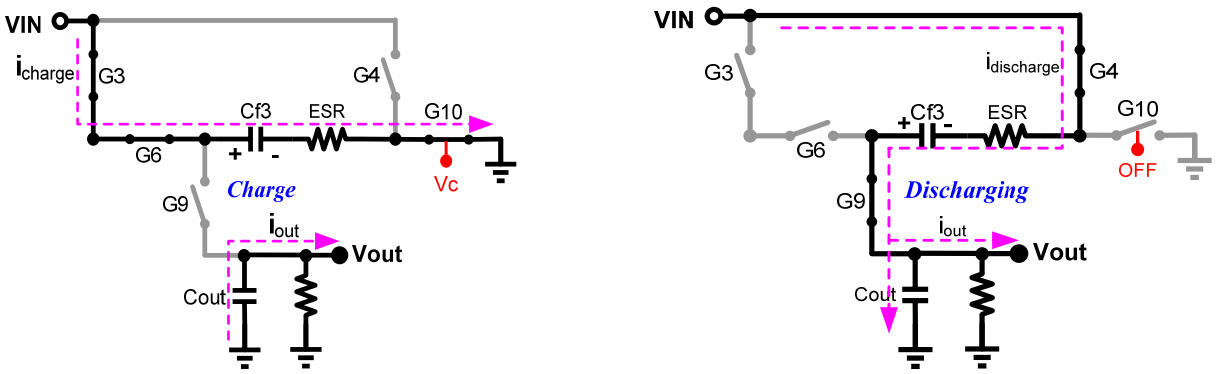

Fig.3.4 Multi-Modes Charge Pump in 2x mode

Model 2x:

Loss in switches: $$P_{Con}=(2I_{out})^2\times 2R_{SW}+(2I_{out})^2R_t\times 0.5=4{I_{out}}^2\times(2R_{SW}+0.5R_t) \quad (3.3)$$

Loss in flying capacitors: $$P_{C_f}={I_{out}}^2/f_sC_f \quad (3.4)$$

Loss in ESR: $$P_{ESR}=(2I_{out})^2\times ESR+{I_{out}}^2\times ESR \quad (3.5)$$

Total Loss: $$P_{Total}=(P_{Con}+P_{C_f}+P_{ESR})+I_qV_{IN}+P_{gate}=R_{out}{I_{out}}^2+I_qV_{IN}+P_{gate} \quad (3.6)$$

$$R_{out}=8R_{SW}+5ESR+1/(f_sC_f)+2R_t \quad (3.7)$$

Similarly, we can derive the losses and R_{out} for Mode 1.5x and 1.33x.

Mode 1.5x:

Loss in switches: $$P_{Con} = I_{out}^{\ 2} \times (3.5R_{SW} + 0.5R_t) \quad (3.8)$$

Loss in flying capacitors: $$P_{C_f} = I_{out}^{\ 2} / (2 f_s C_f) \quad (3.9)$$

Loss in ESR: $$P_{ESR} = 3I_{out}^{\ 2} \times ESR \quad (3.10)$$

Total Loss: $$P_{Total} = I_{out}^{\ 2} \left[3.5R_{SW} + 3ESR + 1/(2 f_s C_f) + 0.5R_t \right] + I_q V_{IN} \quad (3.11)$$

$$R_{out} = 3.5R_{SW} + 3ESR + 1/(2 f_s C_f) + 0.5R_t \quad (3.12)$$

Mode 1.33x:

Loss in switches: $$P_{Con} = I_{out}^{\ 2} \times (2R_{SW} + 0.22R_t) \quad (3.13)$$

Loss in flying capacitors: $$P_{C_f} = I_{out}^{\ 2} / (3 f_s C_f) \quad (3.14)$$

Loss in ESR: $$P_{ESR} = I_{out}^{\ 2} \times 2.33ESR \quad (3.15)$$

Total Loss: $$P_{Loss} = I_{out}^{\ 2} \left[2R_{SW} + 2.33ESR + 1/(3 f_s C_f) + 0.22R_t \right] + I_q V_{IN} \quad (3.16)$$

$$R_{out} = 2R_{SW} + 2.33ESR + 1/(3 f_s C_f) + 0.22R_t \quad (3.17)$$

For Option II, the on-resistance of transistors G2, G3, and G4 located in the discharging paths are regulated; Transistors G1 and G5-G10 have fixed resistance. Using the same method, the output impedance of charge pump at each mode for Option II can be derived.

The results of Option I and Option II are shown in Table 3.1. Once R_{sw}, ESR, and capacitors are fixed, the output impedance of charge pump R_{out} will be determined by R_t.

Table 3.1 Output Impedance of Multi-Modes Charge Pump

Mode	**Output Impedance (R_{out})**	
	Option I	**Option II**
2x	$8R_{sw}+5ESR+1/(f_sC_f)+2R_t$	$8R_{sw}+5ESR+1/(f_sC_f)+2R_t$
1.5x	$3.5R_{sw}+3ESR+1/(2f_sC_f)+0.5R_t$	$3R_{sw}+3ESR+1/(2f_sC_f)+R_t$
1.33x	$2R_{sw}+2.33ESR+1/(3f_sC_f)+0.22Rt$	$1.56R_{sw}+2.33ESR+1/(3f_sC_f)+0.67R_t$

It can be seen that option II can more efficiently regulate the charge pump since the control gain from R_{out} to R_t are larger. However, input current spike during mode change can be huge since the voltage across flying capacitors has a sudden change during mode change, which are shown in Table 3.2. Besides, the voltage run-away can happen among the flying capacitors since they are not in direct parallel with each other during the discharging phase. Compared with Option II, Option I is free of such two issues.

Table 3.2 Voltage of Flying Capacitors at Different Modes

Mode	**Option I**		**Option II**	
	V_{Cf}	**Regulated Transistors**	**V_{Cf}**	**Regulated Transistors**
2x	V_{out}-V_{in}	G10	V_{in}	G4
1.5x	V_{out}-V_{in}	G10	$V_{in}/2$	G3,G4
1.33x	V_{out}-V_{in}	G10	$V_{in}/3$	G2,G3,G4

Finally, Option I is adopted in this design: only regulating transistor G10 in the charging path. The implementation of Multi-Modes Charge Pump is shown in Fig.3.5. To avoid

floating driving issues, G1-G9 are implemented using PMOS, denoted as MP1-MP9. The gate voltage of MP1-MP9 fully swings from ground to V_{out}(5V), so they are unregulated. G10 is implemented using NMOS, denoted as MN1. The output voltage V_{out} will be compared with desired reference voltage and the error will be integrated by a PID compensator. When MN1 is ON, the gate voltage is equal to the output voltage of compensator Vc; When MN1 is OFF, the gate voltage is zero. Therefore, the gate driving voltage of MN1 swings from ground to Vc. It is worth to clarify that the PID compensator controls the gate voltage of MN1, so it may drive MN1 either in saturation or linear region. Generally, MN1 is in saturation region when the impedance needs to be large and in linear region when the impedance needs to be low. However, no matter if it is in linear or saturation region, the regulation principle can still be explained using the same DC model.

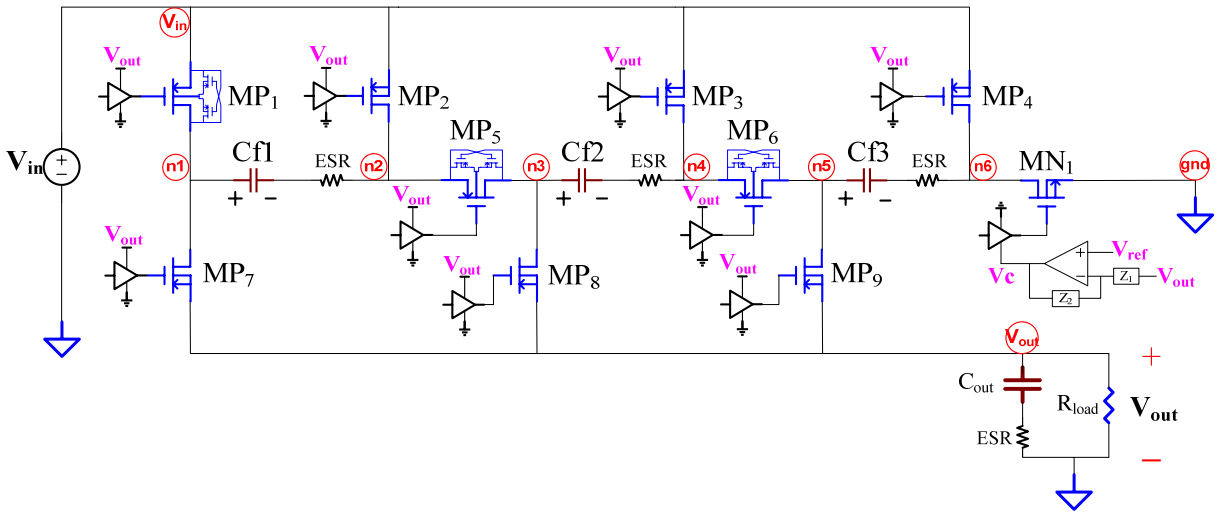

Fig.3.5 Implementation of Multi-Modes Charge Pump in Transistor Level

Table 3.3 The Voltage Swing of Nodes in Multi-Modes Charge Pump

Mode	n1	n2	n3	n4	n5	n6
2X	V_{in}	V_{in}	V_{in}	V_{in}	V_{in} ~V_{out}	gnd~V_{in}
1.5X	V_{in}	V_{in}	V_{in}~V_{out}	1/2V_{in}~V_{in}	1/2V_{in}~V_{out}	gnd~V_{in}
1.33X	V_{in}~V_{out}	2/3V_{in}~V_{in}	2/3V_{in}~V_{out}	1/3V_{in}~V_{in}	1/3V_{in}~V_{out}	gnd~V_{in}

The voltage swing of nodes n1-n6 at different mode is shown in the Table 3.3, which will be the reference to connect the bulk of each transistor correctly. For MP2, MP3 and MP4, it can be seen that nodes n2, n4 and n6 are always less than the node V_{in}. Therefore, the bulk should be connected to V_{in}. For MP7, MP8, and MP9, nodes n1, n3, and n5 are always less than the nodes V_{out}. Therefore, their bulk should be connected to V_{out}. For MN1, the bulk is connected to ground. However, for MP1, MP5, and MP6, the comparison of voltage between both ends is complicated since the result is not consistent when the mode changes. Dynamic Bulk switching technique is proposed by some researchers to solve this problem [50]. Fig.3.6 shows the structure of a PMOS with dynamic bulk switching. The bulk of targeted PMOS will be adaptively connected to the higher voltage between source and drain by adding another two small PMOS across both ends.

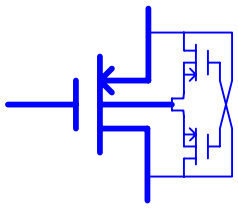

Fig.3.6 Dynamic Bulk Switching for PMOS

3.3 Efficiency Improvement over Wide Input Range

Eq.(3.1) shows that the maximum efficiency of charge pump at given input voltage is determined by its topology. For example, when input voltage is 3.9V, the maximum efficiency of charge pump is 5/(2*3.9)=64.1% in 2x mode, 5/(1.5*3.9)=85.5% in 1.5x mode, and 5/(1.33*3.9)=96.4% in 1.33x mode. Therefore, working at the right operation mode for given input voltage will greatly benefit the efficiency.

In a Multi-Modes Charge Pump, the mode can be easily changed by re-arranging the connection of switches and capacitors according to the input voltage. It is important to know the proper range of V_{in} for each mode. Fig.3.7 shows the Efficiency variations of Multi-Modes Charge Pump over the entire battery voltage range. The x-axis is weighted according to the discharging curve of lithium-ion battery. The dotted line is the minimum voltage that the charge pump can stay in the lower conversion ratio modes. However, the real mode transition point should be selected higher than the minimum voltage considering the voltage drop on charge pump itself. In Fig.3.7, it can be seen that Eff1<Eff2<Eff3 over the entire input range. As a result, when pushing the transition points to higher input voltage, the average efficiency will degrade. On the other side, since the output voltage is regulated to the same value during each mode, it should meet inequalities (3.18)-(3.20).

2X: $$1.5V_{in} - R_{out\_min(1.5x)} * I_{out} \le V_{out} \le 2V_{in} - R_{out\_min(2x)} * I_{out} \quad (3.18)$$

1.5X: $$1.33V_{in} - R_{out\_min(1.33x)} * I_{out} \le V_{out} \le 1.5V_{in} - R_{out\_min(1.5x)} * I_{out} \quad (3.19)$$

1.33X: $$V_{out} \le 1.33V_{in} - R_{out\_min(1.33x)} * I_{out} \quad (3.20)$$

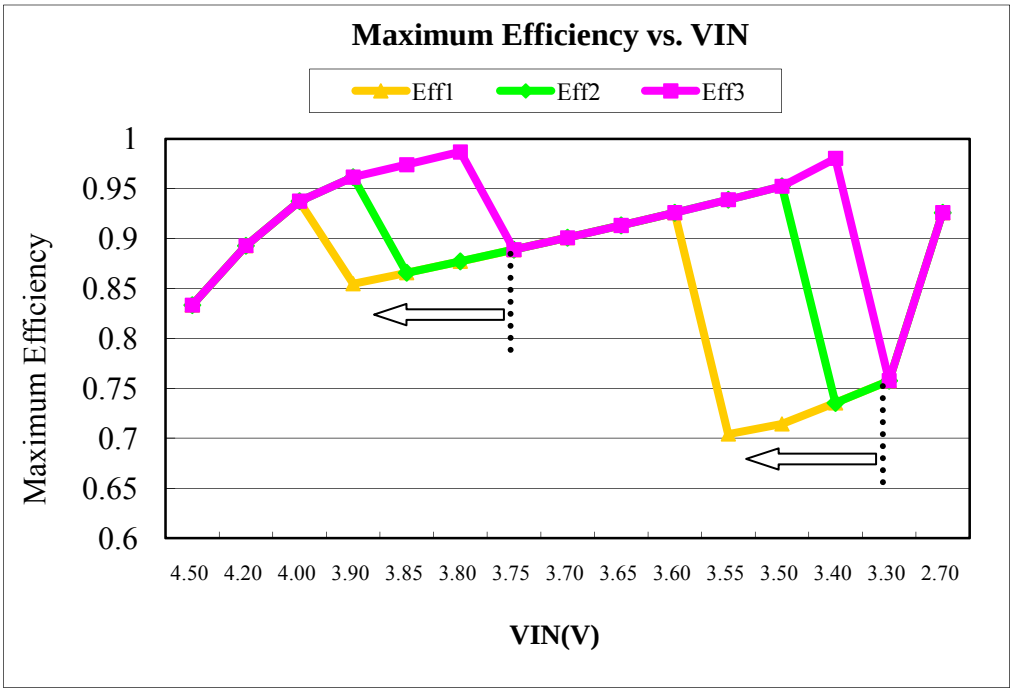

Fig.3.7 Maximum Efficiency vs. VIN of Multi-Modes Charge Pump

Therefore, according to Fig.3.7 and (3.18)-(3.20), the transition voltages should be optimized for overall efficiency while still maintains the regulation of output. In this design, the transition point is set to 3.9V and 3.5V for 1.33x and 1.5x mode respectively.

Based on derived output impedance at each mode, transistor sizes and flying capacitance can be determined. To maintain output regulation over the entire load range, transistor sizes should be chosen based on the worst case, which happens at the full-load condition together with the mode transition. At the worst case, the output impedance of charge pump has the lowest value, thus we can have (3.21).

$$R_{out\_min} \leq (N * V_{in} - V_{out}) / I_{full} \quad (3.21)$$

Assume ESR=10mOhm and Cf=4.7uF. The full load current (I_{full}) is 0.5A and V_{out} is regulated to 5V. The transition points are V_{in}=3.9V (1.33x<->1.5x) and V_{in}=3.5V (1.5x<->2x). According to (3.21) and the expressions of R_{out} in Table 3.1, (3.22)-(3.24) can be derived.

$$2x: \quad 8R_{sw}+2R_t \leq 0.54 \text{ Ohm} \quad (3.22)$$

$$1.5x: \quad 3.5R_{sw}+0.5R_t \leq 0.364 \text{ Ohm} \quad (3.23)$$

$$1.33x: \quad 2R_{sw}+0.22R_t \leq 0.306 \text{ Ohm} \quad (3.24)$$

To simplify the calculation, assume the lowest value of R_t is equal to R_{sw}, so the maximum on-resistance that can maintain regulation at full load can be obtained by solving (3.22)-(3.24). For 2x mode, the on-resistance of switches $R_{sw} \leq 54$ mOhm; For 1.5x mode, $R_{sw} \leq 91$ mOhm; For 1.33x, $R_{sw} \leq 138$ mOhm.

It can be seen that the worst case happens at 2x mode because the switch current is the highest and thus requires the lowest on-resistance. However, the smaller the on-resistance is, the bigger the device size and silicon area will be. In previous calculation, it is assumed that the on-resistances of all un-regulated transistors are equal. It can be seen from Fig.3.5 that the PMOS used in 2x mode are only MP3, MP4, MP6, and MP9. It is undoubted that the on-resistance of these four PMOS needs to be maintained small for high current operation, but it may not be necessary for all the other transistors. Considering the circuit symmetry, the on-resistance of MP2, MP3, and MP4 should be equal and the on-resistance of MP7, MP8, and MP9 should be equal, so we can have: $R_{MP2}=R_{MP3}=R_{MP4}=R_{MP6}=R_{MP7}=R_{MP8}=R_{MP9}=54$

mOhm. As a result, the on-resistances of MP1 and MP5 have some sort of flexibility and can be optimized to reduce the silicon area. It can be calculated that to maintain regulation at full load in 1.5x and 1.33x mode, $R_{MP5} \leq 175$ mOhm and $R_{MP1} \leq 770$ mOhm. Increasing the size of capacitors, the size of transistors will decrease. However, the footprint of capacitors will become bigger.

3.4 Efficiency Improvement over Wide Load Range

In fact, the power loss in a charge pump circuit includes conduction loss, gate driving loss, switching loss, and leakage loss; therefore the efficiency can be expressed using (3.25):

$$\eta = \frac{V_{out} * I_{out}}{V_{in} * N * I_{out} + P_{gate} + P_{sw} + P_{leak}} \tag{3.25}$$

In heavy load condition, the gate driving loss P_{gate}, switching loss P_{sw} and leakage loss P_{leak} are far less than $V_{in}*N*I_{out}$, so the maximum efficiency it can achieve is close to $V_{out}/(N*V_{in})$. However, when the load current decreases until the gate driving loss, switching loss and leakage loss cannot be neglected, the efficiency becomes poor. Improving the light load efficiency is very important when the charge pump needs to work over a very wide load range. According to the gate driving loss equation shown in (3.26), there are several methods to reduce the gate driver loss.

$$P_{gate} \approx C_{iss} V^2_{GS} f_s \tag{3.26}$$

Pulse skipping modulation can reduce the average switching frequency, and thus reduces the gate driver loss, switching loss and leakage loss. The gate driver loss can be further reduced by reducing the capacitance associated with the transistor gates according to (3.26). Since the transistors sizes are optimized to reduce conduction loss and maintain regulation at maximum load condition, they are usually big devices with small on-resistance. The gate capacitances of those devices are very large. However, for the same input voltage, the required output impedances of charge pump R_{out} are different for high and low load current according to the DC model equation shown in (3.2). In light load condition, the R_{out} can be larger than that in heavy load condition. Therefore, small devices with less gate capacitance will be enough to maintain regulation at light load condition and it can help reduce gate driver loss. Ref.[37] proposed the concept of device segmentation in Buck converter. By segmenting each large transistor into several baby-transistors, and shut down part of those baby-transistors when the load current decreases, the gate driver loss can be reduced. The same concept can be used in charge pump as well and achieves better results because there are much more transistors in a charge pump than in a Buck converter.

In this design, a hybrid regulation is used for efficiency and ripple tradeoff. At heavy load, the charge pump is continuously running at 1MHz to reduce output ripple. At light load, switch sizes are reduced by shutting down most parts of the baby-transistors, thus reduce gate driver loss. At very light load, pulse skipping modulation (PSM) is used in addition to device segmentation. By shutting down the controller intermittently, the gate driver loss, switching

loss and leakage loss can be reduced. The shutdown frequency of the controller is designed to be around 50 kHz, which is out of the audible band.

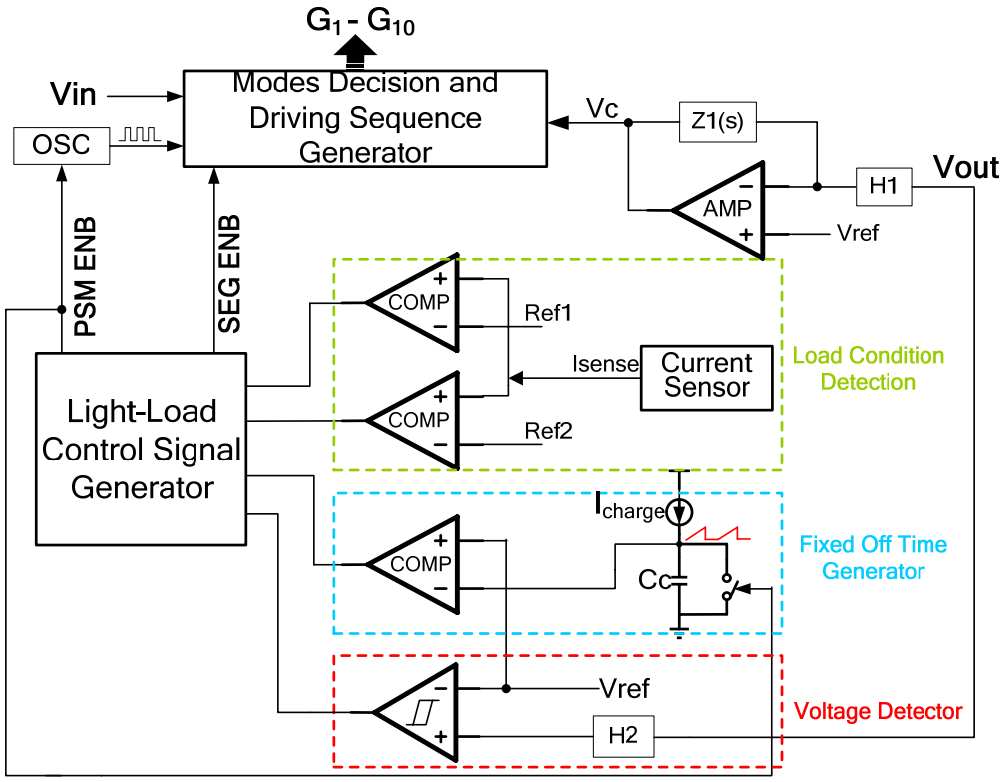

Fig.3.8 Hybrid Regulation Scheme for Improving Light Load Efficiency

Fig.3.8 shows the designed control diagram. Output voltage is regulated using a PID compensator. Compensator output Vc is also used as the gate voltage of current source MN1, so it is proportional to the current flowing through MN1 when it is on. 'Ref1' and 'Ref2' are two references for deciding the load condition. Fixed-off-time generator controls the shut down time in pulse skipping mode using the capacitor-charging circuitry. Voltage detector monitors the output voltage V_{out}. When V_{out} is less than 4.9V, the voltage detector will disable

all the light load control. Light-load control signal generator is responsible for generating the PSM enable (PSM_ENB) and segmentation enable (SEG_ENB) signals based on the circuit condition. Modes decision and driving sequence generator will output the driving signals for ten transistors according to the V_{in}, PSM_ENB, and SEG_ENB.

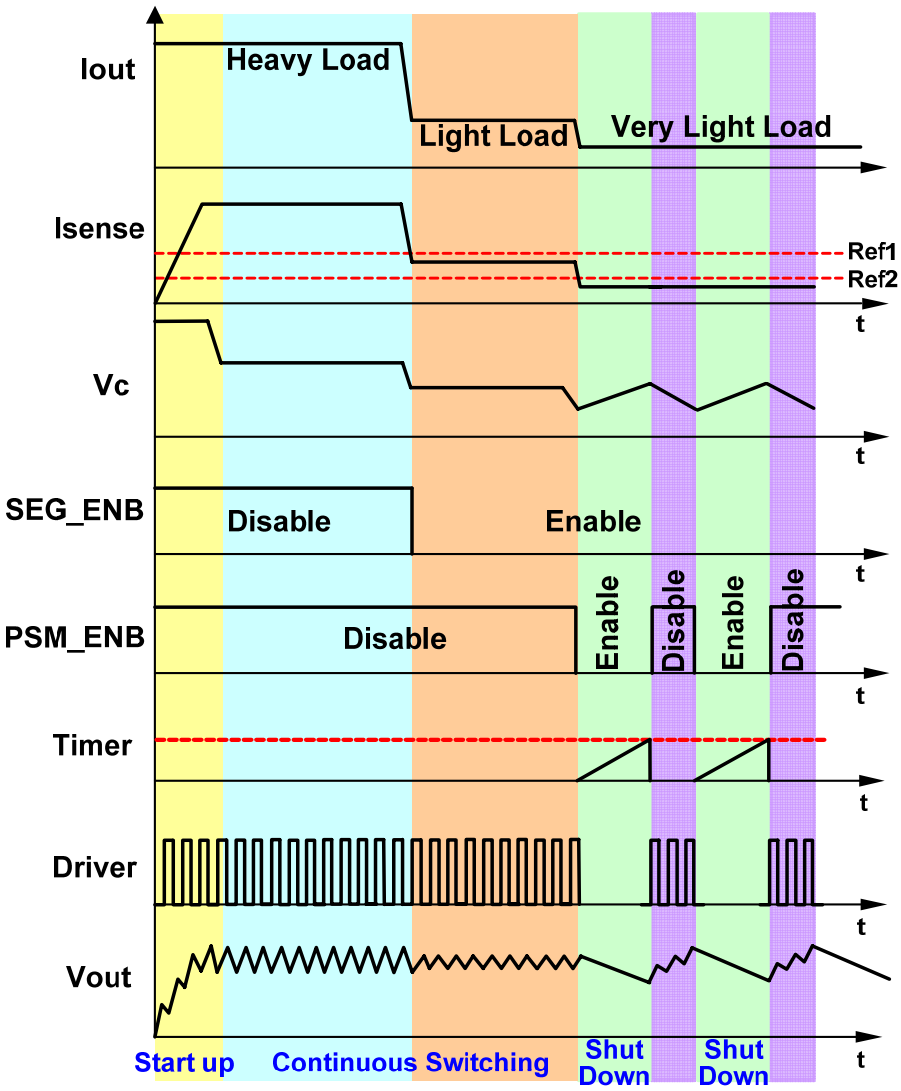

Fig.3.9 Key waveforms in hybrid regulation scheme

The primary nodes waveforms are shown in Fig.3.9. During start-up, V_{out} increases from zero and driving pulses are continuous. Vc decreases when V_{out} reaches 5V. Load condition is judged using the output signal from current sensor. At heavy load condition, I_{sense} is higher than Ref1. When I_{sense} is lower than Ref1 but higher than Ref2, charge pump operates in light load condition. Device segmentation is enabled but the driving frequency is still 1MHz. Ripple is smaller than that in heaving load. When I_{sense} drops below Ref2, charge pump enters very light load condition. The controller will be shut down for a fixed off time and then restart. Eq. (3.27) gives the equation of off time. During the off time, load current is only provided by discharging the output capacitor, and the output voltage drop can be derived using (3.28). Therefore, smaller load current results in less voltage ripple.

$$t_{off} = \frac{C_C V_{ref}}{I_{Charge}} = \text{Constant} \tag{3.27}$$

$$\Delta V\text{-} = \frac{I_{out} t_{off}}{C_{out}} \tag{3.28}$$

When the controller is shut down, it is still able to respond to a load transient quickly using the voltage detector. Since the decreasing slope of output voltage is proportional to the load current during the off time, the output voltage should drop more sharply and results in more voltage drop if a load step up happens. Without waiting for the end of the off time, the controller will wake up once the output voltage touches the threshold. The primary waveforms during load transient are shown in Fig.3.10.

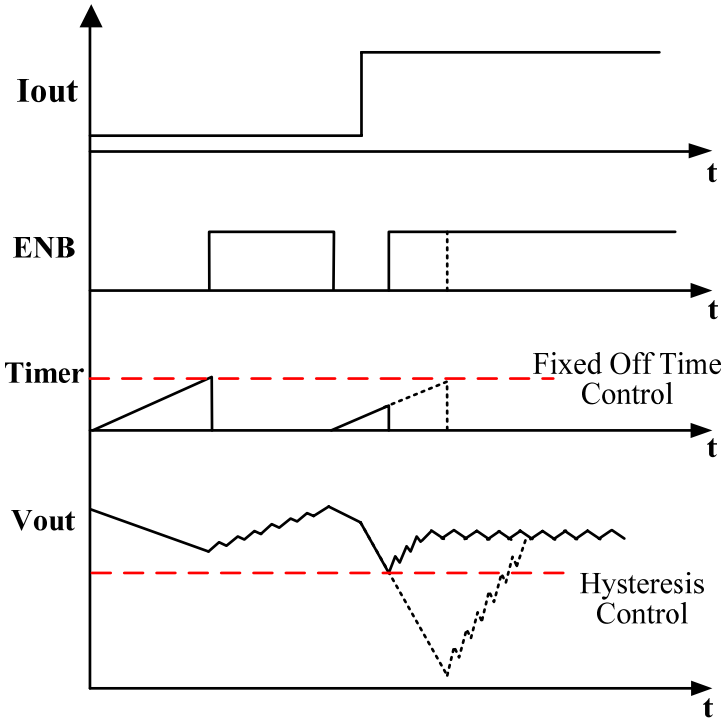

Fig.3.10 Fast Light-Heavy Load Transient Response

3.5 System Stability Analysis

In designed Multi-Modes Charge Pump, the regulated transistor MN1 mostly operates in saturation region and behaves as a controlled current source. The output voltage V_o is regulated by controlling the gate voltage of MN1, thereby controlling the charging current I_{ch}. Small signal modeling is required to obtain the transfer function from the charging current to the output voltage before performing the stability analysis. The small signal model can be derived based on State Space Average analysis [51]. The following analysis uses 1.33x mode charge pump as the example. V_1, V_2, and V_3 represent the voltages across the three flying

capacitors Cf1-Cf3. To simplify the calculation, assume the voltages across the three flying capacitors are equal since the circuit structure is symmetrical. Neglect the ESR of capacitors in the following analysis as they are much smaller than the on-resistance of switches.

[0-0.5Ts]: During the first half cycle, the regulated device behaves like a controlled current source. The charging current for three flying capacitors is the same, as shown in (3.29). The output capacitor is discharging current to the load, as shown in (3.30).

$$I_{ch} = C_f \frac{dV_1}{dt} = C_f \frac{dV_2}{dt} = C_f \frac{dV_3}{dt} \tag{3.29}$$

$$C_o \frac{dV_o}{dt} = \frac{-V_o}{R_L} \tag{3.30}$$

By rearranging the two equations, we can have (3.31) and (3.32).

$$\frac{dV_3}{dt} = 0 \cdot V_3 + 0 \cdot V_o + \frac{1}{C_f} I_{ch} + 0 \cdot V_{in} \tag{3.31}$$

$$\frac{dV_o}{dt} = 0 \cdot V_3 + \frac{-1}{R_L C_o} \cdot V_o + 0 \cdot I_{ch} + 0 \cdot V_{in} \tag{3.32}$$

[0.5Ts-Ts]: During the second half cycle, the regulated device is OFF. The three flying capacitors are in parallel and discharging energy to the output. Since the three flying capacitor paths have the same impedance, the discharging current should be the same as well.

$$C_f \frac{dV_3}{dt} = \frac{V_o - V_3 - V_{in}}{2R_{on}} \tag{3.33}$$

$$C_o \frac{dV_o}{dt} = -3\frac{V_o - V_3 - V_{in}}{2R_{on}} - \frac{V_o}{R_L} \tag{3.34}$$

By rearranging the two equations, we can have (3.35) and (3.36).

$$\frac{dV_3}{dt} = \frac{-1}{2R_{on}C_f} \cdot V_3 + \frac{1}{2R_{on}C_f} \cdot V_o + 0 \cdot I_{ch} + \frac{-1}{2R_{on}C_f} \cdot V_{in} \tag{3.35}$$

$$\frac{dV_o}{dt} = \frac{3}{2R_{on}C_o} \cdot V_3 + (-\frac{3}{2R_{on}C_o} - \frac{1}{R_L C_o}) \cdot V_o + 0 \cdot I_{ch} + \frac{3}{2R_{on}C_o} \cdot V_{in} \tag{3.36}$$

The system state equations in one cycle can be obtained by averaging the equations during [0-0.5Ts] and [0.5Ts-Ts], as shown in (3.37) and (3.38).

$$\frac{dV_3}{dt} = \frac{-1}{4R_{on}C_f} \cdot V_3 + \frac{1}{4R_{on}C_f} \cdot V_o + \frac{1}{2C_f} \cdot I_{ch} + \frac{-1}{4R_{on}C_f} \cdot V_{in} \tag{3.37}$$

$$\frac{dV_o}{dt} = \frac{3}{4R_{on}C_o} \cdot V_3 + (-\frac{3}{4R_{on}C_o} - \frac{1}{R_L C_o}) \cdot V_o + 0 \cdot I_{ch} + \frac{3}{4R_{on}C_o} \cdot V_{in} \tag{3.38}$$

Then by doing Laplace transform to (3.37) and (3.38), the equation of v_o in s-domain can be solved, as shown in (3.39).

$$v_o = \frac{3R_L i_{ch} + 6R_L C_f s v_{in}}{8R_{on}R_L C_f C_o s^2 + (6R_L C_f + 2R_L C_o + 8R_{on}C_f)s + 2} \tag{3.39}$$

Finally, the transfer function from charging current i_{ch} to output voltage v_o can be obtained, which is shown in (3.40).

$$G_{vi\_1p33x} = \frac{v_o}{i_{ch}} = \frac{1.5R_L}{4R_{on}R_L C_f C_o s^2 + (3R_L C_f + R_L C_o + 4R_{on}C_f)s + 1} \tag{3.40}$$

Using the same method, the transfer functions from charging current i_{ch} to output voltage v_o for 1.5x and 2x mode charge pump can be derived as well, which are shown in (3.41) and (3.42) respectively.

$$G_{vi\_1p5x} = \frac{v_o}{i_{ch}} = \frac{R_L}{4R_{on}R_LC_fC_os^2 + (2R_LC_f + R_LC_o + 4R_{on}C_f)s + 1} \tag{3.41}$$

$$G_{vi\_2x} = \frac{v_o}{i_{ch}} = \frac{0.5R_L}{4R_{on}R_LC_fC_os^2 + (R_LC_f + R_LC_o + 4R_{on}C_f)s + 1} \tag{3.42}$$

Table 3.4 System Poles of Charge Pump at Different Mode

Mode	**Pole1**	**Pole2**
1.33x	$f_{p1} = \frac{3C_f + C_o}{4R_{on}C_oC_f}$	$f_{p2} = \frac{1}{R_L(3C_f + C_o)}$
1.5x	$f_{p1} = \frac{2C_f + C_o}{4R_{on}C_oC_f}$	$f_{p2} = \frac{1}{R_L(2C_f + C_o)}$
2x	$f_{p1} = \frac{C_f + C_o}{4R_{on}C_oC_f}$	$f_{p2} = \frac{1}{R_L(C_f + C_o)}$

It can be seen that designed charge pump system is a second-order system and has two poles. Table 3.4 shows the equations of two poles for each mode. Pole1 is formed by the on-resistance of switches R_{on}, C_f and C_o; Pole2 is formed by the output RC network consisting of R_L, C_f and C_o. Since the load resistance is much higher than the on-resistance of switches, Pole 2 will be the dominant pole of system. Based on the small signal analysis above, the equivalent small signal AC model at each mode can also be derived, as shown in Fig.3.11. It can be seen that the difference between each mode is the number of flying-capacitor branches that are in parallel. When switching from 2x mode to 1.5x mode and to 1.33x mode, more flying capacitors are involved and thus results in a significant change in its small signal model. As a result, it will shift the locations of system poles when

the conversion mode changes. When the Multi-Modes Charge Pump switches from high conversion ratio to low conversion ratio, the dominant pole moves to high frequency while the non-dominant pole moves to low frequency. Therefore, the phase margin can get worse at lower conversion ratio.

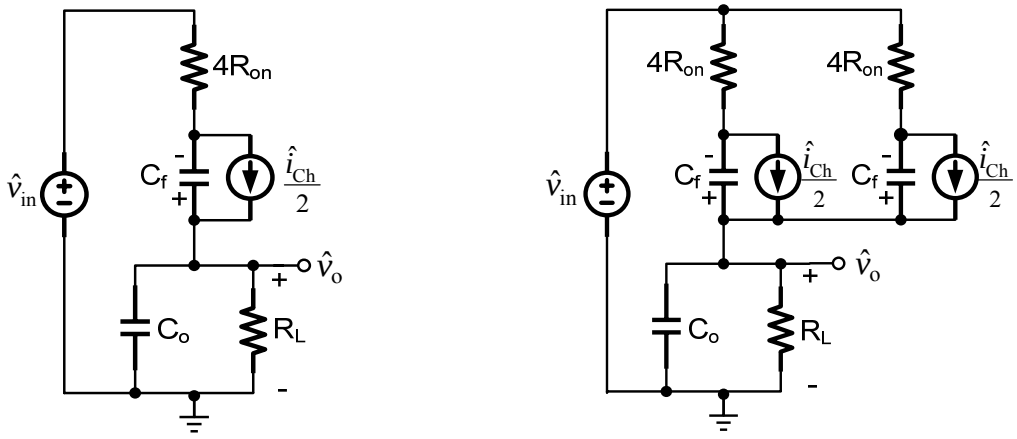

(a) 2x Mode (b) 1.5x Mode

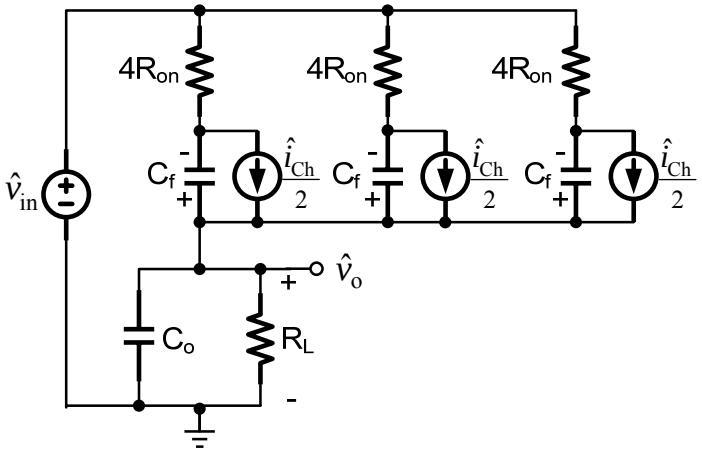

(c) 1.33x Mode

Fig.3.11 Equivalent small signal AC circuit model of Multi-Modes Charge Pump

To verify the accuracy of derived math model, a circuit with the same parameters (C_f=4.7uF, C_o=22uF, R_L=50Ohm, R_{on}=75mOhm, fs=1MHz) is built and simulated in SIMPLIS. Both of the simulated and calculated bode plots are plotted in Fig.3.12. It can be seen that they match each other very well up to half of the switching frequency.

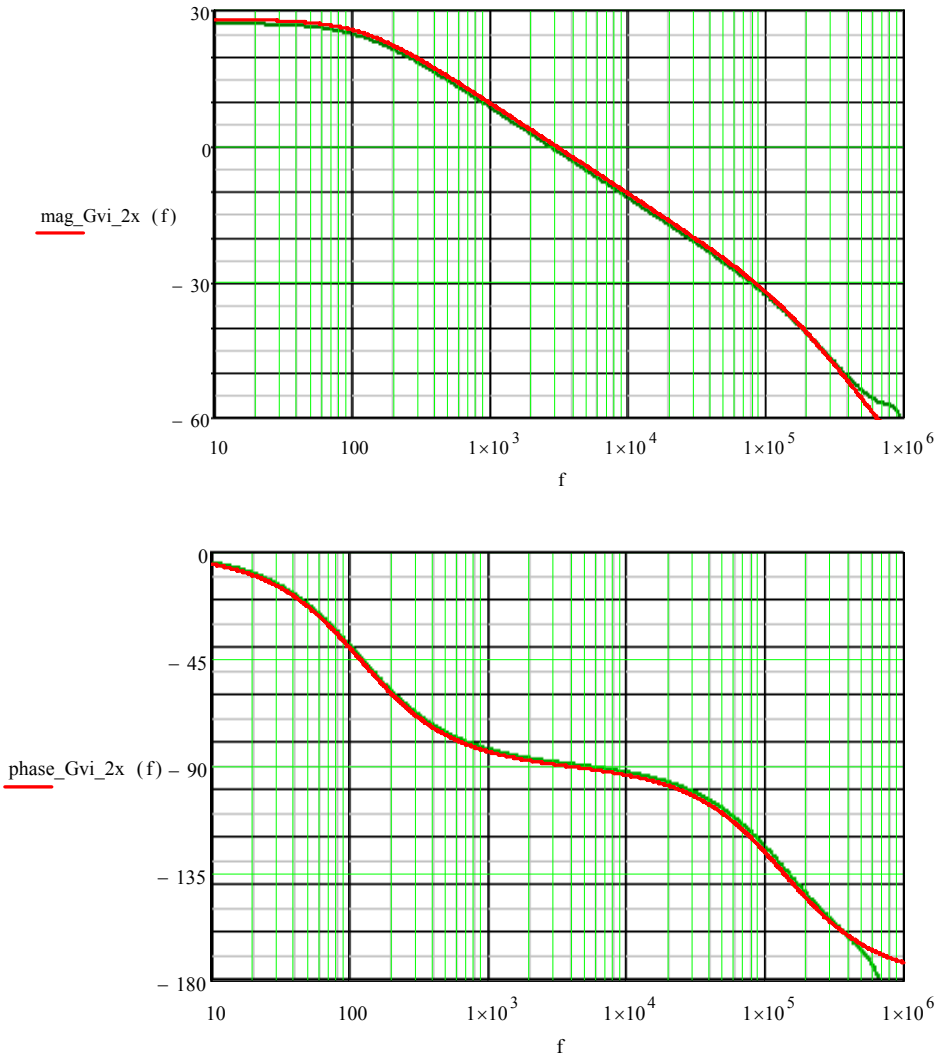

Fig.3.12 Comparison between Calculated and Simulated G_{vi} at 2x mode.

(Red: Calculation; Green: Simulation)

Designed regulated Multi-Modes Charge Pump is a complex feedback system. In addition to adaptively switching conversion modes at different input voltage, it also uses device segmentation and pulse skipping modulation control at different load condition. As a result, the transfer function G_{vi} may change dramatically at different circuit conditions. To make the system stable over all conditions, it is necessary to analyze the G_{vi} at all cases and design the compensator based on the worst case.

1) G_{vi} at Different Input Voltage (Different Mode)

It can be seen from Table 3.4 that the transfer function G_{vi} at each mode is not the function of input voltage v_{in}, so it has a consistent bode plot at different input voltage as long as it stays within the same mode. Fig.3.13 shows the bode plots of G_{vi} in 2x, 1.5x and 1.33x modes when I_{out}=66mA. It can be seen that the magnitude plots vary a lot with modes while the phase plots vary a little. The worst case happens at 2x mode, which has the lowest cross-over frequency and low-frequency gain.

2) G_{vi} at Different Load Current

The equations of G_{vi} show that they also vary with the load current I_{out}. Fig.3.14 gives the bode plots of G_{vi} in 2x mode charge pump at different load current. It can be seen that the low-frequency portions of G_{vi} vary a lot with I_{out} while the high-frequency portions are very consistent. The cross-over frequencies are the same for all the load conditions. The phase margins are different but all are greater than 90 degrees. The low-frequency gain decreases when load current increases.

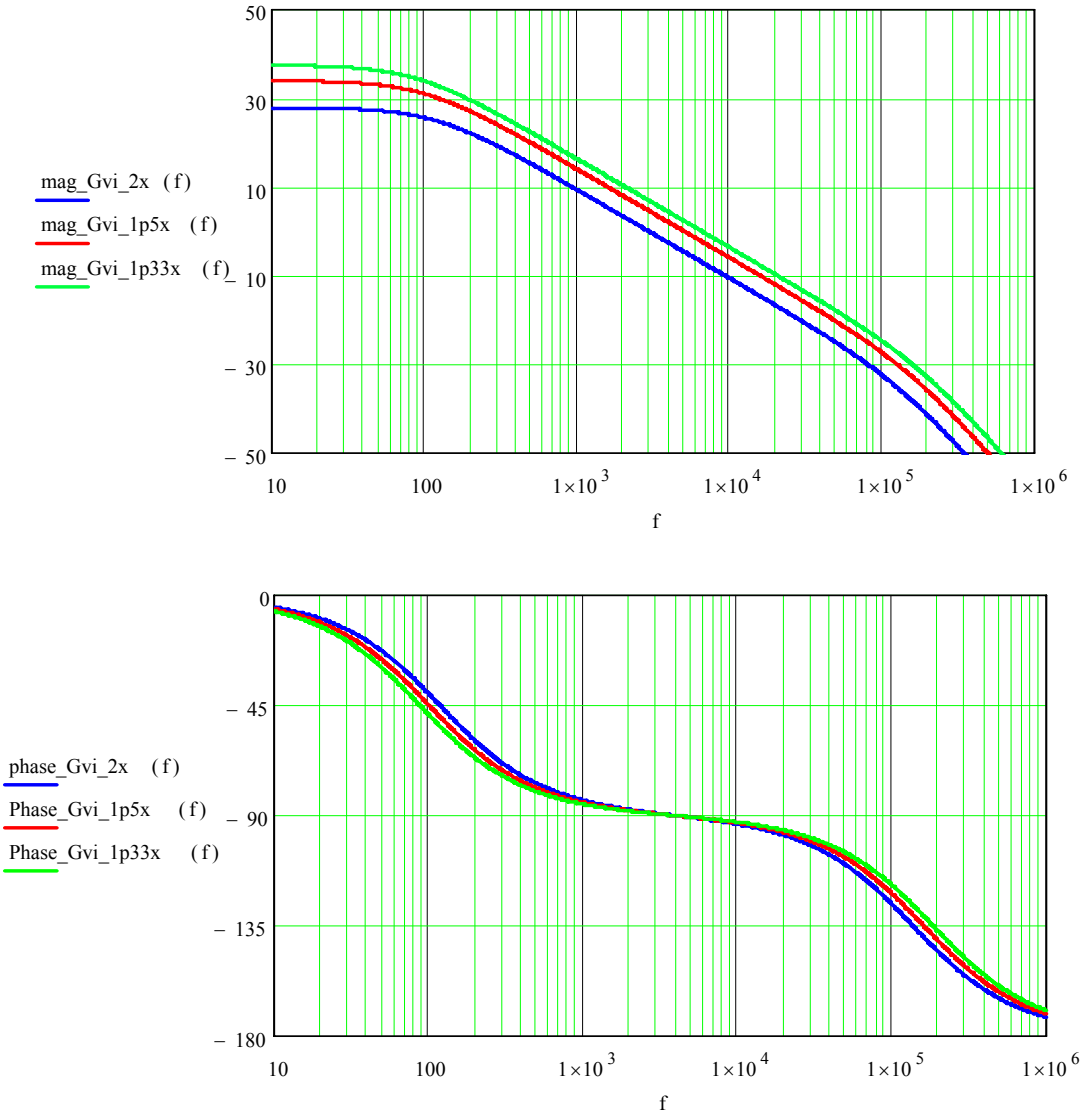

Fig.3.13 G_{vi} at Different Input Voltage (Mode)

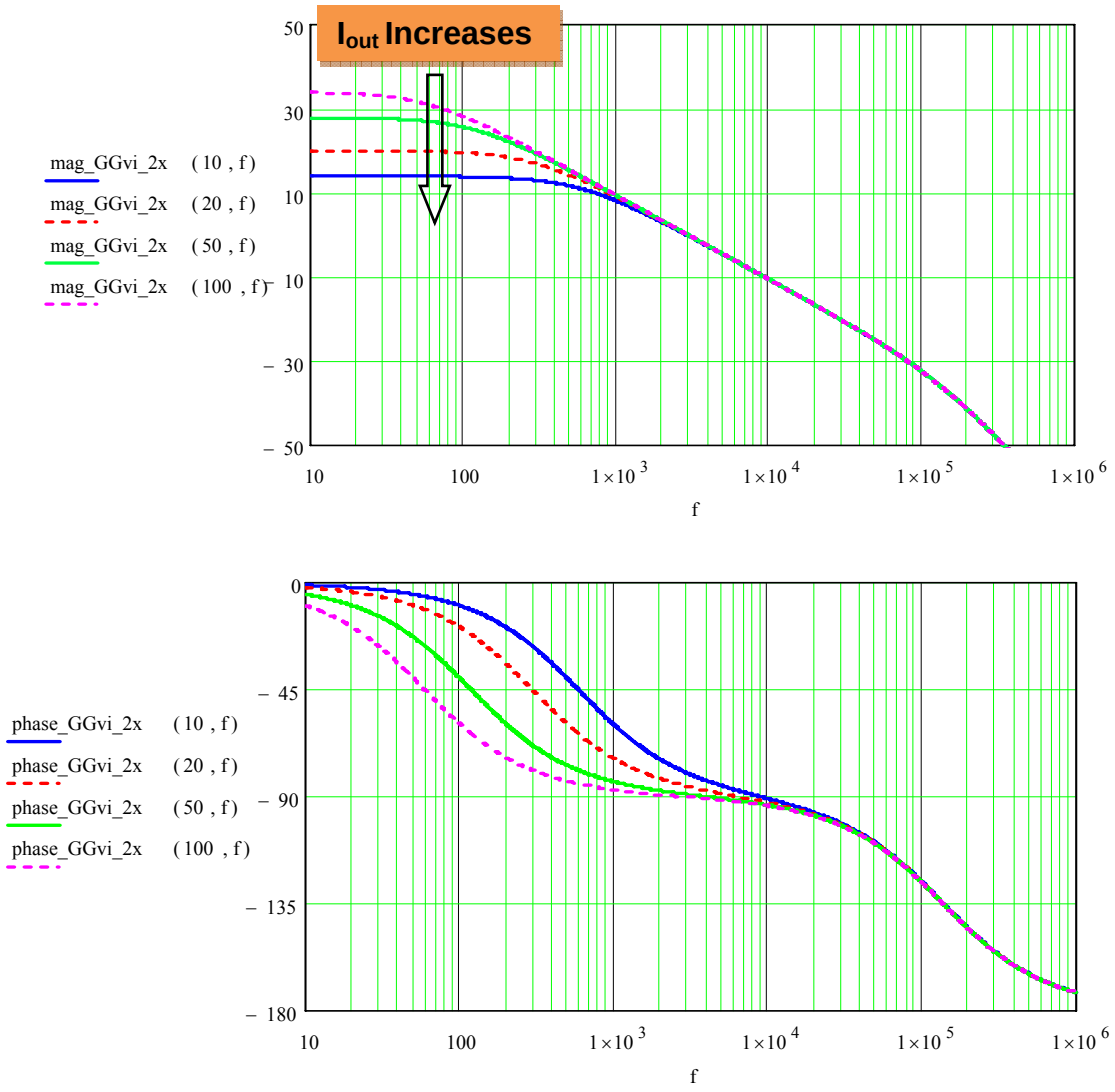

Fig.3.14 Bode Plot of G_{vi} in 2x Mode at Different Load Current

3) G_{vi} w and w/o Device Segmentaion Control

When device segmentation control is enabled, parts of baby-transistors are shut down at light load and the on-resistance greatly increases. Although the circuit topology remains, the change of devices' on-resistance finally alters G_{vi}. The bode plots of G_{vi} in 2x mode before

and after device segmentation are shown in Fig.3.15. It can be seen that the low-frequency portions of G_{vi} are consistent but the high-frequency portions vary a lot, especially the phase plots. After device segmentation, Pole1 moves to lower frequency and results in a large phase drop. Therefore, the compensator should be carefully designed to be able to compensate the phase drop after device segmentation.

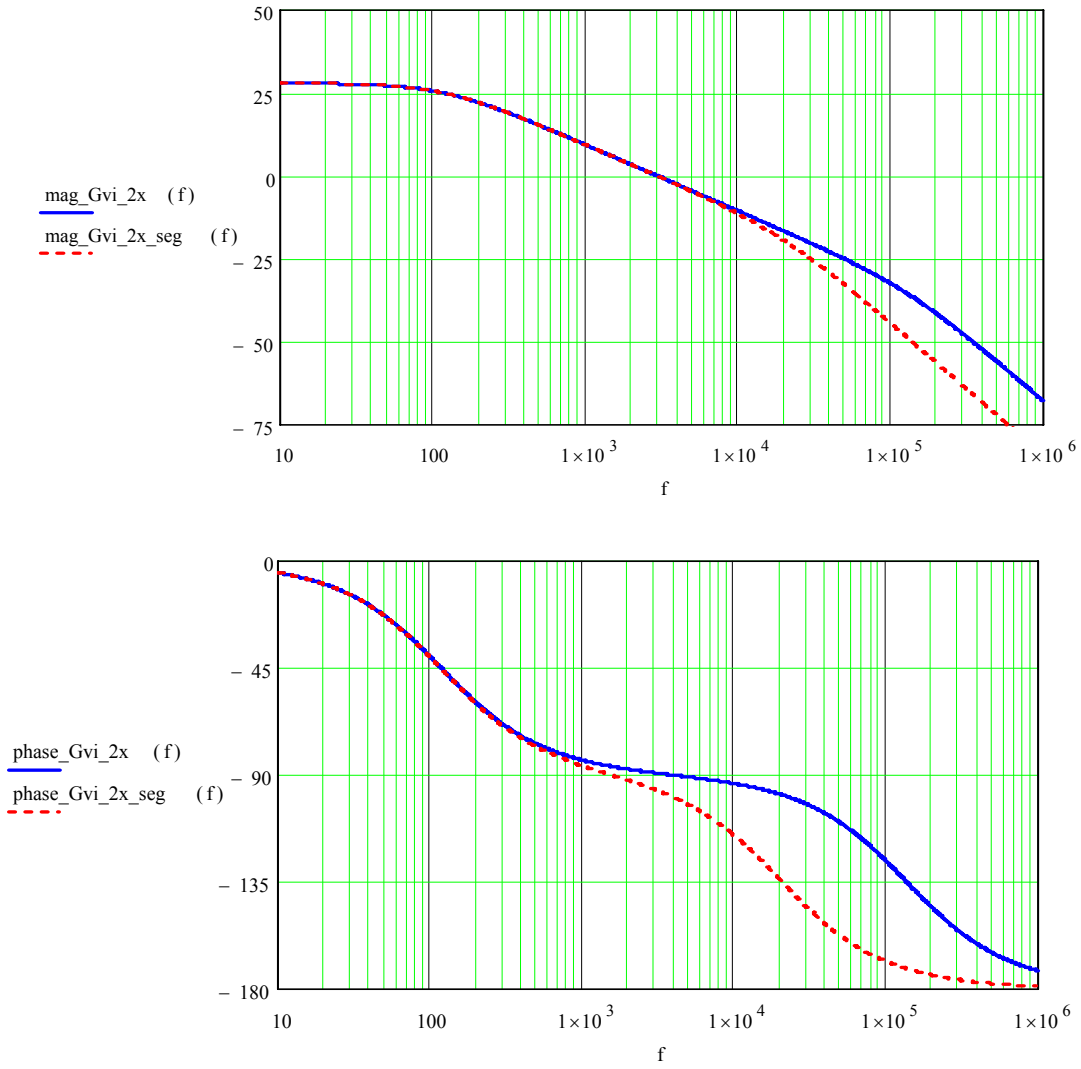

Fig.3.15 Bode Plot of G_{vi} in 2x Mode before and after Device Segmentation

4) G_{vi} w and w/o Pulse Skipping

At very light load condition, pulse skipping modulation is used in addition to device segmentation. The pulse skipping modulation will force the controller turn ON and OFF intermittently. When controller is ON, PID compensator is working normally; when controller is OFF, the compensator will not affect the system. The ON/OFF frequency is much lower than the switching frequency. To check the system stability, the circuit models in Fig.3.11 are still valid for deriving the new G_{vi}. Since the charge pump circuit is originally a linear system, the derived small signal AC equivalent circuit in Fig.3.11 can also be considered as a large signal circuit equivalent model. A switch S1 can be manually added to emulate the ON/OFF of the control system. Using 2x mode charge pump as the example, the modified circuit is shown in Fig.3.16. T_{PSM} is the period of pulse skipping modulation and D is the duty cycle of switch S1.

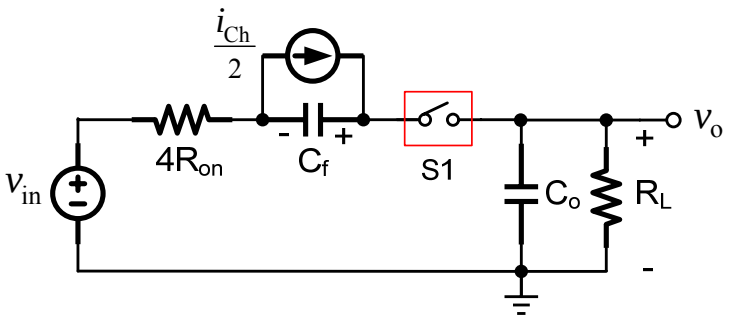

Fig.3.16 Modified Equivalent Circuit Model of 2x mode Charge Pump in PSM

[0-D*T_{PSM}]: S1 is ON, and the control system is working normally.

$$V_{in} - \left(\frac{I_{ch}}{2} - C_f \frac{dV_3}{dt} \right) 4R_{on} + V_3 = V_o \tag{3.43}$$

$$\left(\frac{I_{ch}}{2} - C_f \frac{dV_3}{dt} \right) - C_o \frac{dV_o}{dt} = \frac{V_o}{R_L} \tag{3.44}$$

By rearranging the two equations above, we can get (3.45) and (3.46).

$$\frac{dV_3}{dt} = -\frac{1}{4R_{on}C_f} V_3 + \frac{1}{4R_{on}C_f} V_o + \frac{1}{2C_f} I_{ch} - \frac{1}{4R_{on}C_f} V_{in} \tag{3.45}$$

$$\frac{dV_o}{dt} = \frac{1}{4R_{on}C_o} V_3 - (\frac{1}{R_L C_o} + \frac{1}{4R_{on}C_o}) V_o + \frac{1}{4R_{on}C_o} V_{in} \tag{3.46}$$

[$D*T_{PSM}$-T_{PSM}]: S1 is OFF, and the control system is shut down.

$$C_f \frac{dV_3}{dt} = 0 \tag{3.47}$$

$$\frac{dV_o}{dt} = -\frac{V_o}{R_L C_o} \tag{3.48}$$

According to the design, the duty cycle of S1 at very light load condition is almost fixed to 0.3446. By averaging the state equations in one cycle we can get (3.49) and (3.50).

$$\frac{dV_3}{dt} = -\frac{0.08615}{R_{on}C_f} V_3 + \frac{0.08615}{R_{on}C_f} V_o + \frac{0.1723}{C_f} I_{ch} - \frac{0.08615}{C_f R_{on}} V_{in} \tag{3.49}$$

$$\frac{dV_o}{dt} = \frac{0.08615}{R_{on}C_o} V_3 + (-\frac{0.08615}{R_{on}C_o} - \frac{1}{R_{on}C_o}) V_o + \frac{0.08615}{R_{on}C_o} V_{in} \tag{3.50}$$

Using Laplace transform, the transfer function G_{vi} at pulse skipping modulation can be derived, which is shown in (3.51).

$$G_{vi} = \frac{0.29687R_L}{20R_{on}R_LC_fC_os^2 + (1.723R_LC_f + 1.723R_LC_o + 20R_{on}C_f)s + 1.723} \tag{3.51}$$

Compared with the G_{vi} without using pulse skipping modulation, the equation is similar but the gain and poles are changed. To verify the derived math model, the same circuit is simulated in SIMPLIS with PSM enabled. Both of the simulated and calculated Bode plots are plotted in Fig3.17. It can be seen that they almost match each other.

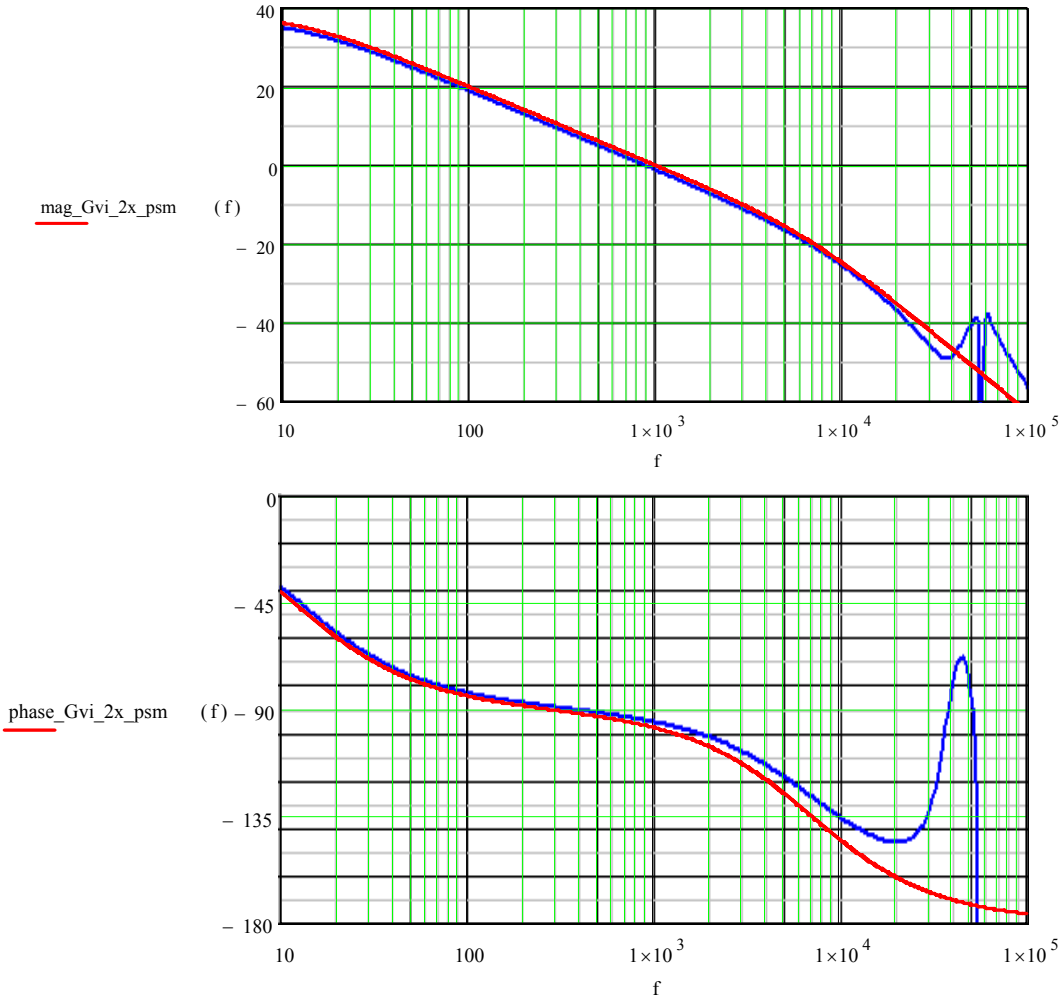

Fig.3.17 Comparison between Calculated G_{vi} (Red) and Simulated G_{vi} (Blue)

Fig.3.18 shows the bode plots of G_{vi} in 2x Mode with and without pulse skipping modulation. It can be seen that the phase margin of system with PSM enabled remains but both of the bandwidth and low-frequency gain decrease.

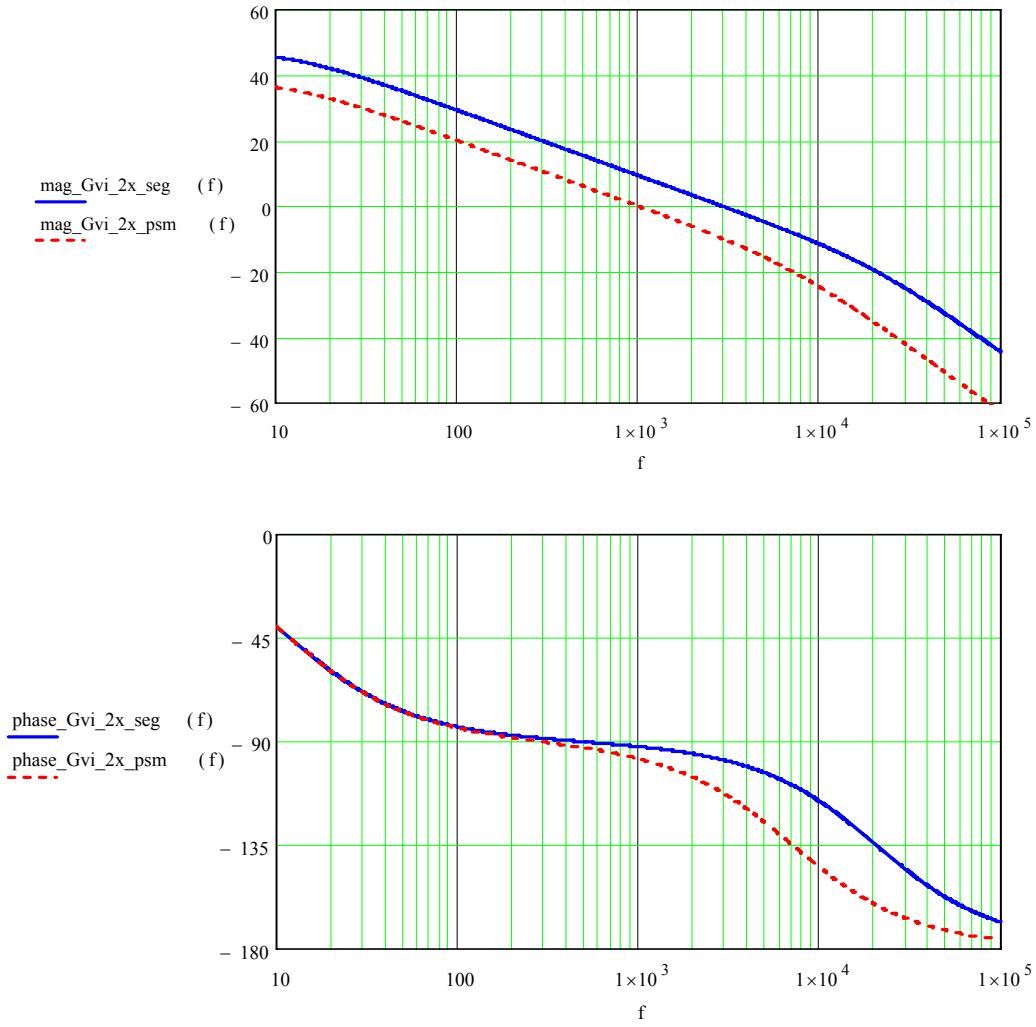

Fig.3.18 Bode plots of G_{vi} in 2x Mode with (Red) and without (Blue) pulse skipping modulation

4) Compensator Selection

From the above analysis, it can be seen that the transfer function G_{vi} changes with modes, load current, and control schemes. The worst case happens at 2x Mode, and the upper limit of very light load condition with both of device Segmentation and PSM enabled. Since the phase drop can be around 45 degree after using device segmentation control, a type III PID compensator will be good for improving phase margin and ensure system stability over wide input and load range.

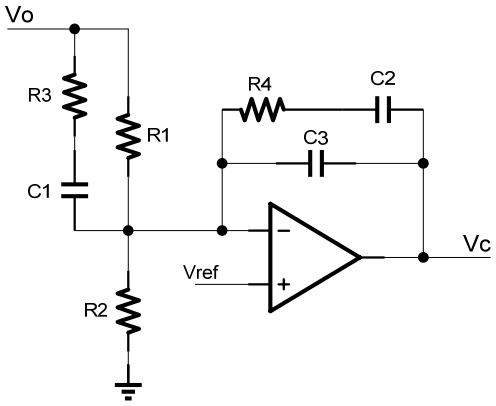

Fig.3.19 Type III PID Compensator

3.6 Key Blocks Design

The Block Diagram of designed the regulated Multi-Modes Charge Pump is shown in Fig.3.20. It includes charge pump power stage, driver, control logic, protection, and etc. The

controller and the power stage will be integrated on the same silicon chip while the three flying capacitors will be packaged together within the chip. The most important function blocks are: Mode Change Control Logic, Universal Current Sensor, Device Segmentation and PSM Selector, and Soft Start Block. The operating principles of these blocks will be demonstrated as follows.

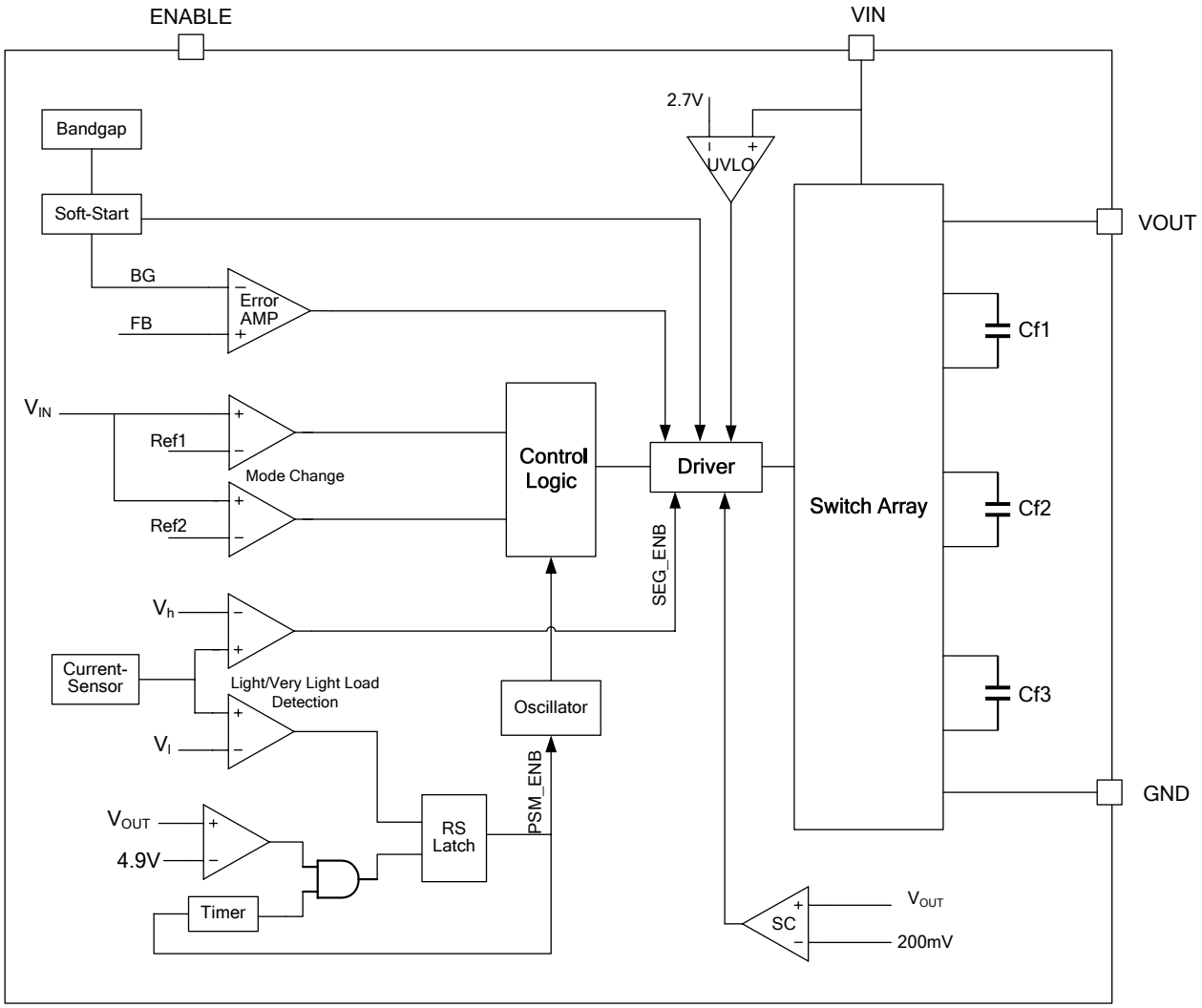

Fig.3.20 Block Diagram

3.6.1. Mode Change Control Logic

When input voltage V_{in} varies, the mode change block will choose the best mode the charge pump should operate at and generate corresponding gate signals. Fig.3.21 shows the Mode Change Control logic. It senses the input voltage and compares with given reference voltages. The truth table of Mode selector is shown in Table 3.5. Once the output mode has been decided, the gate signal logic is generated respectively. Non-overlapping signals CLK and CLK_Bar are used to insert certain deadtime between the Charging phase and Discharge phase.

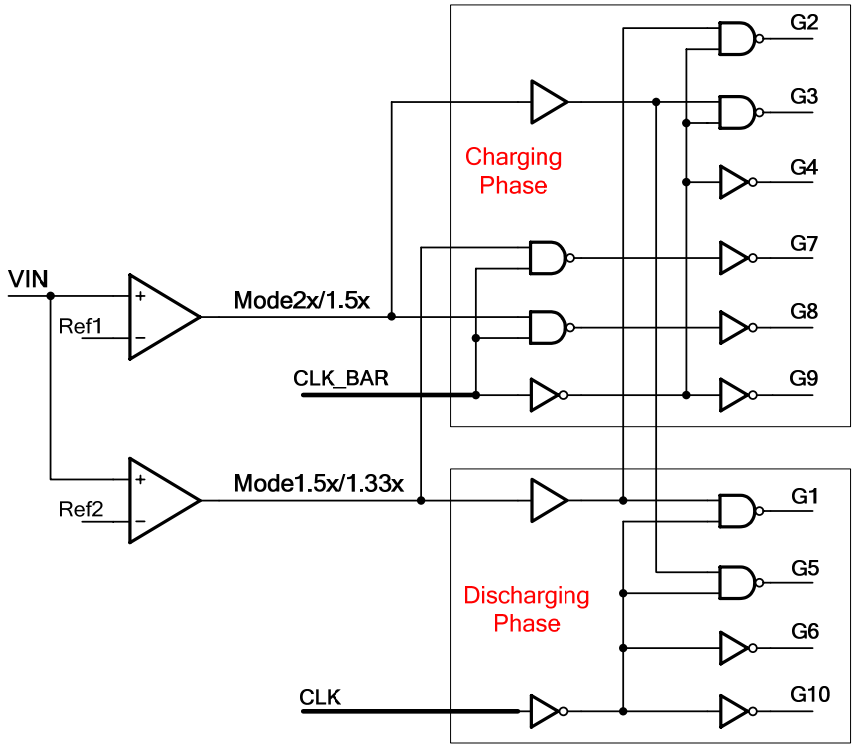

Fig.3.21 Mode Change Control Logic

Table 3.5 Truth Table of Mode Decision

Mode2x/1.5x	Mode1.5x/1.33x	Output Mode
0	------	2x
1	0	1.5x
------	1	1.33x

3.6.2. Universal Current Sensor

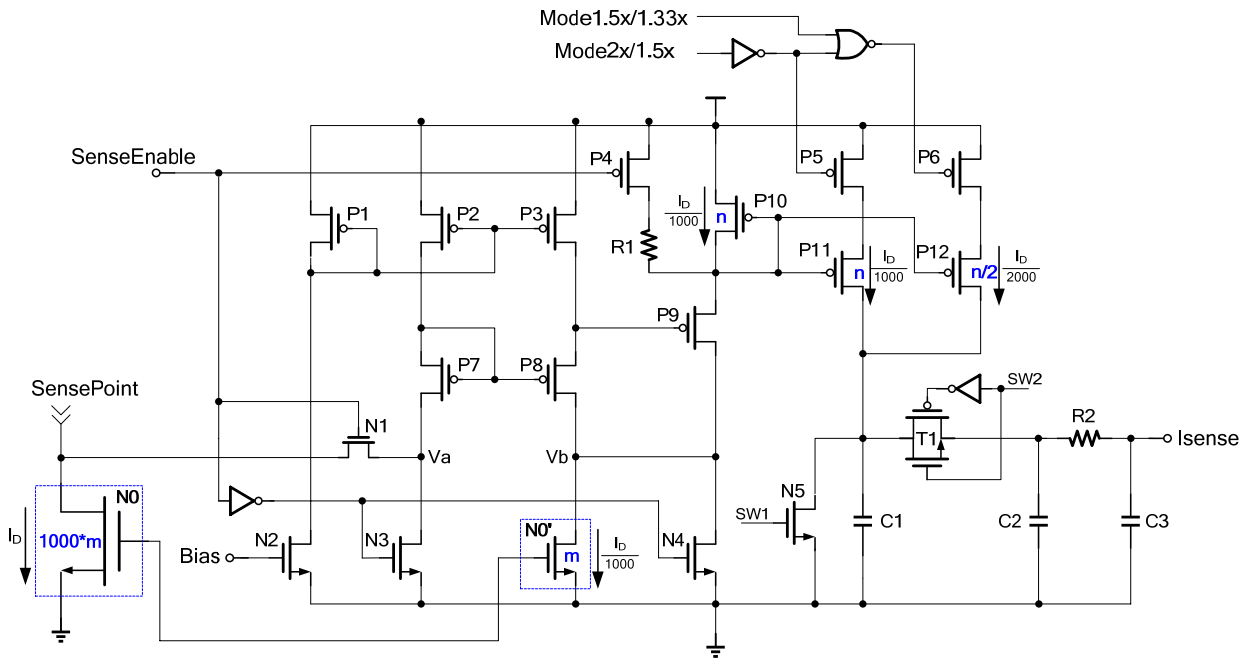

Fig.3.22 Universal Current Sensor

The universal current sensor is designed using Sense-FET technique. N0 and N0' is a pair of NMOS with the same gate voltage. The size of N0' is 1000 times smaller than N0.

[0-0.5Ts]: SenseEnable is high, N1 is ON and N3, N4 are OFF. The voltage of Va is equal

to SensePoint. Transistor P2, P3, P7 and P8 form a current bias and mirror and force the voltage Vb equal to Va. Therefore, the current flowing through N4 is 1/1000 of the current through N0. The current of N4 is then mirrored to P9-P10. The sensed current will be mirrored again to P11, P12 and charge the capacitor C1. When P5 is ON, the current in P10 is 1:1 mirrored to P11; When P6 is ON, the current in P10 is 2:1 mirrored to P12; When P5 and P6 are ON, the current in P10 is mirrored to P11 and P12. P5 and P6 are controlled by the mode select signal.

[0.5Ts-Ts]: SenseEnable is low, N0 and N0' are OFF. N3 and N4 are ON to provide paths for bias current to flow. P10 is OFF, so the sensed current is zero. The peak voltage of C1 is sampled and held at C2 when transmission gate T1 is ON. At the end of the half cycle, T1 is OFF and N5 is ON to discharge C1 to zero.

The relationship between the voltage of C2 (I_{sense}) and load current (I_{out}) can be found using the following analysis. During 0-Ts, the average current in one cycle through one flying capacitor is zero, so we can have (3.52),

$$\int_0^{T_s} i_{Cf} = \int_0^{0.5T_s} i_{Ch}dt - \int_{0.5T_s}^{T_s} i_{Dis}dt = 0 \tag{3.52}$$

Therefore, the average current during 0-0.5Ts can be obtained using (3.53).

$$\frac{1}{0.5T_s}\int_0^{0.5T_s} i_{Ch}dt = \begin{cases} 2I_{out} & \text{for 2x Mode} \\ 2I_{out}/2 & \text{for 1.5x Mode} \\ 2I_{out}/3 & \text{for 1.33x Mode} \end{cases} \tag{3.53}$$

It can be seen from (3.53), the ratio of average value of current i_{ch} to output current I_{out} is different at each mode. However, by using P5 and P6 to turn ON/OFF the current source P11 and P12, the variation of ratios can be compensated, which is shown as (3.54). Finally, the

ratio of sensed current I_{sense} to I_{out} is the same for all three modes.

$$I_{sense} = \begin{cases} \dfrac{\int_0^{0.5T_s} i_{Ch}\,dt}{C_1} \times \dfrac{1}{2} = \dfrac{T_s}{2C_1} I_{out} & \text{for 2x Mode} \\ \dfrac{\int_0^{0.5T_s} i_{Ch}\,dt}{C_1} \times 1 = \dfrac{T_s}{2C_1} I_{out} & \text{for 1.5x Mode} \\ \dfrac{\int_0^{0.5T_s} i_{Ch}\,dt}{C_1} \times \dfrac{3}{2} = \dfrac{T_s}{2C_1} I_{out} & \text{for 1.33x Mode} \end{cases} \tag{3.54}$$

3.6.3. Device Segmentation and PSM Selector

The sensed current I_{sense} will be compared with references to determine the load condition and control scheme.

When I_{sense} is lower than V_L for 5 continuous cycles and PG is high, PSM_ENB is low. The charge pump is in very light load condition. SEG_ENB keeps low so device segmentation is enabled. All switches turn OFF, so the output current is provided by the output capacitor only. A timer is started to produce a constant OFF time (10 cycles) for very light load condition. When time is up, or PG is low, the charge pump will be restarted.

When I_{sense} is lower than V_{H1} but higher than V_L, SEG_ENB is low but PSM_ENB is high. Pulse Skipping Modulation is disabled and Device segmentation is still enabled. The charge pump is in light load condition.

When I_{sense} is higher than V_{H2}, SEG_ENB is high and device segmentation is disabled. The

charge pump is in heavy load condition.

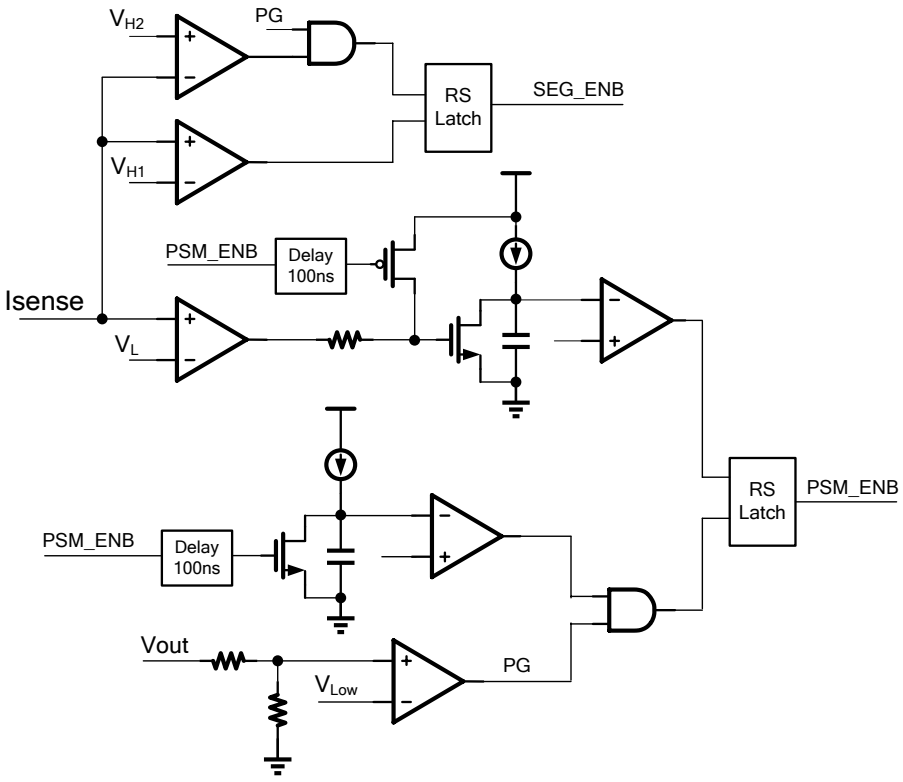

Fig.3.23 Device Segmentation and PSM Selector

3.6.4. Soft Start

At the beginning, the voltage across the output capacitor is zero. When charge pump begins to switch, a huge current will be pulled from the input source to get the output capacitor being fast charged. A soft start function is designed to reduce the inrush current during start-up. PMOS G1 and G7 will be turned ON only, and the turn-on speed of G1 is controlled by slowly decreasing its gate voltage. The input source is directly charging the

output capacitor though G1 and G7. If the decreasing speed of gate voltage G1 is slow enough, the inrush current can be limited. Once G1 is fully turned on, the output capacitor will be charged to the input voltage. Then the charge pump begins to switch normally. The FB of error amplifier will be firstly pulled up 100-200mV higher than REF, and gradually decreases until FB and REF are equal. The saturation of the compensator is avoided, so the settling time and overshoot of output voltage is reduced. During this period, the output voltage will continuously to increase until it reaches 5V.

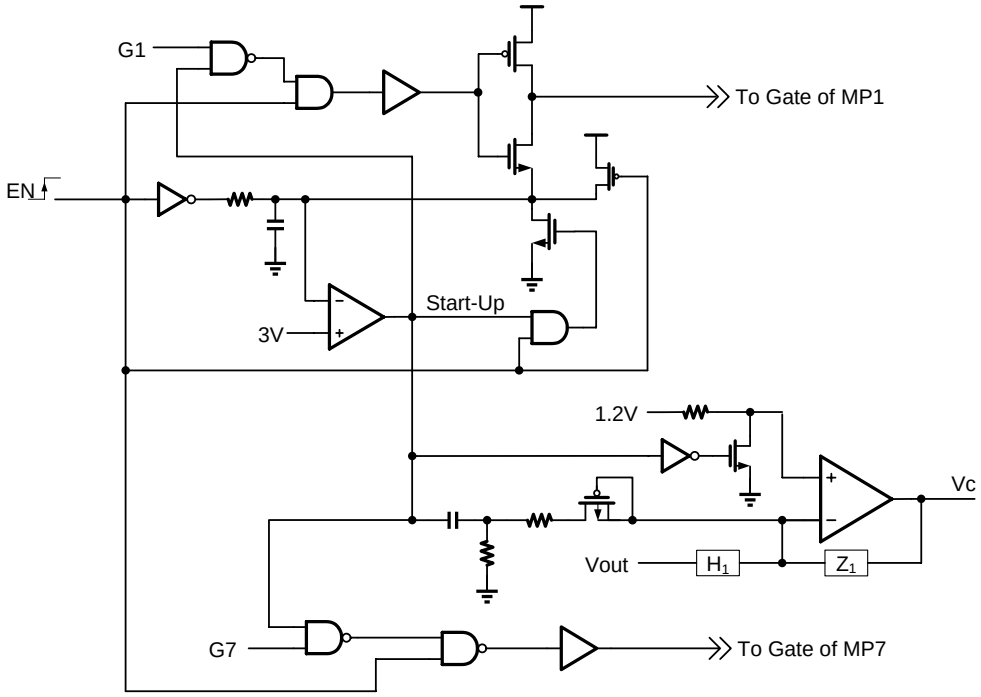

Fig.3.24 Soft Start Control

3.7 Simulation and Experiment Verifications

The designed regulated Multi-Modes Charge Pump with improved light load efficiency is implemented using IBM7RF 5V process and simulated in Cadence Spectre. Three flying capacitors Cf1-Cf3 are 2.2μF and the output capacitor C_{out} is 4.7μF. Each capacitor has a 10mOhm ESR resistance. The whole system will be fit in a 4*4mm^2 package.

Fig.3.25. shows the slow transition from very light to light to heavy load condition when V_{in} is 3.7V. It can be seen that only device segmentation is used for current between 70mA and 205mA; Both of PSM and segmentation are used for current below 70mA. The output voltage is regulated at 5V over all load conditions. Fig.3.26 shows the frequency and output ripple change with the load current at V_{in}=3.7V. The frequency is 1MHz when load current is above 70mA, but decreases to around 70 kHz for lower current. The maximum output voltage ripple 78mV happens at the upper limit of very light load condition. However, the ripple decreases with load current no matter if it is in heavy, light, or very light load condition. The ripple also decreases with more output capacitances.

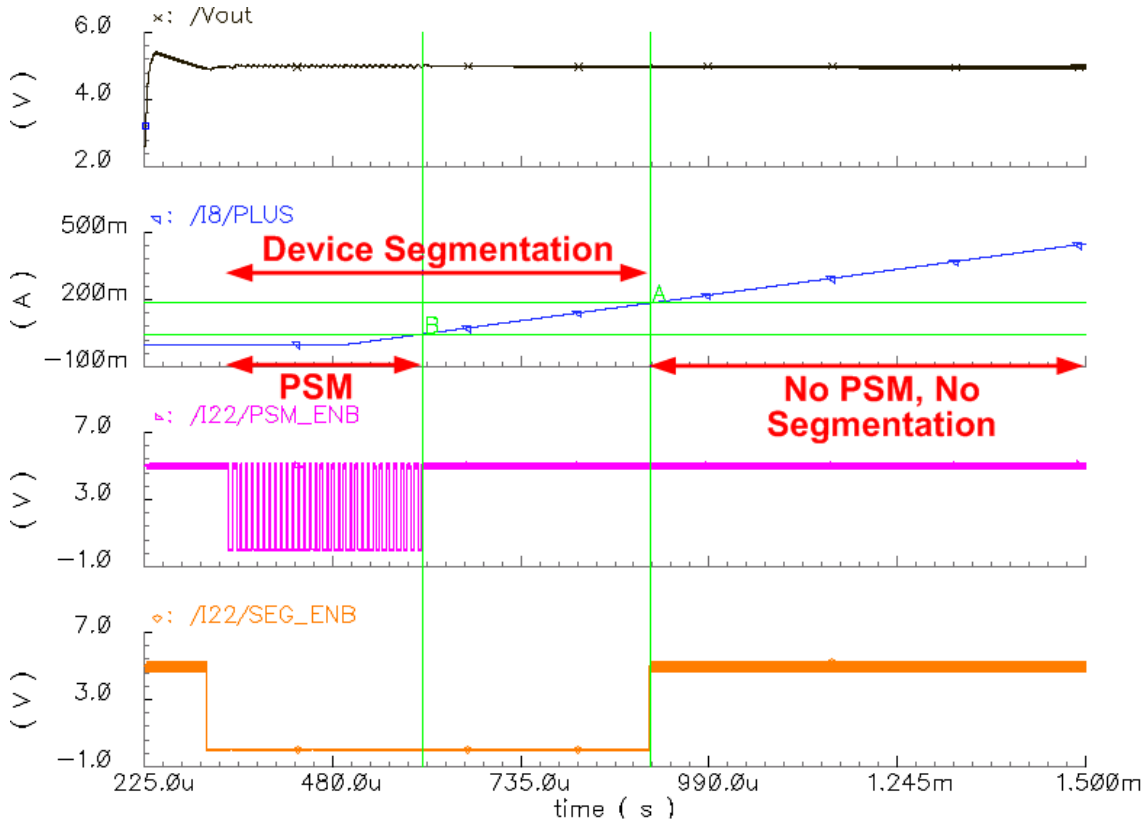

Fig.3.25 Load Transition from 50 mA to 500mA@ V_{in}=3.7V

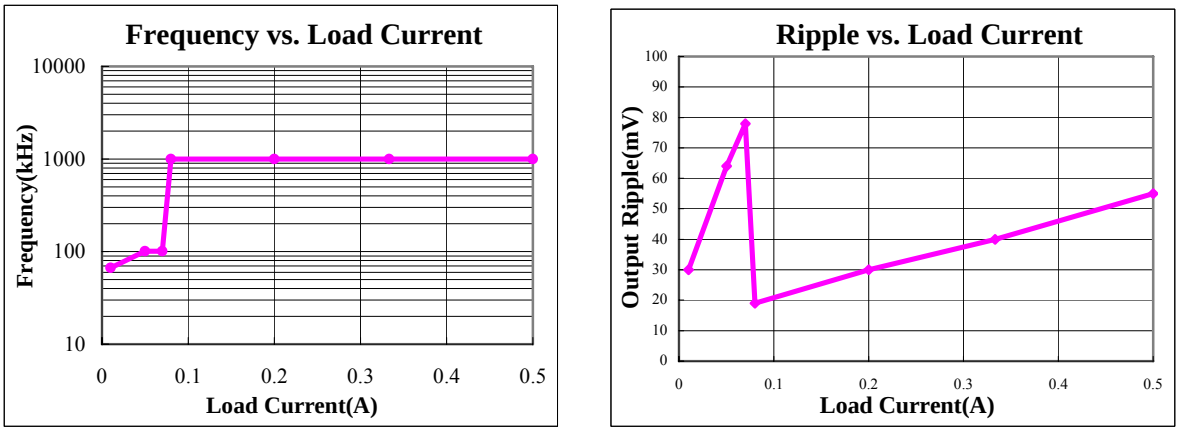

Fig.3.26 (Left) Frequency vs. Load Current; (Right) Ripple vs. Load Current

Fig.3.27 shows the simulated charge pump efficiency at 10mA load current using different control schemes. Comparing with a multi-modes charge pump without using any light load efficiency control scheme, the charge pump with both of PSM and device segmentation have the highest efficiency. It can improve the efficiency by 10-30% over the entire input voltage. Fig.3.28 shows the simulated charge pump efficiency at different load conditions. It can be seen that the average efficiency at 500mA and 50mA load are around 80% when the input voltage varies from 2.7V to 4.5V. The average efficiency at 10mA load over the entire input range is around 60%.

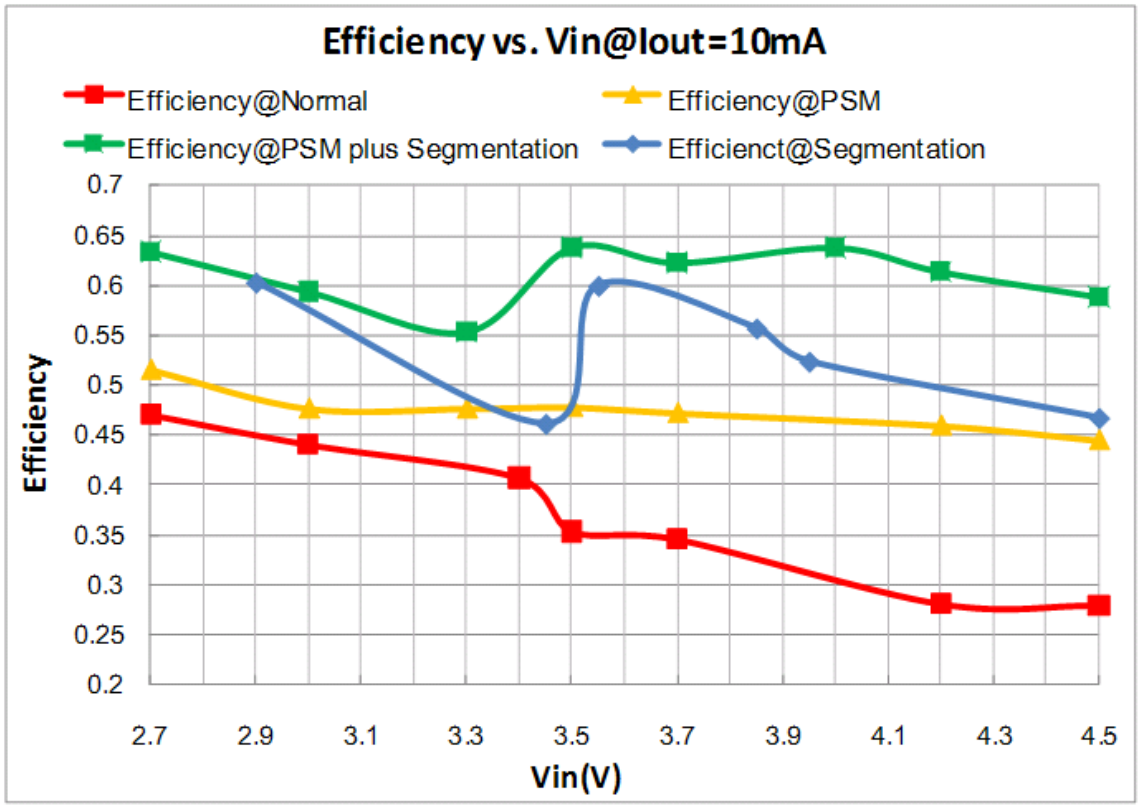

Fig.3.27. Efficiency of Charge pump with Different Control Schemes at very Light Load Condition

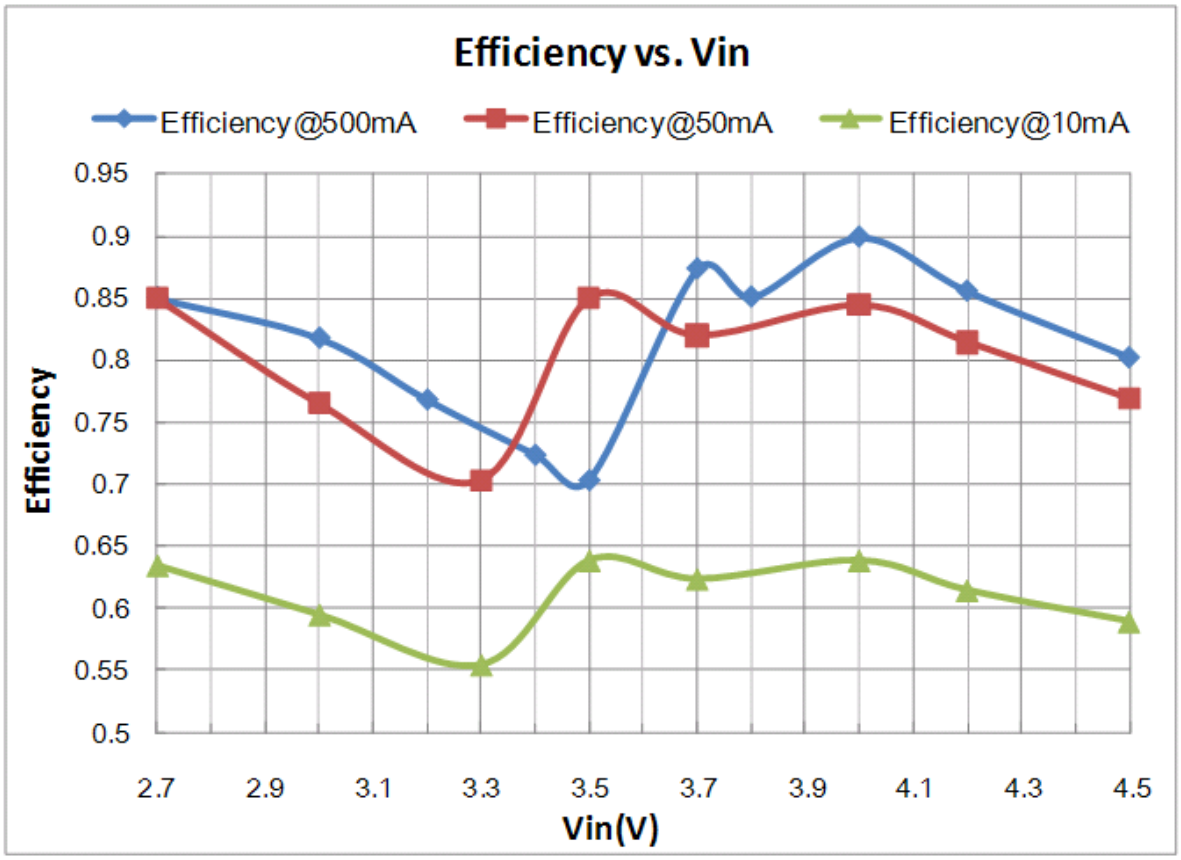

Fig.3.28. Efficiency of Designed Charge Pump at Different Load Currents

A PCB prototype is built to verify proposed control methods, as shown in Fig.3.29. Table 3.6 shows the circuit parameters used in the prototype. The circuit is running at 1MHz at heavy and light load condition, but the frequency will decease at very light load condition. Transistors MP1-MP9 are PMOS while MN1 is NMOS. The gate charge ratio of PMOS before and after the device segmentation control is 7.8:1.

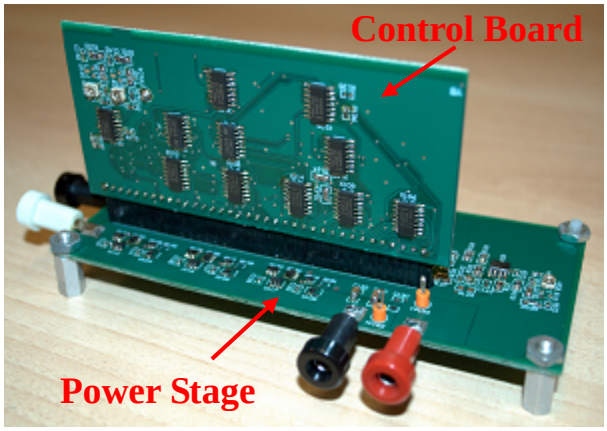

Fig.3.29. Test Bench of Designed Multi-modes Regulated Charge Pump

Table 3.6 Circuit Parameters for the Prototype

V_{in}	2.7-4.5V	**V_o**	5V
f_s	1MHz	**I_{out}**	10-500mA
C_{fly}	4.7uF	**C_o**	10uF*2
PMOS (Before Segmentation)	Qg=14nC , R_{on}=35mΩ@V_{GS}= –4.5 V		
PMOS (After Segmentation)	Qg=1.8nC, R_{on}=0.4Ω@V_{GS} = –4.5 V		
NMOS(Regulated)	R_{on}=36mΩ @V_{GS}= 4.5 V		

Fig.3.30 (a) and (b) are experiment results for fast load transitions between different load conditions. In Fig.3.30 (a), load steps down from 300mA to 100mA, and SEG_ENB is automatically enabled after transition while PSM_ENB is always disabled. In Fig.3.30 (b), load steps down from 100mA to 25mA, and PSM_ENB is automatically enabled after transition while SEG_ENB is always enabled. Fig.3.31 shows the output voltage ripple and control signals in steady state at different load conditions.

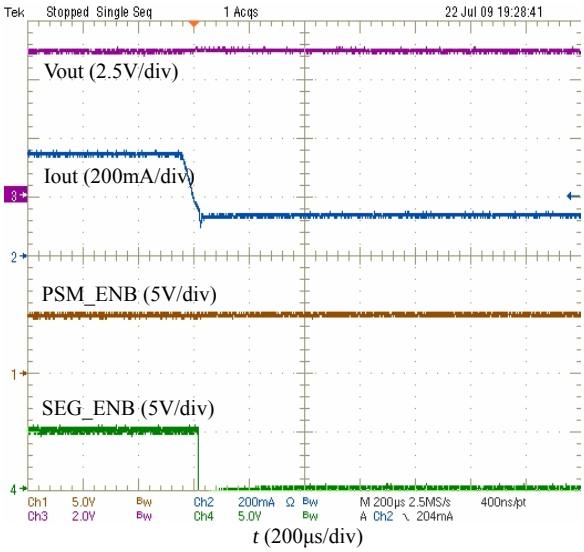

(a) Heavy->Light Load

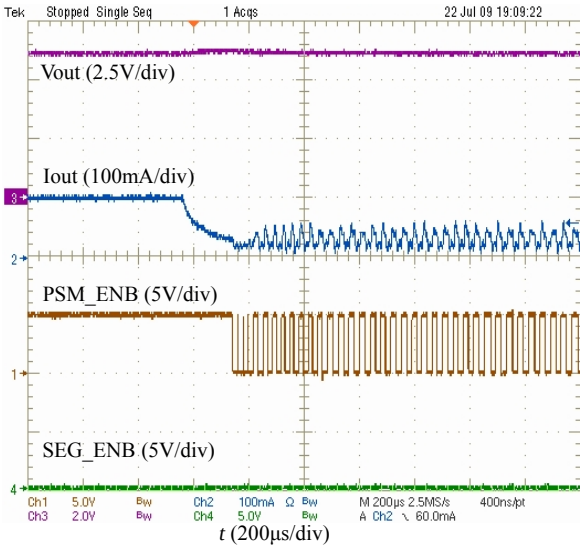

(b) Light-> Very Light Load

Fig.3.30 Test Results of Load Transitions from Very light->light->heavy load @ V_{in}=3.7V

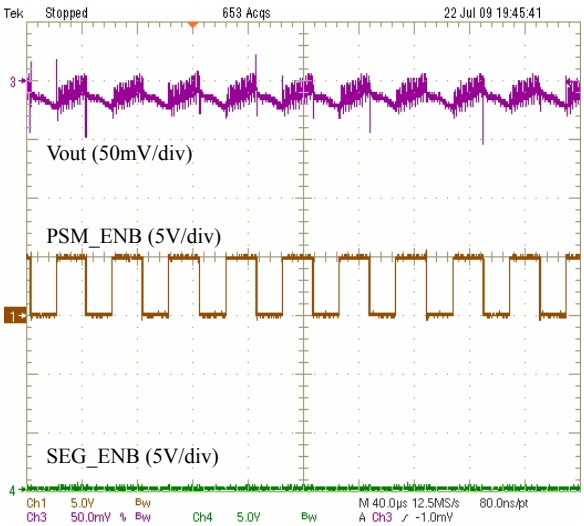

(a) I_{out}=25mA(very light load)

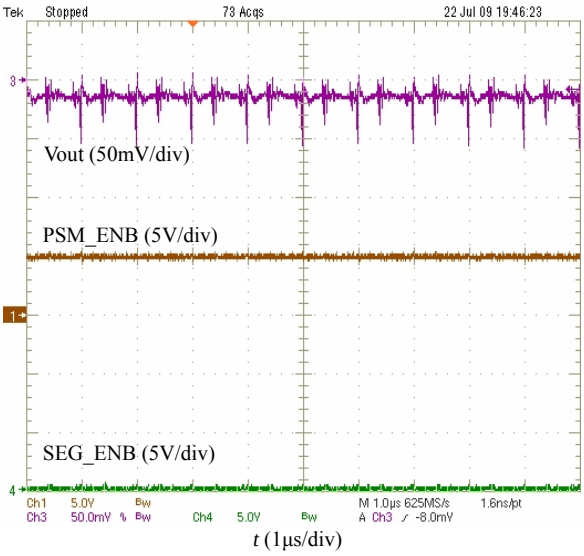

(b) I_{out}=100mA(light load)

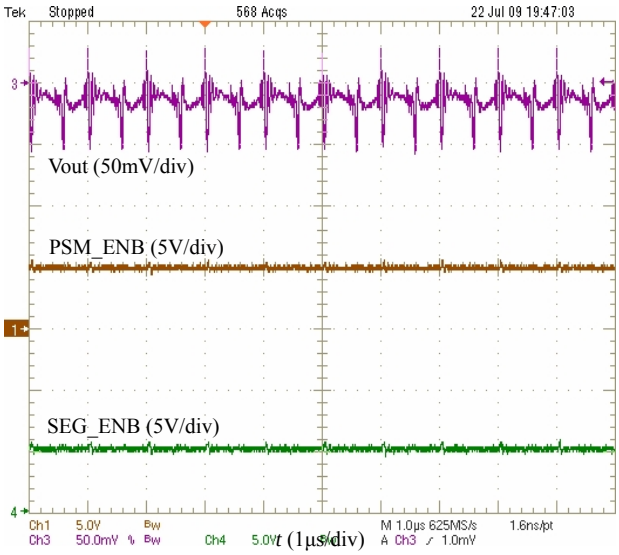

(c) I_{out}=300mA(heavy load)

Fig.3.31 Steady State at different load conditions when V_{in}=3.7V

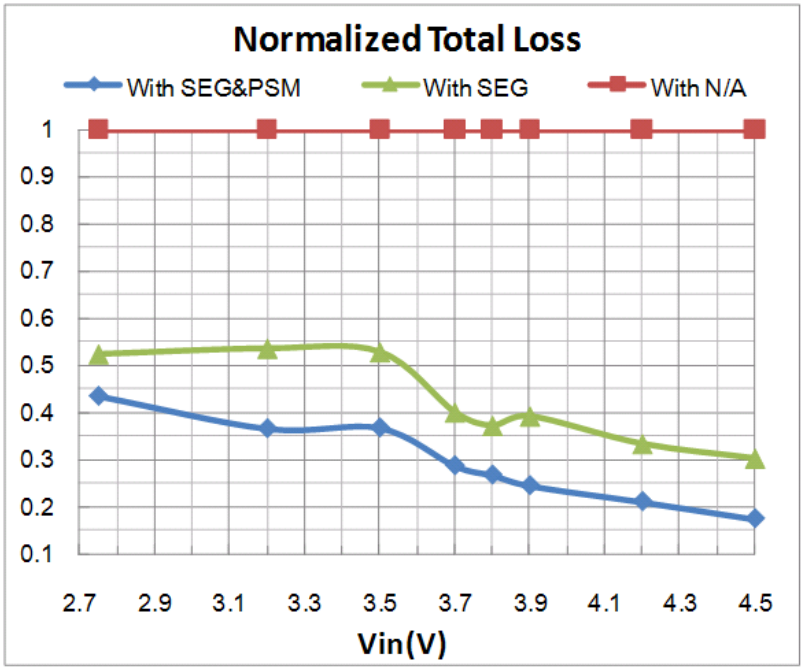

Fig.3.32 Total Loss Comparisons @ I_{out}=25mA

Fig.3.32 shows the total loss comparison between different light load control methods. The total loss of charge pump without any light load improvement has been normalized to 1. The experiment results show the charge pump with only device segmentation saves the loss by 47%-70%, while the one combining both of device segmentation and PSM can reduce the total loss by 56% to 83%.

3.8 Summary

A multi-modes regulated charge pump with improved efficiency over wide input and load range is proposed. The output voltage is regulated to 5V when input is 4.5-2.7V. By alternating the switch network, it can realize 2x, 1.5x, and 1.33x conversion modes, which improves the efficiency over wide input range. During each mode, the output voltage is regulated by a controlled current source. The regulated charge pump is designed for a very wide load range (10mA to 500mA). Pulse skipping regulation and device segmentation are used to improve light load efficiency, especially for very light load conditions. A hybrid control scheme is designed to achieve a high efficiency over wide load range. Both of the simulation and test results are provided to verify the control scheme. The results show that the total loss at light load can be reduced by 56% to 83%.

Chapter 4. High Efficiency Multi-Modes Charge-Pump Based Buck Converter for Wide Input Range Applications

4.1 Research Motivation

Wide input range DC-DC converters are widely used in automotive, telecom and industrial systems. For example, a 42V automotive battery system usually requires the DC-DC converter to operate over 18-58V input range [16]. Sometimes, the input voltage range can be even wider depending on different manufacture's requirement. The output voltage is regulated to 5V, 3.3V or even lower, therefore the step-down ratio could be high. In industrial applications where the front-end Bus voltage can change (12V, 24V, or 48V), instead of redesigning the DC-DC converter, a wide input range DC-DC converter can save the time and cost. However, these wide input range converters usually come with several issues. First, switching loss increases fast as the input voltage becomes higher and thus results in a low efficiency at high input voltage. Conduction loss increases very little with input voltage, but high voltage rating low on-resistance devices are required to keep it down. Second, it is impractical for a standard single inductor Buck converter to step down very high voltage to very low voltage because of the duty cycle limit [52]. With a high step-down ratio, it is

difficult to control at extremely low duty cycle because very little room is left to reduce the duty cycle further once there is a load step-down transient. Transformer based converter is a better choice; however it is bulky and expensive for applications that do not need isolation. Third, compensator design is not easy as the loop gain can vary a lot with input voltage. Feed forward control can be used to cancel the variation; however it will increase the complexity of control circuit. Fourth, the maximum switching frequency is also limited because of the extremely narrow duty cycle at high step down.

To overcome these drawbacks, a multi-modes charge-pump based wide input range DC-DC converter is proposed. An unregulated multi-modes charge pump is used as a pre-regulator of standard buck converter and does a rough voltage conversion. It has three modes: 1/3x, 1/2x and 1x. According to the input voltage, the charge pump can adaptively select the best mode to step down the input voltage. The input voltage range of Buck converter is greatly reduced and therefore low voltage standard devices can be used in Buck converter, which reduces both of the conduction loss and switching loss. Since the charge pump is unregulated, the efficiency usually is very high (>90%). As Buck converter and charge pump converter exhibit different efficiency tendency within the same input range, it is proved that the total efficiency can be improved by combining them, especially at high input voltage. It also directly benefits the design of compensator and output LC filter because the input range of Buck converter becomes much narrower. In addition, extremely low duty cycle will not happen in steady state.

Compared with a wide input range single Buck converter, the proposed charge-pump based DC-DC converter not only improves the efficiency, but also can improve the transient response without using feed forward control. Instead of a bulky transformer, the added charge pump can be integrated with Buck regulator (except flying capacitors) for single chip solution and saves space.

In this Chapter, the theoretical efficiency analysis of multi-modes charge-pump based Buck converter is given. Benefits for control over wide input range are also analyzed. A 10W prototype is built to verify the benefits of proposed solution. Experiment results show that the highest efficiency improvement is 7% at heavy load and 16% at light load.

4.2 Proposed Structure of Wide Input Range Buck Converter

Fig.4.1 shows the proposed topology of wide input range converter. The first stage is an unregulated multi-modes charge-pump and the second stage is a synchronous buck converter. As the pre-stage of synchronous Buck converter, the multi-modes charge pump includes eight MOSFETs M1-M8 and three flying capacitors Cf1-Cf3. All of the MOSFETs operate in triode region and behave like switches with fixed on-resistance. By alternating the arrangement of switches and capacitors, it can realize three different conversion modes: 1/3x, 1/2x and 1x.

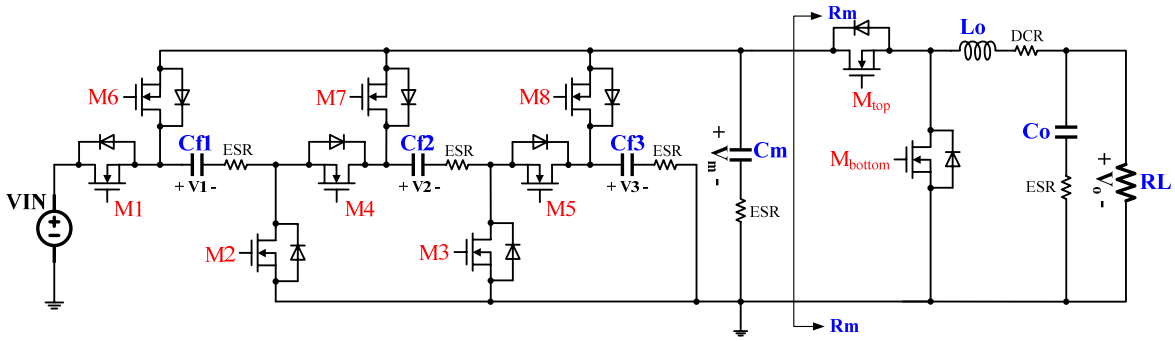

Fig.4.1 Proposed topology of wide input range DC-DC converter

1) Mode 1/3x: During 0-0.5Ts, M1, M4 and M5 are on. Cf1, Cf2, and Cf3 are in series connection and are charged by the input source VIN. The input voltage is evenly distributed across the three flying capacitors. During 0.5Ts-Ts, M2, M3, M6, M7, and M8 are on. Cf1, Cf2, and Cf3 are in parallel connection, and discharge energy to capacitor Cm.

2) Mode 1/2x: During 0-0.5Ts, M1, M4 and M3 are on. Cf1 and Cf2 are in series connection and are charged by the input source VIN. VIN is evenly distributed across the two flying capacitors. During 0.5Ts-Ts, M2, M3, M6, and M7 are on. Cf1 and Cf2 are in parallel connection, and charge the capacitor Cm.

3) Mode 1x: Only M1 and M6 are on, while other switches are off. The input source VIN will directly charge the capacitor Cm.

The charge pump is unregulated with duty cycle fixed to 50%, thus its output voltage will be affected by modes, input voltage, load resistance and internal impedance. Use 1/3X mode

charge pump as the analysis model. Assume all the switches have equal on-resistance R_{on}, and all the capacitors have the same ESR. The voltages across capacitors Cf1, Cf2, Cf3, and C_m are represented as $v1$, $v2$, $v3$, and v_m respectively. The input impedance of Buck converter is R_m, which is also the load of the charge pump. During 0-0.5Ts, Cf1, Cf2 and Cf3 are charged by the same current i_{ch} while C_m discharges energy to the output. The equations are shown in (4.1)-(4.3). During 0.5Ts-Ts, Cf1, Cf2, Cf3 and C_m are in parallel connection. The three flying capacitors will discharge current to load and charge C_m up as well. The corresponding equations are shown in (4.4) and (4.5).

[0 to 0.5Ts]

$$i_{ch} = Cf_1 \frac{dv_1}{dt} = Cf_2 \frac{dv_2}{dt} = Cf_3 \frac{dv_3}{dt} \tag{4.1}$$

$$(3ESR + 3R_{on})i_{ch} + v_1 + v_2 + v_3 = \mathrm{V_{in}} \tag{4.2}$$

$$-C_m \frac{dv_m}{dt}(ESR + R_m) = v_m \tag{4.3}$$

[0.5Ts to Ts]

$$Cf_1 \frac{dv_1}{dt}(ESR + 2R_{on}) + v_1 = Cf_2 \frac{dv_2}{dt}(ESR + 2R_{on}) + v_2 = Cf_3 \frac{dv_3}{dt}(ESR + R_{on}) + v_3 \tag{4.4}$$

$$v_m + C_m \frac{dv_m}{dt} ESR = (-Cf_1 \frac{dv_1}{dt} - Cf_2 \frac{dv_2}{dt} - Cf_3 \frac{dv_3}{dt} - C_m \frac{dv_m}{dt})R_m = Cf_1 \frac{dv_1}{dt}(ESR + 2R_{on}) + v_1 \tag{4.5}$$

To simplify the calculation, neglect the ESR as they are much smaller than the R_{on}. The output voltage of charge pump V_m can be obtained using state-space average analysis [17]. The calculated output voltage V_m and its ideal value for each mode are shown in Table 4.1.

Table 4.1 Output Voltage of Charge Pump at Each Mode

Mode	V_m	Ideal V_m
1/3x	$V_m = \frac{V_{in}}{3 + 8R_{on}/(3R_m)}$	$\frac{V_{in}}{3}$
1/2x	$V_m = \frac{V_{in}}{2 + 7R_{on}/(2R_m)}$	$\frac{V_{in}}{2}$
1x	$V_m = \frac{V_{in}}{1 + 2R_{on}/R_m}$	V_{in}

It can be seen that when R_{on} is selected much smaller than R_m, V_m will get close to the ideal value. After inserting the charge pump between the input source and the Buck converter, the input voltage range of Buck converter has been reduced by 2/3 compared with a single Buck converter. As a result, instead of using high voltage rating devices, standard voltage rating devices can be used in Buck converter. The on-resistance will be lower and the cost is reduced as well.

Since the charge pump stage only roughly steps down the input voltage, the fine regulation of output voltage will be achieved by Buck converter using feedback and PID control.

4.3 Loss Break Down of Charge Pump

A single Buck converter operating over wide input range shows a low efficiency at high input voltage. However, using a multi-mode charge pump as the pre-stage can improve the

efficiency. In this section, the losses in charge pump stage are analyzed.

To perform a reasonable efficiency analysis of charge pump, the expressions of charging and discharging current in the charge pump need to be derived first. A 1/3X mode charge pump is used as the example, and analyzed in time domain during each half cycle. To simplify the calculation, use Cf to represent the three flying capacitors since they are selected to be equal, and also consider *v*2 and *v*3 having the same equation as *v*1.

[0 to 0.5Ts]

During this half cycle, the flying capacitors are being charged by the input source, so we have (4.6).

$$3R_{on}C_f\frac{dv_1}{dt}+3v_1=\mathrm{V_{in}} \tag{4.6}$$

Assume the peak ripple voltage of *v*1 is u_p and the valley ripple voltage is u_v. Therefore the initial voltage of flying capacitor Cf1 during charging stage is u_v, and the initial voltage during discharging stage is u_p. The equation of *v*1(t) during [0-0.5Ts] can be solved from (4.6), as shown in (4.7).

$$v_{1\_Ch}(t)=\frac{\mathrm{V_{in}}}{3}+(\mathrm{u_v}-\frac{\mathrm{V_{in}}}{3})e^{-\frac{t}{R_{on}C_f}} \tag{4.7}$$

From (4.7), we can verify the initial voltage of *v*1 during charging stage and also get the voltage when t=0.5Ts, as shown in (4.8).

$$\begin{cases} v_{1\_Ch}(0)=\mathrm{u_v} \\ v_{1\_Ch}(0.5T_s)=\frac{\mathrm{V_{in}}}{3}+(\mathrm{u_v}-\frac{\mathrm{V_{in}}}{3})e^{-\frac{0.5T_s}{R_{on}C_f}} \end{cases} \tag{4.8}$$

During the same half cycle, C_m is discharging energy to load, as shown in (4.9).

$$-C_m R_m \frac{dv_m}{dt} = v_m \tag{4.9}$$

Assume the peak ripple of v_m is um_p and the valley ripple is um_v. Therefore the initial voltage of C_m during charging stage is um_v, and the initial voltage during discharging stage is um_p. The equation of $v_m(t)$ during 0-0.5Ts can be solved from (4.9), which is shown in (4.10).

$$v_{m\_Dis}(t) = \mathrm{um_p} e^{-\frac{t}{C_m R_m}} \tag{4.10}$$

From (4.10), we can verify the initial voltage and also get the voltage of v_m when t=0.5Ts, as shown in (4.11).

$$\begin{cases} v_{m\_Dis}(0) = \mathrm{um_p} \\ v_{m\_Dis}(0.5T_s) = \mathrm{um_p} e^{-\frac{T_s}{2R_m C_m}} \end{cases} \tag{4.11}$$

[0.5Ts to Ts]

During this half cycle, the flying capacitors are discharging energy to the output capacitor C_m, so we can have (4.12) and (4.13).

$$v_m = 2R_{on} C_f \frac{dv_1}{dt} + v_1 \tag{4.12}$$

$$-C_f \frac{dv_1}{dt} = C_m \frac{dv_m}{dt} + \frac{v_m}{R_m} \tag{4.13}$$

Then the equation of $v1(t)$ during 0.5Ts-Ts can be solved from (4.12) and (4.13), which is shown in (4.14). ‘xa’ and ‘xb’ are constants determined by the R and C parameters in the charge pump circuit. The expressions of ‘xa’ and ‘xb’ are given in (4.15).

$$v_{1\_Dis}(t)=\frac{\dfrac{3C_fR_m\mathrm{u_p}+C_mR_m\mathrm{um_v}+2C_fR_{on}\mathrm{u_p}}{2R_{on}C_fC_mR_m}-xa\cdot\mathrm{u_p}}{xb-xa}e^{-xa(t-\frac{T_s}{2})}+\frac{xb\cdot\mathrm{u_p}-\dfrac{3C_fR_m\mathrm{u_p}+C_mR_m\mathrm{um_v}+2C_fR_{on}\mathrm{u_p}}{2R_{on}C_fC_mR_m}}{xb-xa}e^{-xb(t-\frac{T_s}{2})} \tag{4.14}$$

$$\begin{cases} xa=\dfrac{\sqrt{\dfrac{9C_f{}^2R_m{}^2+12C_f{}^2R_mR_{on}+4C_f{}^2R_{on}{}^2+6C_fC_oR_m{}^2-4C_fC_oR_oR_{on}+C_o{}^2R_m{}^2}{2}}+\dfrac{3C_fR_m}{2}+\dfrac{C_mR_m}{2}+C_fR_{on}}{2C_fC_oR_oR_{on}} \\ xb=\dfrac{-\sqrt{\dfrac{9C_f{}^2R_m{}^2+12C_f{}^2R_mR_{on}+4C_f{}^2R_{on}{}^2+6C_fC_oR_m{}^2-4C_fC_oR_oR_{on}+C_o{}^2R_m{}^2}{2}}+\dfrac{3C_fR_m}{2}+\dfrac{C_mR_m}{2}+C_fR_{on}}{2C_fC_oR_oR_{on}} \end{cases} \tag{4.15}$$

From (4.14), we can verify the initial voltage of *v*1 during discharging stage and also get the voltage when t=Ts, which are shown in (4.16).

$$\begin{cases} v_{1\_Dis}(0.5T_s)=\mathrm{u_p} \\ v_{1\_Dis}(T_s)=\dfrac{\dfrac{3C_fR_m\mathrm{u_p}+C_mR_m\mathrm{um_v}+2C_fR_{on}\mathrm{u_p}}{2R_{on}C_fC_mR_m}-xa\cdot\mathrm{u_p}}{xb-xa}e^{-0.5xaT_s}+\dfrac{xb\cdot\mathrm{u_p}-\dfrac{3C_fR_m\mathrm{u_p}+C_mR_m\mathrm{um_v}+2C_fR_{on}\mathrm{u_p}}{2R_{on}C_fC_mR_m}}{xb-xa}e^{-0.5xbT_s} \end{cases} \tag{4.16}$$

At the same time, capacitor C_m is being charged by three flying capacitors. Therefore, the equation of $v_m(t)$ can be obtained according to the equation of $v_1(t)$.

$$v_{m\_Ch}(t) = 2R_{on}C_f \frac{dv_{1\_Dis}(t)}{dt} + v_{1\_Dis}(t) \tag{4.17}$$

From (4.17), the initial condition of $v_m(t)$ during 0.5Ts-Ts can be verified and the voltage at t=Ts can also be found, as shown in (4.18).

$$\begin{cases} v_{m\_Ch}(0.5T_s) = \mathrm{um_v} \\ v_{m\_Ch}(T_s) = \dfrac{(\dfrac{3C_fR_m\mathrm{u_p} + C_mR_m\mathrm{um_v} + 2C_fR_{on}\mathrm{u_p}}{2R_{on}C_fC_mR_m} - xa\cdot \mathrm{u_p})(1-2C_fR_{on}xa)}{xb-xa} e^{-0.5xaT_s} \\ \qquad + \dfrac{(xb\cdot \mathrm{u_p} - \dfrac{3C_fR_m\mathrm{u_p} + C_mR_m\mathrm{um_v} + 2C_fR_{on}\mathrm{u_p}}{2R_{on}C_fC_mR_m})(1-2C_fR_{on}xb)}{xb-xa} e^{-0.5xbT_s} \end{cases} \tag{4.18}$$

Since the end of the charging stage is the start of the discharging stage, and vice versa, based on the results shown in (4.8), (4.11), (4.16), and (4.18), we can get (4.19).

$$\begin{cases} v_{1\_Ch}(0.5T_s) = \mathrm{u_p} \\ v_{1\_Dis}(T_s) = \mathrm{u_v} \\ v_{m\_Dis}(0.5T_s) = \mathrm{um_v} \\ v_{m\_Ch}(T_s) = \mathrm{um_p} \end{cases} \tag{4.19}$$

Then according to (4.19), the expressions of $\mathrm{u_p}$, $\mathrm{u_v}$, $\mathrm{um_v}$, and $\mathrm{um_p}$ can be solved, which are shown in (4.20).

Finally, the equations of $v1(t)$ and $v_m(t)$ during 0-Ts can be obtained by substituting the solved initial conditions $\mathrm{u_p}$, $\mathrm{u_v}$, $\mathrm{um_v}$, and $\mathrm{um_p}$ into the equations (4.7), (4.10), (4.14) and (4.17). Once the voltage equations are derived, the current flowing through Cf1 can be found

using (4.21).

$$\begin{cases} u_p = \dfrac{\dfrac{V_{in}(e^{\frac{T_s}{2C_f R_{on}}}-1)}{3}(xa-xb)}{\dfrac{(e^{-xa\frac{T_s}{2}}-e^{-xb\frac{T_s}{2}})^2\dfrac{3}{2C_m R_{on}}}{2C_f R_{on}(xa-xb)e^{\frac{T_s}{2C_m R_m}}-e^{-xa\frac{T_s}{2}}(2C_f R_{on}xa-1)+e^{-xb\frac{T_s}{2}}(2C_f R_{on}xb-1)}-\left[(xa-xb)e^{\frac{T_s}{2C_f R_{on}}}-e^{-xa\frac{T_s}{2}}(xa-\frac{3C_f R_m+2C_f R_{on}}{2C_f C_m R_m R_{on}})+e^{-xb\frac{T_s}{2}}(xb-\frac{3C_f R_m+2C_f R_{on}}{2C_f C_m R_m R_{on}})\right]} \\ u_v = e^{\frac{T_s}{2C_f R_{on}}}(u_p-\dfrac{V_{in}}{3}+\dfrac{V_{in}e^{-\frac{T_s}{2C_f R_{on}}}}{3}) \\ um_v = \dfrac{-(e^{-\frac{T_s}{2}xa}-e^{-\frac{T_s}{2}xb})\dfrac{3C_f}{C_o}}{2C_f R_{on}(xa-xb)e^{\frac{T_s}{2C_m R_m}}-e^{-\frac{T_s}{2}xa}(2C_f R_{on}xa-1)+e^{-\frac{T_s}{2}xb}(2C_f R_{on}xb-1)} \\ um_p = \dfrac{um_v}{e^{-\frac{T_s}{2C_m R_m}}} \end{cases} \tag{4.20}$$

$$\begin{cases} i_{1\_Ch}(t) = C_f \dfrac{dv_{1\_Ch}(t)}{dt} \\ i_{1\_Dis}(t) = C_f \dfrac{dv_{1\_Dis}(t)}{dt} \end{cases} \tag{4.21}$$

The calculated $v_m(t)$, $v1(t)$, and $i1(t)$ in one cycle are plotted in red using MathCAD, as shown in Fig.4.2. To verify the accuracy of calculation, the charge pump circuit is also simulated using SIMPLIS with the same circuit parameters, and the simulation results are plotted in blue. It can be seen from Fig.2 that they are matched perfectly.

By solving the expressions of current and voltage in the circuit, the RMS, peak and valley value of charging and discharging current can be easily calculated, which are denoted as $I_{1\_Ch\_RMS}$, I_{p_Ch}, I_{v_Ch}, $I_{1\_Dis\_RMS}$, I_{p_Dis} and I_{v_Dis} respectively.

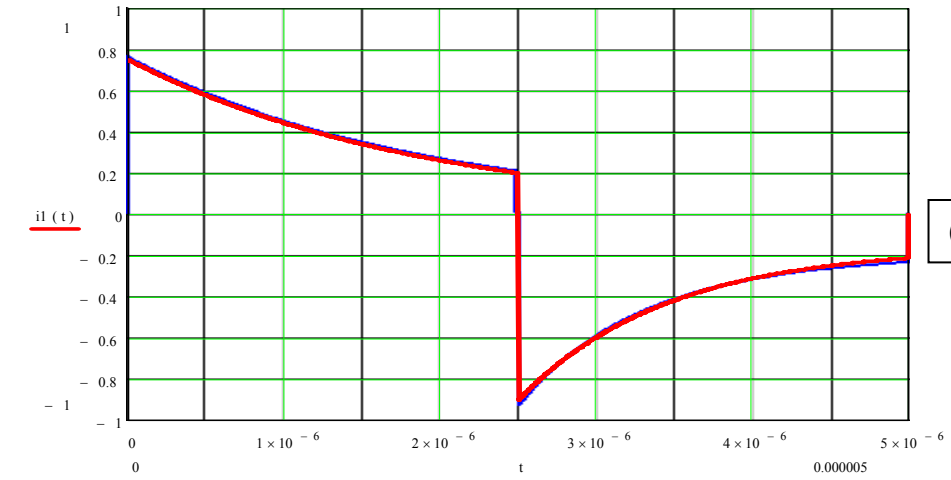

(a) $i1(t)$

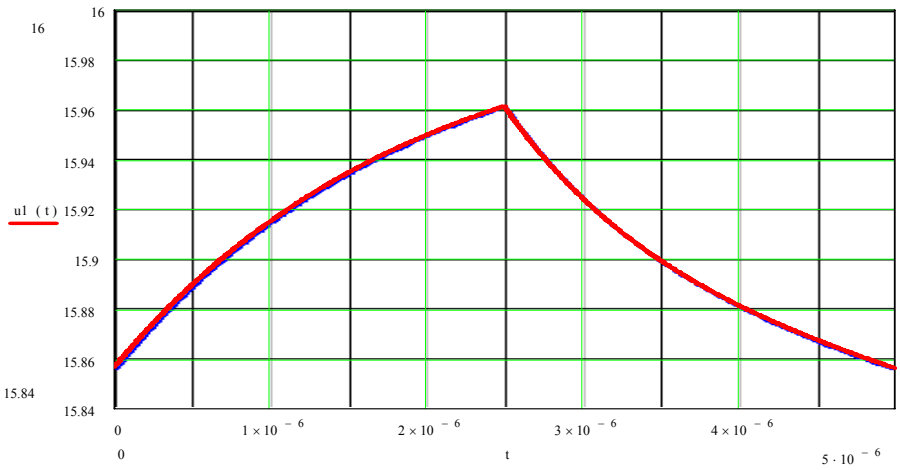

(b) $v1(t)$

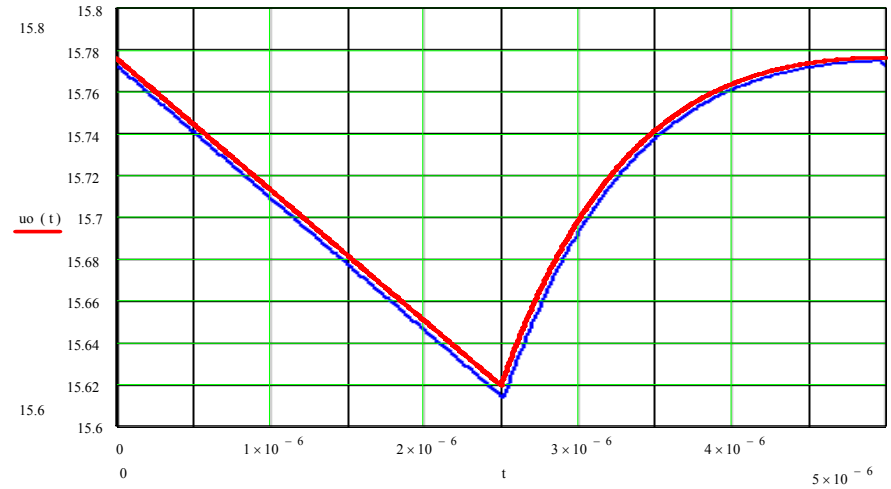

(c) $v_m(t)$

Fig.4.2 Comparisons of $i1(t)$, $v1(t)$, and $v_m(t)$ between simulation results and calculations.

Based on calculated current information, the loss equations can be accurately derived. In a charge pump, the major loss can usually be broken down to two categories: conduction loss and switching loss. The quiescent loss will not be the focus of this analysis.

1) Conduction Loss

The conduction loss includes on-resistance loss of switches and ESR loss of the capacitors. During 0-0.5Ts, G1, G4 and G5 are ON. During 0.5Ts-Ts, G2, G3, G6, G7, and G8 are ON. The on-resistance loss (P_{ron}) and ESR loss (P_{esr}) can be derived using (4.22) and (4.23). Fig.4.3 plots the variation of total conduction loss (P_{Con}) with input voltage in a 1/3x mode charge pump. It can be seen that the conduction loss quickly decreases when the input voltage is increasing, because the current passing through charge pump becomes smaller at the same time.

$$P_{ron} = I_{1\_Ch\_rms}{}^2 3R_{on} + I_{1\_Dis\_rms}{}^2 5R_{on} \tag{4.22}$$

$$P_{esr} = (I_{1\_Ch\_rms}{}^2 + I_{1\_Dis\_rms}{}^2)3R_{esr} + I_{m\_rms}{}^2 R_{esr} \tag{4.23}$$

2) Switching Loss

The switching loss of charge pump will include V-I overlapping loss, C_{oss} charging loss, and Gate driver loss. During the analysis, assume G1, G4, and G5 are on and off simultaneously; G2, G3, G6, G7, and G8 are on and off simultaneously.

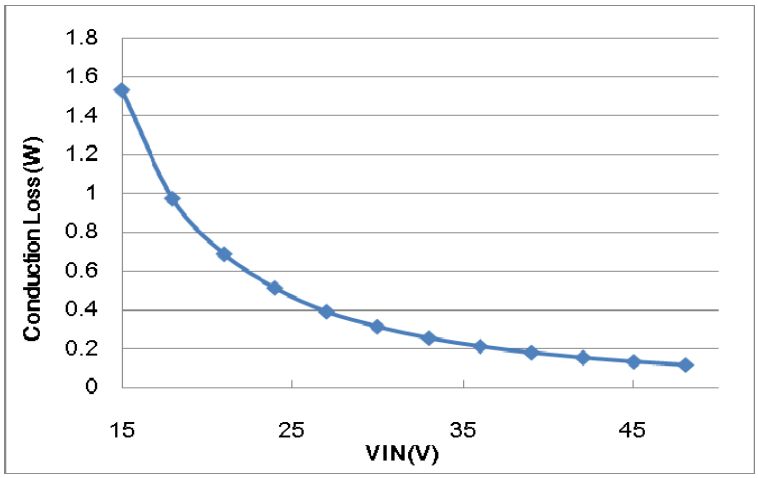

Fig.4.3 Conduction Loss vs. Input Voltage in 1/3x Charge Pump (P_o=10W)

a. V-I Overlapping Loss.

All switches in the charge pump are hard-switching, therefore V-I overlapping losses exist. The turn on and turn off transients of switches are shown in Fig.4.4. Since there are only switches and capacitors in the circuit, the transition of voltage and current can be considered as occurring at the same time. The equations to calculate the turn-on and turn-off losses are shown in (4.24). V_{ds} is the blocking voltage when the switch is off. During 0-0.5Ts, the blocking voltage of G1 is V_{in}-V_{out}=2/3V_{in}, and the blocking voltage of G4 and G5 is V_{out}=1/3V_{in}. During 0.5Ts-Ts, the blocking voltages of G2, G3, G6, G7, and G8 are 2/3V_{in}, 1/3V_{in}, 2/3V_{in}, 1/3V_{in} and 0 respectively. The turn-on and turn off losses of each switch are summarized in Table 4.2. The total V-I overlapping loss will be the sum of turn-on and turn-off loss of all switches, which is shown in (4.25).

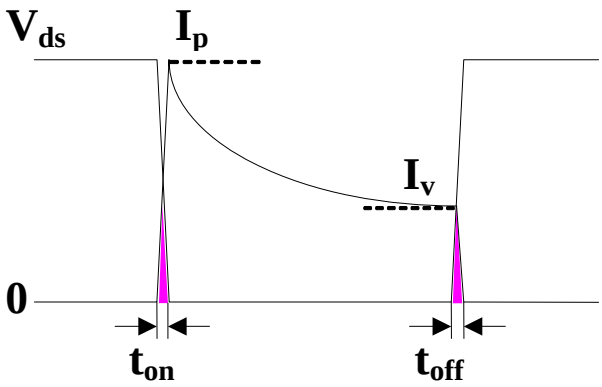

Fig.4.4 Turn on and Turn off Transients of the switches

$$\begin{cases} P_{turn-on} = \frac{1}{6} V_{ds} I_p t_{on} f_s \\ P_{turn-off} = \frac{1}{6} V_{ds} I_v t_{off} f_s \end{cases} \tag{4.24}$$

$$P_{overlapping} = P_{Turn-on} + P_{Turn-off} \tag{4.25}$$

b. C_{oss} Charging Loss.

The parasitic C_{oss} of each switch will be charged to the blocking voltage of that switch when it is off, and will be fully discharged when the switch is on. The charging efficiency is only 50% and half of the energy gets wasted. C_{oss} is a nonlinear capacitor and strongly depends on the drain to source voltage V_{ds}. The C_{oss} is normally tested at V_{gs}=0 and V_{ds}=V_{in}, but the real C_{oss} is inversely proportional to the square root of the V_{ds} [53]. Since it will change when it is being charged or discharged, a coefficient 4/3 is added during the loss calculation for a better approximation. The C_{oss} charging losses of each switch are summarized in Table 4.3. The total C_{oss} charging loss will the sum of C_{oss} charging loss of

each switch, as shown in (4.26).

$$P_{Coss} = P_{oss1} + P_{oss2} + P_{oss3} + P_{oss4} + P_{oss5} + P_{oss6} + P_{oss7} + P_{oss8} \tag{4.26}$$

Table 4.2 Summary of Turn-on and Turn-off Losses

	Switch	Turn-on Loss($P_{Turn-on}$)	Turn-off Loss($P_{Turn-off}$)
0-0.5Ts	G1	$\frac{1}{6}(\frac{2}{3}V_{in})I_{p\_Ch}t_{on}f_s$	$\frac{1}{6}(\frac{2}{3}V_{in})I_{v\_Ch}t_{off}f_s$
	G4	$\frac{1}{6}(\frac{1}{3}V_{in})I_{p\_Ch}t_{on}f_s$	$\frac{1}{6}(\frac{1}{3}V_{in})I_{v\_Ch}t_{off}f_s$
	G5	$\frac{1}{6}(\frac{1}{3}V_{in})I_{p\_Ch}t_{on}f_s$	$\frac{1}{6}(\frac{1}{3}V_{in})I_{v\_Ch}t_{off}f_s$
0.5Ts-Ts	G2	$\frac{1}{6}(\frac{2}{3}V_{in})I_{p\_Dis}t_{on}f_s$	$\frac{1}{6}(\frac{2}{3}V_{in})I_{v\_Dis}t_{off}f_s$
	G3	$\frac{1}{6}(\frac{1}{3}V_{in})I_{p\_Dis}t_{on}f_s$	$\frac{1}{6}(\frac{1}{3}V_{in})I_{v\_Dis}t_{off}f_s$
	G6	$\frac{1}{6}(\frac{2}{3}V_{in})I_{p\_Dis}t_{on}f_s$	$\frac{1}{6}(\frac{2}{3}V_{in})I_{v\_Dis}t_{on}f_s$
	G7	$\frac{1}{6}(\frac{1}{3}V_{in})I_{p\_Dis}t_{on}f_s$	$\frac{1}{6}(\frac{1}{3}V_{in})I_{v\_Dis}t_{off}f_s$
	G8	0	0

Table 4.3 Summary of C_{oss} Charging Loss

G1	$P_{oss1} = \frac{1}{2}(\frac{4}{3}C_{oss})(\frac{2}{3}V_{in})^2 f_s$	G5	$P_{oss5} = \frac{1}{2}(\frac{4}{3}C_{oss})(\frac{1}{3}V_{in})^2 f_s$
G2	$P_{oss2} = \frac{1}{2}(\frac{4}{3}C_{oss})(\frac{2}{3}V_{in})^2 f_s$	G6	$P_{oss6} = \frac{1}{2}(\frac{4}{3}C_{oss})(\frac{2}{3}V_{in})^2 f_s$
G3	$P_{oss3} = \frac{1}{2}(\frac{4}{3}C_{oss})(\frac{1}{3}V_{in})^2 f_s$	G7	$P_{oss7} = \frac{1}{2}(\frac{4}{3}C_{oss})(\frac{1}{3}V_{in})^2 f_s$
G4	$P_{oss4} = \frac{1}{2}(\frac{4}{3}C_{oss})(\frac{1}{3}V_{in})^2 f_s$	G8	0

c. Gate Driver loss.

There are eight transistors in the charge pump; therefore, the gate driving loss can be derived according to (4.27).

$$P_{dr} = 8C_{iss}V_{gs}^{2}f_{s} \tag{4.27}$$

In summary, the switching loss can be obtained by adding the three losses up, which is shown in (4.28). Fig.4.5 plots the switching loss versus input voltage in a 1/3x mode charge pump. It can be seen that the total switching loss is not monotonously increasing with the input voltage. From Table 4.2, the turn-on and turn-off losses are the functions of both input voltage and the charging/discharging current. However, when input voltage goes up, the current will go down and results in a non-monotonic loss increase with input voltage.

$$P_{SW} = P_{overlapping} + P_{Coss} + P_{dr} \tag{4.28}$$

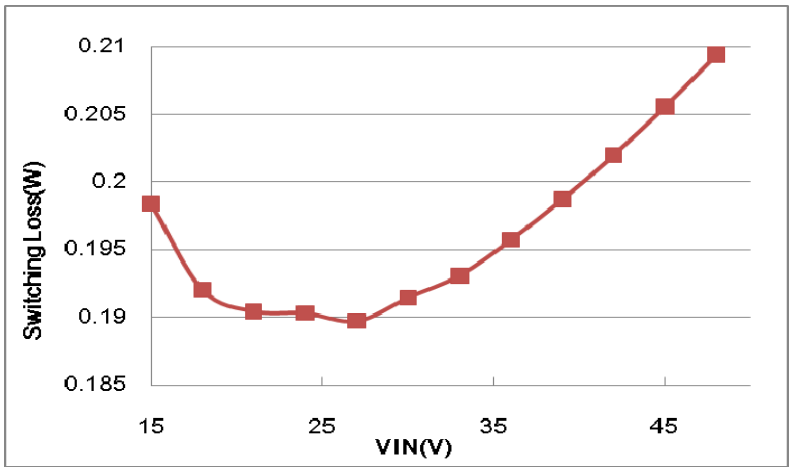

Fig. 4.5. Switching Loss vs. Input Voltage in 1/3x Charge Pump(P_o=10W)

4.4 Loss Break Down of Synchronous Buck Converter

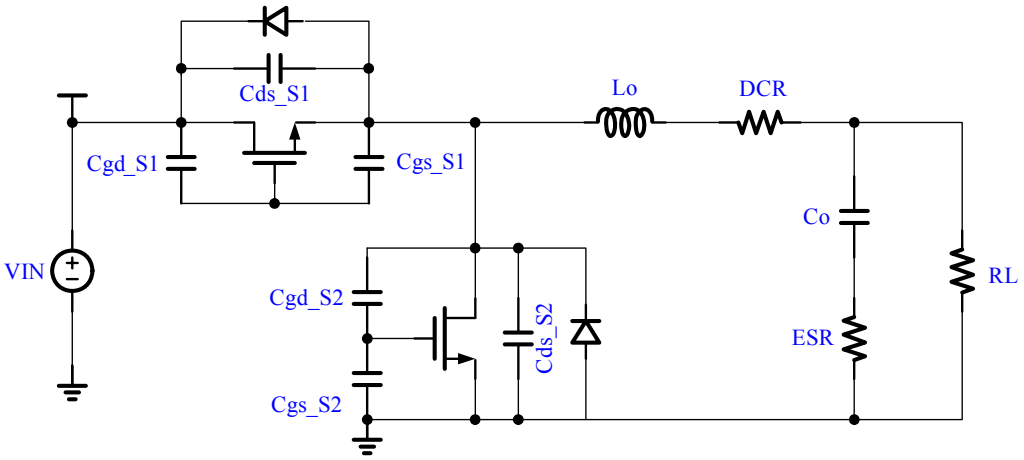

Fig.4.6. Power Stage of Synchronous Buck Converter

The loss break down of Buck converter has already been analyzed in lots of papers [54-56]. Based on these literatures, we can category the loss into conduction loss and switching loss. Assume the Buck converter operates in CCM. The peak and valley inductor current are I_p and I_v, as shown in (4.29). The RMS current of inductor and switches are denoted as I_{RMS}^2(Inductor), $I_{HS\_RMS}^2$(Top FET), and $I_{LS\_RMS}^2$(Bottom FET), as shown in (4.30).

$$\begin{cases} I_p = I_o + \dfrac{(V_{in} - V_o)V_o}{2L_o f_s V_{in}} \\ I_v = I_o - \dfrac{(V_{in} - V_o)V_o}{2L_o f_s V_{in}} \end{cases} \tag{4.29}$$

$$\begin{cases} I_{RMS}{}^2 = \dfrac{1}{3}(I_p{}^2 + I_p I_v + I_v{}^2) = \dfrac{V_o{}^4 - 2V_{in}V_o{}^3 + V_{in}{}^2V_o{}^2 + 12I_o{}^2L_o{}^2V_{in}{}^2 f_s{}^2}{12L_o{}^2V_{in}{}^2 f_s{}^2} \\ I_{HS\_RMS}{}^2 = \dfrac{\dfrac{V_o}{V_{in}}}{3}(I_p{}^2 + I_p I_v + I_v{}^2) = \dfrac{V_o{}^5 - 2V_{in}V_o{}^4 + V_{in}{}^2V_o{}^3 + 12I_o{}^2L_o{}^2V_{in}{}^2 f_s{}^2 V_o}{12L_o{}^2V_{in}{}^3 f_s{}^2} \\ I_{LS\_RMS}{}^2 = \dfrac{1-\dfrac{V_o}{V_{in}}}{3}(I_p{}^2 + I_p I_v + I_v{}^2) = \dfrac{(V_{in}-V_o)(V_o{}^4 - 2V_{in}V_o{}^3 + V_{in}{}^2V_o{}^2 + 12I_o{}^2L_o{}^2V_{in}{}^2 f_s{}^2)}{12L_o{}^2V_{in}{}^3 f_s{}^2} \end{cases} \tag{4.30}$$

1) Conduction Loss

The conduction loss of Buck converter includes top and bottom FETs on-resistance losses P_{HS} and P_{LS}, body diode conduction loss P_{BD}, inductor DCR loss P_{DCR} and capacitor ESR loss P_{ESR}. They are independent of switching frequency. The equations are shown in (4.31). V_{BD} is the forward voltage drop of the body diode and t_d is the dead time between high-side and low-side switches.

$$\begin{cases} P_{HS} = I_{HS\_RMS}{}^2 R_{HS} \\ P_{LS} = I_{LS\_RMS}{}^2 R_{LS} \\ P_{DCR} = I_{RMS}{}^2 R_{DCR} \\ P_{ESR} = (\dfrac{I_p - I_v}{2})^2 R_{ESR} \\ P_{BD} = (V_{BD} I_p t_d + V_{BD} I_v t_d) f_s = 2V_{BD} I_o t_d f_s \end{cases} \tag{4.31}$$

The total conduction loss is shown in (4.32). Fig.4.7 plots the variation of conduction loss with input voltage. Since the conduction loss in Bottom FET increases with input voltage, while the conduction loss in Top FET decreases, the total conduction loss only has slight increase with input voltage.

$$P_{Con} = P_{HS} + P_{LS} + P_{DCR} + P_{ESR} + P_{BD} \tag{4.32}$$

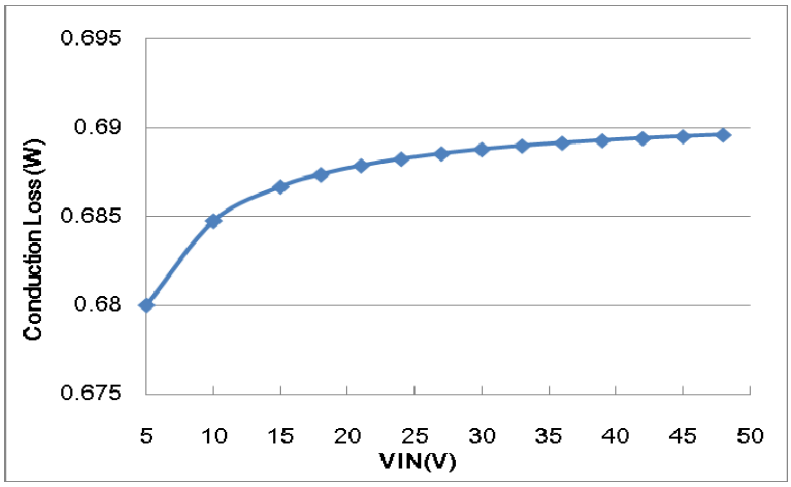

Fig.4.7 Conduction Loss vs. Input Voltage in Buck Converter (V_o=5V, I_{out}=2A)

2) Switching Loss

The switching loss in Buck Converter includes V-I overlapping loss, C_{oss} charging loss, Gate driver loss, and Reverse recovery loss. They are frequency dependent.

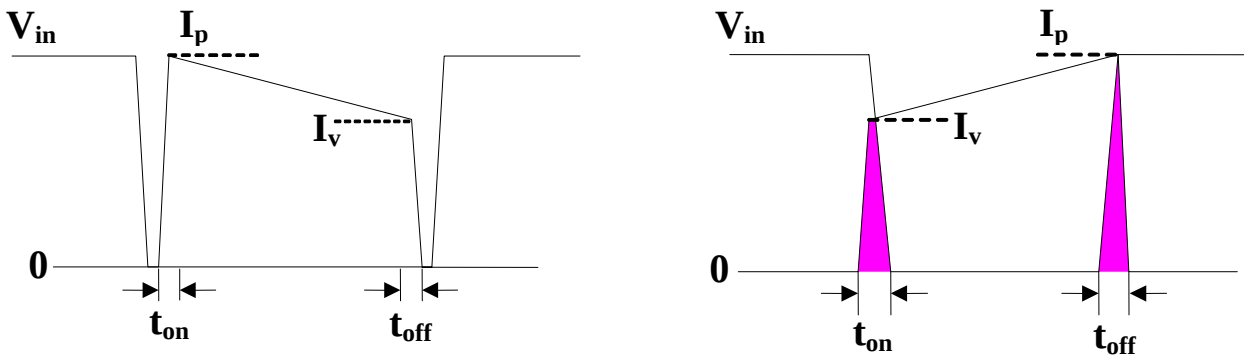

(a) Bottom FET (b) Top FET

Fig.4.8 V_{ds} and I_{ds} during Turn-On and Turn-Off of Switches

a. V-I Overlapping Loss

Fig.4.8 shows the voltage and current transitions during Turn-on and Turn-off of Top FET and Bottom FET. The Bottom FET is ZVS turn on and ZVS turn off due to the freewheeling body diode, so there is no turn-on and turn-off overlapping loss. For Top FET, during the turn-on process, V_{ds} begins to drop at the end of I_{ds} rising edge, therefore it is easy to get the expression of turn-on overlapping loss, as shown in (4.33).

$$P_{HS\_Turn-on} = \frac{1}{2} V_{in} I_v t_{on} f_s = \frac{1}{2} V_{in} (I_o - \frac{(V_{in} - V_o)V_o}{2L_o f_s V_{in}}) t_{on} f_s \tag{4.33}$$

During the turn-off process, the current begins to drop at the end of V_{ds} rising edge. The Turn-off overlapping loss is shown in (4.34).

$$P_{HS\_Turn-off} = \frac{1}{2} V_{in} I_p t_{off} f_s = \frac{1}{2} V_{in} (I_o + \frac{(V_{in} - V_o)V_o}{2L_o f_s V_{in}}) t_{off} f_s \tag{4.34}$$

Thereby, the loss due to the V-I overlapping can be obtained by (4.35).

$$P_{overlapping} = P_{HS\_Turn-on} + P_{HS\_Turn-off} \tag{4.35}$$

b. C_{oss} Charging Loss

Both of Top FET and Bottom FET in Buck converter have the same blocking voltage V_{in} when they are OFF. The total C_{oss} charging loss will be the sum of high side and low side C_{oss} charging loss, as shown in (4.36).

$$P_{Coss} = P_{Coss\_HS} + P_{Coss\_LS} = \frac{1}{2} (\frac{4}{3} C_{oss\_HS}) V_{in}^{\ 2} f_s + \frac{1}{2} (\frac{4}{3} C_{oss\_LS}) V_{in}^{\ 2} f_s \tag{4.36}$$

c. Gate Driving Loss

The gate driving loss in Buck converter includes the losses for driving Top FET and Bottom FET. The equation can be derived using (4.37).

$$P_{dr} = P_{dr\_HS} + P_{dr\_LS} = (C_{iss\_HS} + C_{iss\_LS})V_{gs}^{\ 2} f_s \tag{4.37}$$

d. Reverse Recovery Loss

Because of the existence of inductor in the Buck converter, the body diode of Bottom FET will be on during the dead time between Bottom FET turn-off and Top FET turn-on, which results in a reverse recovery loss, as shown in (4.38).

$$P_{rr} = V_{in} Q_{rr\_LS} f_s \tag{4.38}$$

$$P_{SW} = P_{overlapping} + P_{Coss} + P_{dr} + P_{rr} \tag{4.39}$$

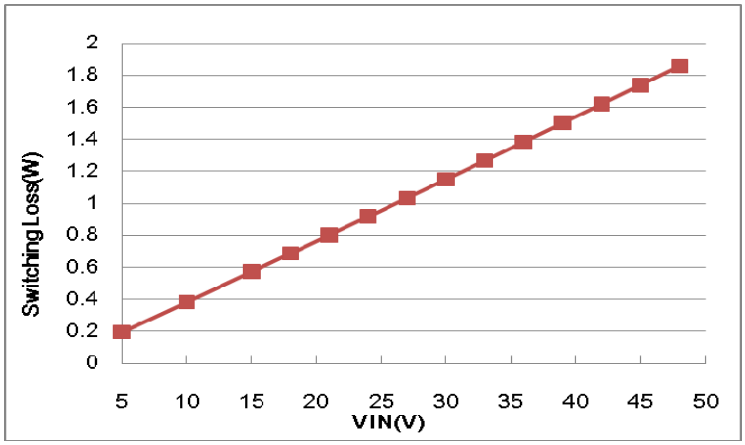

Fig.4.9 Switching Loss vs. Input Voltage in Buck Converter (V_o=5V, I_{out}=2A)

Finally, the total switching loss of Buck converter can be obtained using (4.39). Fig.4.9.

plots the switching loss over a wide input voltage. The switching loss is increasing quickly with the input voltage. The major two losses are V-I overlapping loss and diode reverse recovery loss.

Comparisons can be made by putting together the switching loss and conduction loss curves of 1/3x mode charge pump and singe Buck converter, as shown in Fig.4.10. It can be seen that the dominant loss in charge pump is conduction loss, and it decreases much faster than the increasing speed of switching loss when V_{in} increases. The situation is just reversed in Buck converter: the dominant loss is switching loss, and it increases much faster than conduction loss as V_{in} increases. Such a complimentary characteristic made it possible to get a better efficiency curve over a wide input range by combining the two converters, especially at a high input voltage.

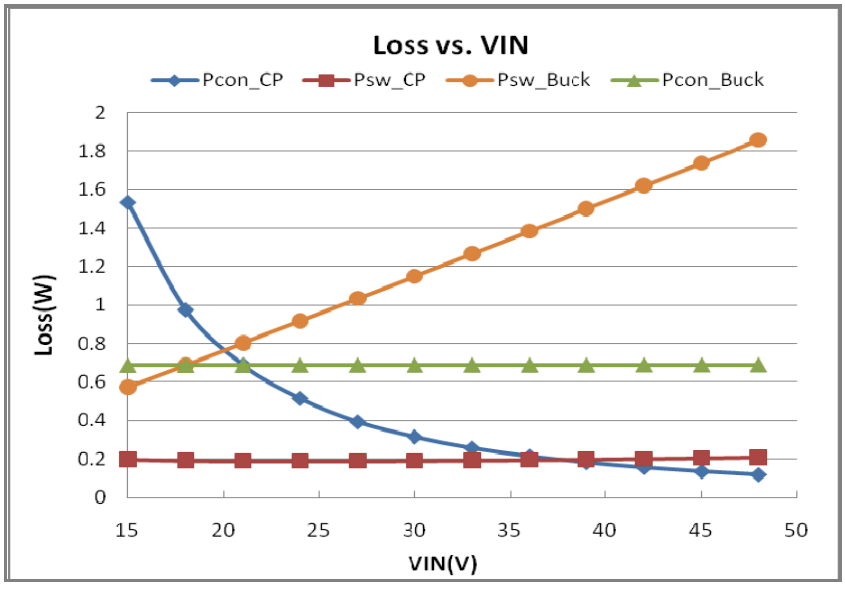

Fig.4.10 Losses vs. Input Voltage@P_o=10W

4.5 Efficiency Analysis of Charge-pump based Buck Converter

According to the loss analysis in section 4.3 and 4.4, the efficiency curves of multi-modes charge pump and single Buck converter can be plotted. Fig.4.11 (a) shows the efficiency vs. input voltage when the multi-modes charge pump is in 1x, 0.5x and 0.33x mode. Fig.4.11 (b) shows the efficiency curves of Buck converter when its input voltage range is reduced to half and one third of the original range. The efficiency of charge pump increases with V_{in} while the efficiency of Buck converter decreases with V_{in}. A 1/3x mode charge pump has a lower efficiency than 1x mode charge pump, but the efficiency difference will not be significant at a high input voltage. With only one third of the original input voltage range, the Buck converter can have a much better efficiency, especially when the original input voltage is high. The total efficiency when combining multi-modes charge pump and Buck converter is shown in Fig.4.12.

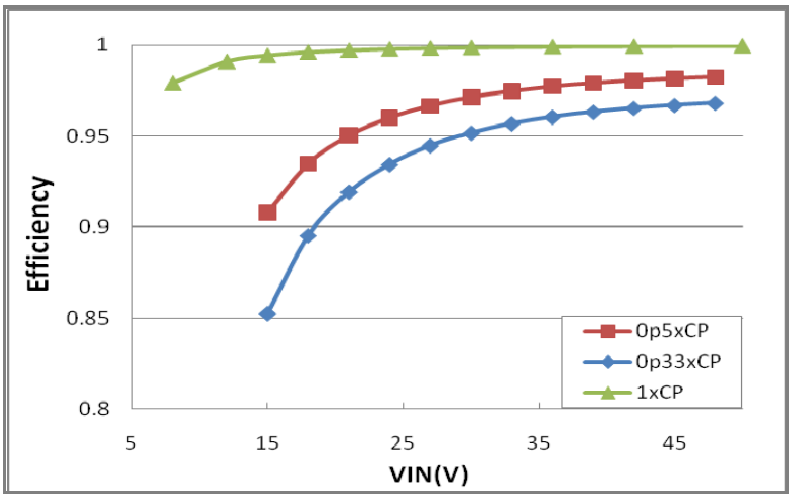

Fig.4.11 (a) Efficiency of Charge Pump at Different Modes

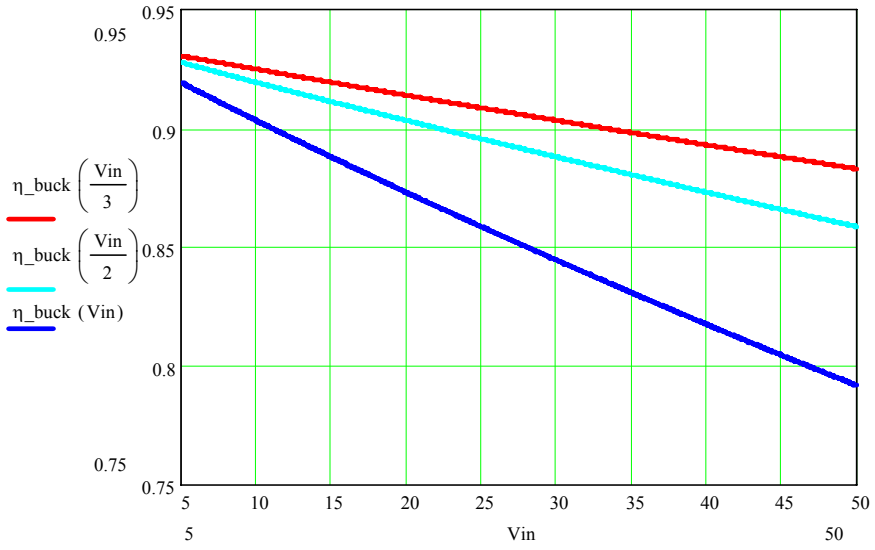

Fig.4.11 (b) Efficiency of Buck converter with Different Input Ranges

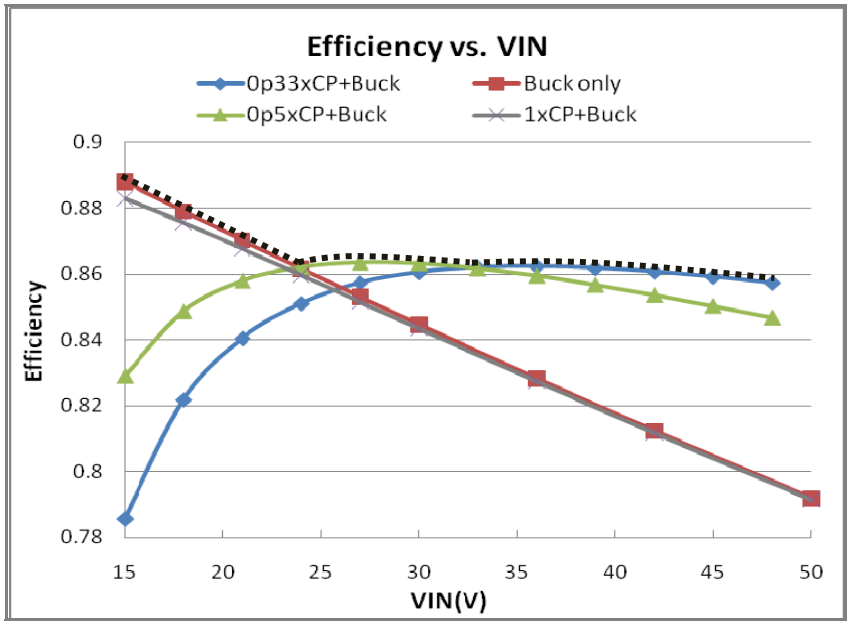

Fig.4.12 Efficiency of Charge Pump based Converters vs. Vin

It can be seen that the Buck converter with 1/3x mode charge pump has the highest efficiency at high input voltage while the Buck converter with 0.5x mode charge pump has the highest efficiency at medium input voltage. The Buck converter with 1x mode charge pump has a comparable efficiency to single Buck converter at low input voltage. Thus by changing the modes of charge pump according to the input voltage, the best efficiency curve can be achieved over wide input range, which is shown as the black dashed line. Compared with single buck converter, the overall efficiency can get greatly improved, especially from medium to high input voltage range.

If the input is a continuously changing voltage source, such as a battery, the controller can adaptively change the modes by comparing V_{in} with predetermined references. If the input is a loosely regulated front-end voltage Bus, the mode can also be manually switched according to the actual operation input voltage for the efficiency optimization.

4.6 Control Benefits of Charge-Pump based Buck Converter

For wide input range DC-DC converter, the loop gain can vary a lot with the input voltage and the compensator is often designed at its worst case. However, it is desired that converters have good performance over the entire input range, such as good output regulation and fast transient response. To compensate for input variations, feed forward control is usually used [52]. By varying the ramp amplitude according to the input voltage, constant loop gain,

bandwidth and phase margin can be achieved over the full input range. However, the implementation of feed forward control sophisticates the control part design. Current mode Buck converters will have better performance than voltage mode Buck converters when operating over a wide input range. In this section, the control benefits brought by using a multi-modes charge pump with a voltage/current Mode Buck converter will be discussed.

Since the multi-modes charge pump is unregulated, the transfer function will be the ratio of the output voltage to the input voltage, as shown in (4.40). It is a linear system and the low-frequency gain is determined by its conversion mode.

$$T_{CP} = \frac{v_{out}}{v_{in}} \tag{4.40}$$

1) Multi-mode charge pump Based Voltage mode Buck Converter

For voltage mode Buck converters, the type III compensator is usually used to improve the stability and bandwidth. It can be seen from (4.41), the closed loop gain T_v will directly depend on the input voltage V_{in}. The loop gains of a single voltage mode Buck converter and a Multi-mode charge pump based voltage mode Buck converter are plotted in Fig.4.13.

For the single Buck converter, the wider the input voltage range is, the more divergent the magnitude of loop gains will be. The phase plots are the same at any input voltage. It can be seen that with the same compensator, the maximum bandwidth variation can be 80% and the phase margin differs by 20 degrees.

$$T_v = H \cdot F_m \cdot G_C \cdot G_{vd} = \frac{V_{in}}{V_m} \frac{R_2}{R_1 + R_2} \frac{\omega_i}{s} \frac{(1+\frac{s}{\omega_{z1}})(1+\frac{s}{\omega_{z2}})}{(1+\frac{s}{\omega_{p1}})(1+\frac{s}{\omega_{p2}})} \frac{(1+R_{ESR}C_o s)}{(\frac{s}{\omega_0})^2 + \frac{1}{Q\omega_0}s + (1+\frac{R_{LS}}{R_L})} \qquad (4.41)$$

$$\left(\omega_0 = \frac{1}{\sqrt{L_o C_o}}, \quad Q = \frac{1}{\omega_0} \frac{1}{(\frac{L_o}{R_L} + C_o(R_{LS} + R_{DCR}))} \right)$$

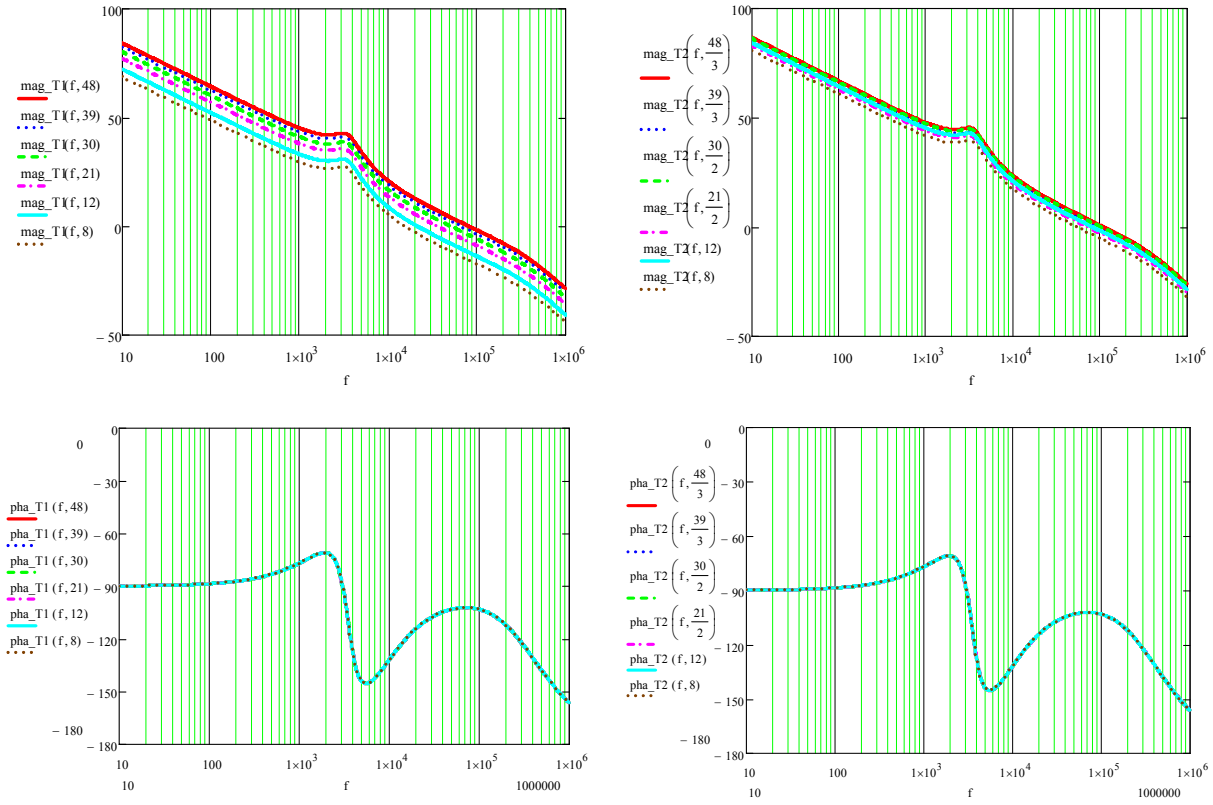

Fig. 4.13 Comparison of Loop-Gain Variations over Wide Input Range between Single Voltage Mode Buck converter(Left) and Multi-modes Charge-Pump based Voltage Mode Buck Converter(Right).

For the Buck converter with a multi-modes charge pump as the pre-stage, the input voltage range of Buck converter is reduced by 2/3. As a result, the loop gains at different input voltage become more centralized even without using feed forward control. The bandwidth variation is reduced from 80% to 40%, and the phase margin variation is within 5 degrees. The great reduction of variations on bandwidth and phase margin not only simplifies the compensator design but also improves the bandwidth at low input voltage. In the single Buck converter, the compensator is often designed around the highest input voltage (Worst case). The bandwidth can be very low at the lowest input voltage. However, when loop gains become centralized, the bandwidth can be pushed higher at low input voltage.

It also can be seen from the block diagram shown in Fig.4.14 that the existence of charge pump as the pre-stage of Buck converter will not affect the loop gain of total system since the added charge pump is out of the feedback loop. However, the G_{vd} of Buck converter will be changed because its input voltage is reduced by the charge pump.

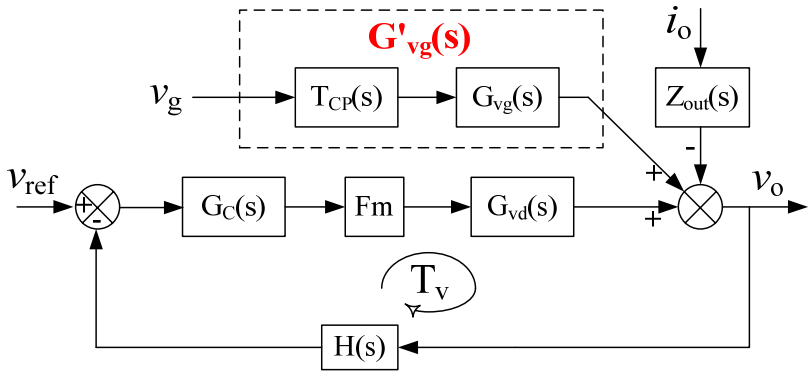

Fig.4.14 Block Diagram of Charge Pump Based Buck Converter in Voltage Mode

2) Multi-mode charge pump Based Current mode Buck Converter

For current mode Buck converter, a type II compensator is usually good for bandwidth improvement and stability. The loop gain equation is given in (4.42). The equation shows that the loop gain is a weak function of input voltage. It does not vary with input voltage at low frequency since the dominant pole only strongly depends on the output capacitor and the load resistor. However, it will vary with input voltage at high frequency. Fig.4.15 shows the loop gains of a single current mode Buck converter and a Multi-modes Charge Pump based current mode Buck converter at different input voltage. For the single Buck converter, although the loop gains at different input voltage are quite consistent below 100kHz, it begins to diverge at higher frequency. The situation is similar for Charge Pump base Buck converter but less divergence at higher frequency. Therefore, combining a multi-modes charge pump with a current mode Buck converter does not benefit the control as much as the voltage mode Buck converter because of the different mechanisms of voltage mode and current mode control. The block diagram is shown in Fig. 4.16. Similar to charge-pump based voltage-mode Buck converter, the loop gain will not be changed by adding the multi-modes charge pump to the Buck converter. Only the transfer function from V_{in} to V_{out} is changed, which becomes more concentrated as well.

$$T_i = H \cdot G_C \cdot G_{vc} = \frac{R_2}{R_1 + R_2} \frac{\omega_i}{s} \frac{(1+\frac{s}{\omega_{z1}})}{(1+\frac{s}{\omega_{p1}})} \frac{F_m G_{vd}}{1 + F_m (G_{id} + F_v G_{vd})} \tag{4.42}$$

$$(F_m = \frac{1}{M_a T_s},\ F_v = \frac{(1-2D)T_s}{2L_o},\ G_{id} = \frac{V_{in}}{R_L} \frac{(1+R_L C_o s)}{(\frac{s}{\omega_0})^2 + \frac{1}{Q\omega_0} s + (1+\frac{R_{LS}}{R_L})},\ G_{vd} = \frac{V_{in}(1+R_{ESR} C_o s)}{(\frac{s}{\omega_0})^2 + \frac{1}{Q\omega_0} s + (1+\frac{R_{LS}}{R_L})})$$

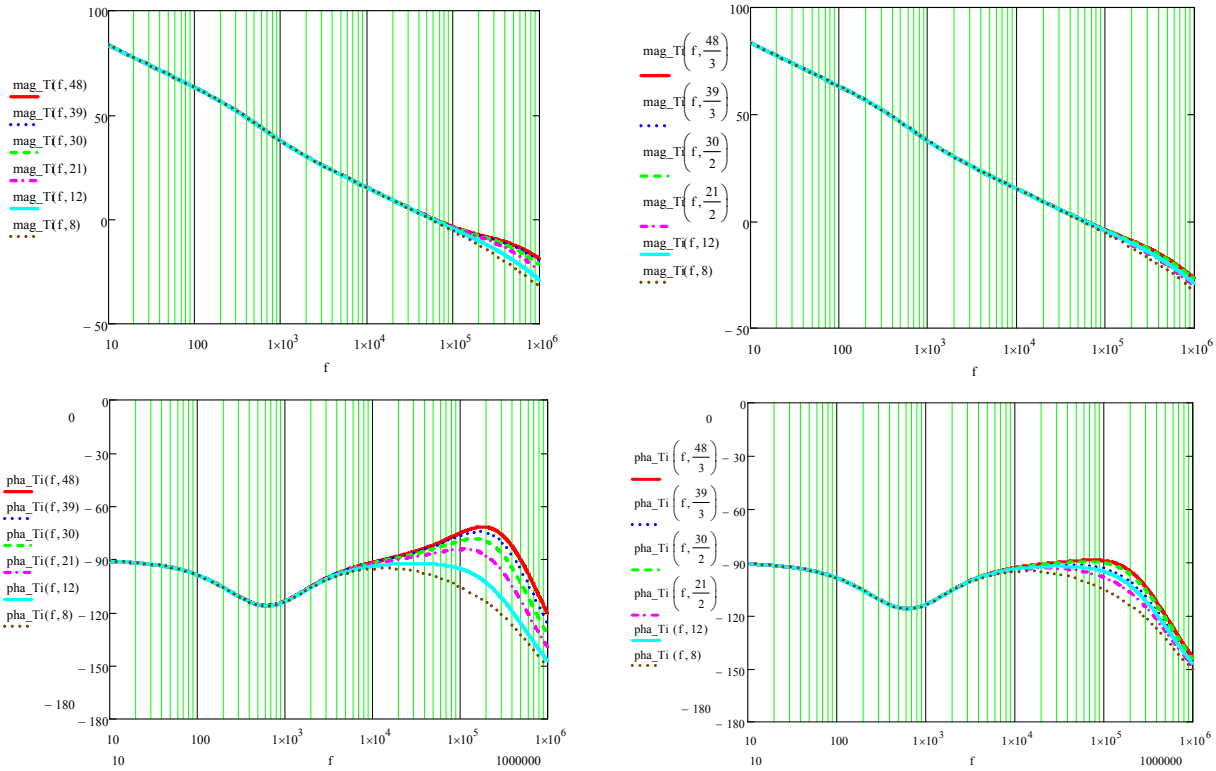

Fig.4.15 Comparison of Loop-Gain Variations over Wide Input Range between Single Current Mode Buck converter(Left) and Multi-modes Charge-Pump based Current Mode Buck Converter(Right).

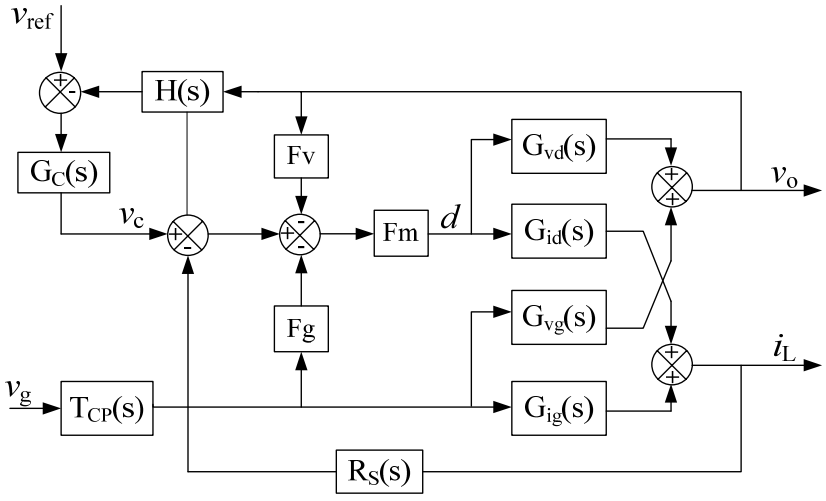

Fig.4.16 Block Diagram of Charge Pump Based Current Mode Buck Converter

In the Buck converter, the highest inductor current ripple I_{pp} appears at the maximum input voltage. When input voltage decreases, the ripple current decreases as well. Fig.4.17 shows the inductor current ripple comparisons between a single Buck converter and a multi-modes charge pump based Buck converter. If the maximum ripple current of the single Buck converter is normalized to one, then the ripple current in the charge pump based Buck converter can be reduced by 24%. The mode determines how much ripple will be reduced. At 1x mode, there is no change.

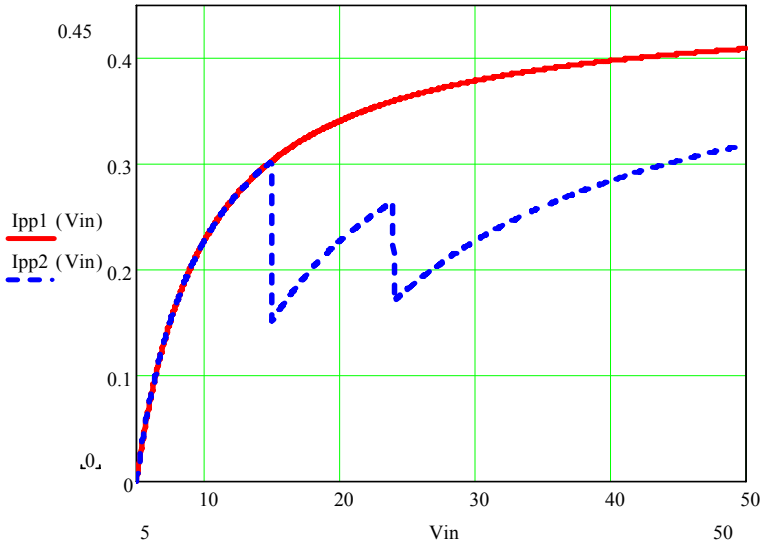

Fig.4.17 Inductor Current Ripple in Single Buck Converter (Red) and Multi-modes Charge Pump Based Buck Converter (Blue)

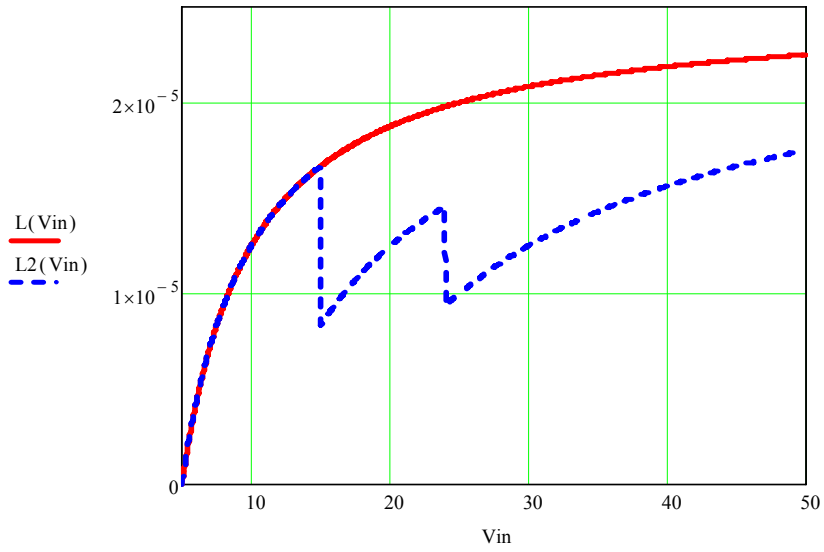

Fig.4.18 Minimum Inductance of Single Buck Converter (Red) and Multi-modes Charge Pump Based Buck Converter (Blue)

The minimum inductor value is determined based on the worst case when the current ripple is the largest. At high input voltage, duty cycle is low, and the peak-peak current will be high. To meet the ripple requirement, the minimum inductance at input=48V has the highest value over the entire input range and should be used as the reference for designing the inductor. Fig.4.18 shows the minimum inductance of single Buck converter and multi-modes charge pump based Buck converter. Compared with single Buck solution, the required inductance can be reduced by 24% when using multi-modes charge pump based Buck converter for same current ripple. Meanwhile, the reduction of inductance can benefit the control bandwidth and improve transient response.

4.7 Experiment Verifications

To verify the performance of the proposed solution, a 10W prototype is built. Since the charge pump is unregulated, its switching frequency can be selected lower than the Buck converter to improve light load efficiency. The circuit parameters are shown in Table 4.4.

Table 4.4 Parameters of Circuit under Test

Multi-Modes Charge Pump					**Single Buck Converter**			
MOSFETs	**f_s**	**C_f**	**C_o**		**Regulator**	**L_o**	**f_s**	**C_o**
Si2308BDS	200kHz	10μF	10μF*3		ISL8560	22μH	500kHz	470μF

The desired input range is 9-48V, and the output voltage is regulated to 5V with load current up to 2A. Fig.4.19 shows the efficiency curves of the single Buck converter and the charge-pump based Buck converter over the entire input range when I_{out}=1A. The mode change happens at the boundary of areas in different color. It can be seen that the efficiency of the single Buck converter drops fast as V_{in} increases; however the efficiency of the charge-pump based Buck converter drops much slower from medium to high voltage. Therefore, the overall efficiency has been greatly improved using charge-pump based Buck converter. The maximum efficiency improvement is 7%. Fig.4.20 shows the efficiency curves of a single Buck and a charge-pump based Buck converter over the entire load range when V_{in}=48V. The overall efficiency is also greatly improved, especially from medium to light

load condition. Without using any light load control method, the highest efficiency improvement is around 16% at light load.

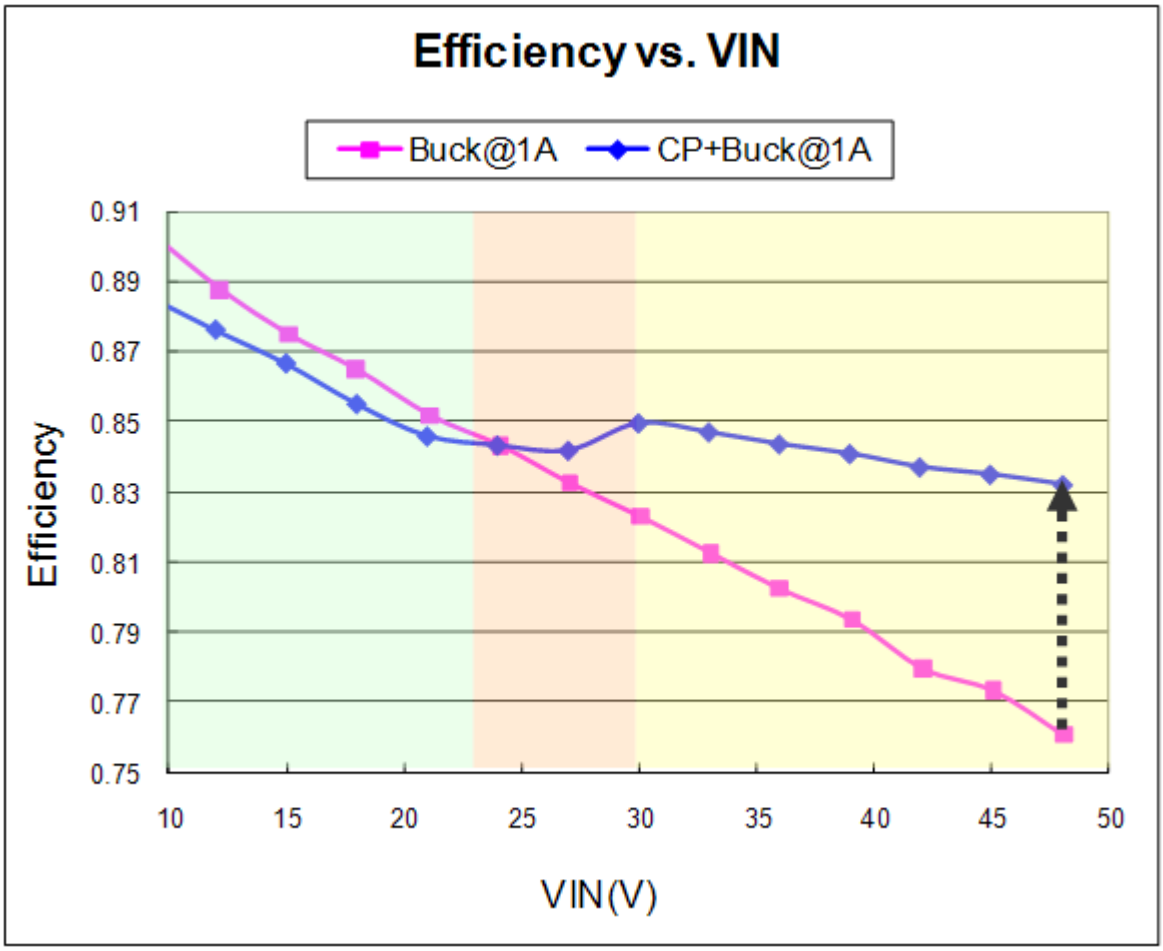

Fig.4.19 Tested Efficiency of Single Buck Converter and Multi-modes Charge Pump based Buck Converter over Wide Input Range

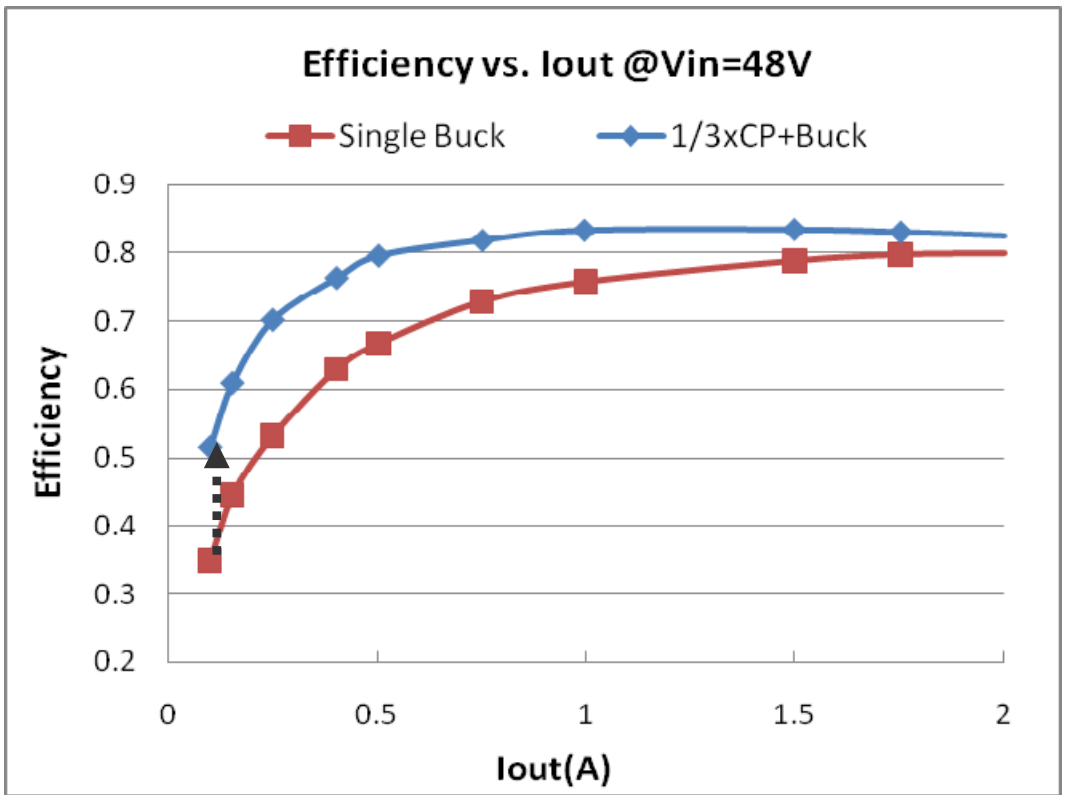

Fig.4.20 Tested Efficiency of Single Buck Converter and Multi-modes Charge Pump based Buck Converter vs. Load Current

4.8 Summary

A high efficiency charge-pump based wide input range DC-DC converter for automotive, telecommunication and industrial applications is proposed. Using an unregulated multi-modes charge pump as the pre-stage of a Buck converter to roughly step down high

voltage, low cost devices can be used in Buck converter and extremely low duty cycle is avoided. The overall efficiency can be improved by adaptively switching among different modes according to input voltage. In addition, the compensator design is simplified and inductance can be reduced due to reduced input range of Buck converter, which directly benefits the transient response. Both of the theoretical calculations and experiment results verify the performance of proposed solution.

Chapter 5. A High Efficiency Transformerless Step-up DC-DC Converter with High Voltage Gain for LED Backlighting Applications

5.1. Introduction

White LEDs are obtaining increasing popularity in small backlighting systems due to their falling costs, longer life, and smaller size [62]. To power the LEDs from a commonly used Li-Ion battery in hand-held devices, a step-up DC-DC converter is required. Boost converter is the typical solution to drive a number of LEDs in series [63-65]. There is no current mismatch issue since all the LEDs are sharing the same current. However, the number of LEDs in series is limited by the gain of Boost converter. An single boost converter (M= 1/(1-D)) would have to operate at a very high steady-state duty-cycle (> 90%) in order to provide a DC gain greater than 10. Such an extreme duty cycle will result a very high di/dt in the circuit, attracting large EMI. Operation at very high switching frequency may not be easy because it requires the control switch to switch fast enough otherwise the diode does not have enough time to conduct current. A latch-up problem can also happen due to the extreme duty cycle. There will be very little room left to increase the duty cycle further when there is a load step-up or line step-down transients. The output voltage varies with the number of LEDs

in series, and the efficiency varies as well. Switching loss increases very fast with output voltage, and results the lowest efficiency when driving maximum LED numbers. Therefore it is hard to maintain a high efficiency when driving different LED numbers.

Transformer based step-up converter can provide a high voltage gain, but it is bulky and expensive for applications that do not require isolation in the power flow. Its efficiency will also drastically degraded by losses associated with the leakage inductors [66, 67].

High gain can also be achieved by cascading two Boost converters [68]. By establishing an intermediate voltage between the two stages, extreme duty cycle can be avoided. However, an extra inductor is required, the control circuit is sophisticated and the total efficiency is low, which is the product of each stage.

An integration of a switched-capacitor (SC) circuit within a boost converter is proposed in [69, 70]. The charge pump is located in front of the Boost converter, but is lumped together with Boost converter by eliminating the capacitor between the two converters. The charge pump is unregulated therefore high efficiency can be achieved. However, the charge pump is at the high-current side, which results in a considerable conduction loss and degrades the total efficiency. In addition, the charge pump is only designed to have fixed conversion ratio, therefore optimal efficiency cannot be achieved for variable gain applications [71].

To overcome these drawbacks, this chapter proposed a multi-modes charge-pump based

step-up DC-DC converter for LED backlighting applications. An unregulated multi-modes charge pump is used as the post-stage of boost converter and performs a rough voltage conversion. The charge pump is located at the low current side therefore can have very high efficiency. It can switch between 1x, 2x and 3x conversion modes according to the number of LEDs in series. With the charge pump, the maximum output voltage of Boost converter is greatly reduced, therefore a low cost device can be used in Boost converter and extremely duty cycle is avoided. Although the two stages are cascaded, it is proved in this paper that the overall efficiency can be improved, especially at high gain. Without a transformer, the proposed charge-pump based step-up converter not only achieves high gain, but also improves the efficiency. Compared with bulky transformers, the added charge pump can be integrated with a Boost regulator (except flying capacitors) for single chip solution and saves space.

5.2. Operation of Proposed High Gain Transformerless Step-up Converter

The structure of the proposed step-up converter is shown in Fig.5.1. A current-mode Boost converter and a multi-modes step-up charge pump are cascaded. To generate the required voltage for the LED string and regulate the output current, the duty cycle of Boost converter is adjustable. The charge pump has a 50% fixed duty cycle. Three conversion modes (1x, 2x, 3x) are obtained by alternating the connections between switches and capacitors. The

topology transformations are shown in Table 5.1. Assume M1-M7 have equal on-resistance R_{on}, and ignore the ESR as they are much smaller than R_{on}. The steady-state output voltage of the charge pump can be obtained using state-space average analysis, which is similar to the derivations in Chapter 4. Unlike the Boost converter, the equations are different at each mode. The output equation of the cascaded converter therefore can be obtained by combining the equations of the Boost converter and Charge Pump converter. Table 5.2 shows the output equations of single Boost converter, multi-modes charge Pump, and multi-modes charge pump based Boost converter. Then the duty cycle can be solved according to input voltage, output voltage and load current. Fig.5.2 shows the duty cycle versus voltage gain of a single Boost converter (D_0x) and multi-modes charge pump based Boost converter(D_1x, D_2x, D_3x). The input voltage is fixed to 2.7V and the load current is 0.125A. At the same voltage

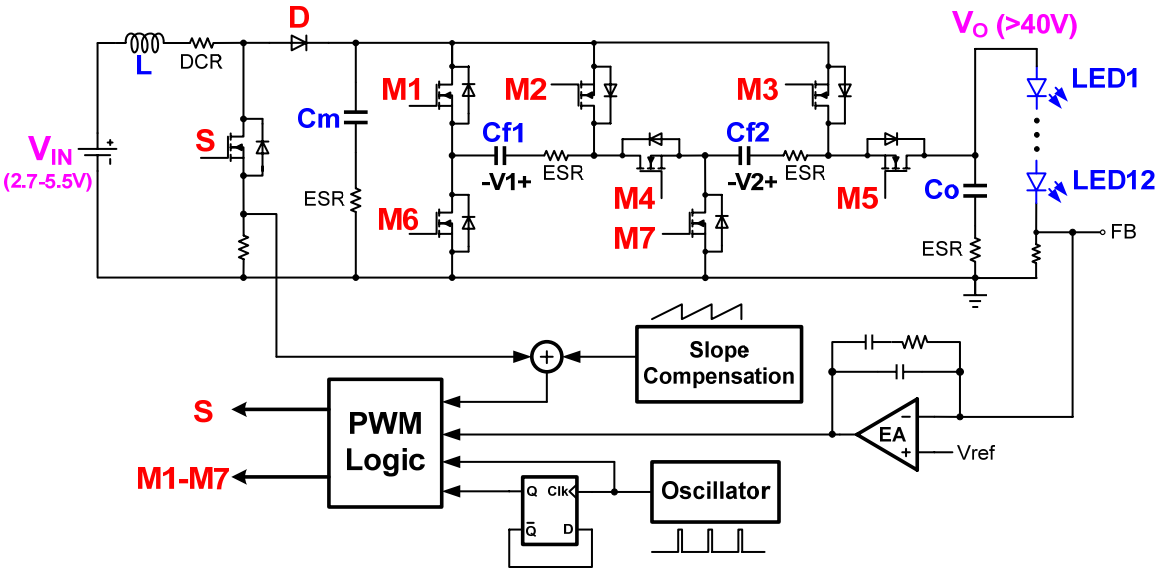

Fig.5.1 Proposed Multi-modes Charge-pump based High gain Step-up DC-DC converter

gain, the required duty cycle decreases when the conversion mode of charge pump increases. It can be seen that the duty cycle is 93% for a single Boost converter to generate 37V output (10 LEDs) and only 80% for a 3x charge pump combined with Boost converter. Extreme duty cycle at high gain is avoided.

Table 5.1 Topology Transformations of Multi-modes Step-up Charge Pump

Mode	0-0.5Ts	0.5Ts-Ts
3x	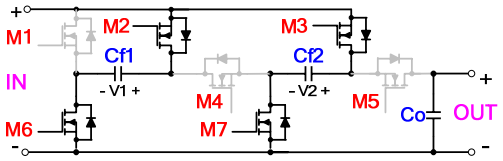	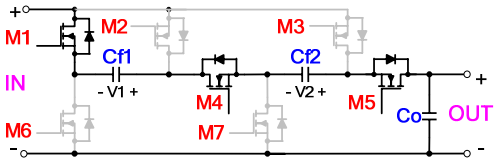
2x	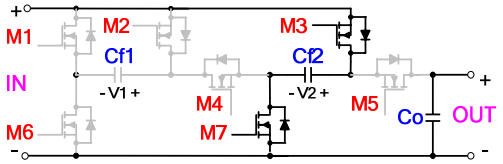	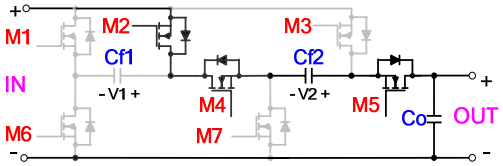
1x	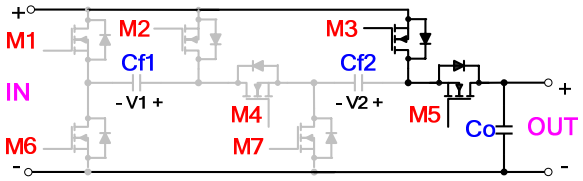	

Table 5.2 Output Equations for Each Stage

Modes	Boost Converter	Charge Pump	Total System
3x	$V_{OUT}=\frac{V_{IN}}{1-D}-V_d-\frac{R_{DCR}+D\cdot R_{son}}{(1-D)^2}I_o$	$V_{OUT}=3V_{IN}-14I_oR_{on}$	$V_{OUT}=3\frac{V_{IN}}{1-D}-3V_d-(9\frac{R_{DCR}+D\cdot R_{son}}{(1-D)^2}+14R_{on})I_o$
2x		$V_{OUT}=2V_{IN}-10I_oR_{on}$	$V_{OUT}=2\frac{V_{IN}}{1-D}-2V_d-(4\frac{R_{DCR}+D\cdot R_{son}}{(1-D)^2}+10R_{on})I_o$
1x		$V_{OUT}=V_{IN}-2I_oR_{on}$	$V_{OUT}=\frac{V_{IN}}{1-D}-V_d-(\frac{R_{DCR}+D\cdot R_{son}}{(1-D)^2}+2R_{on})I_o$

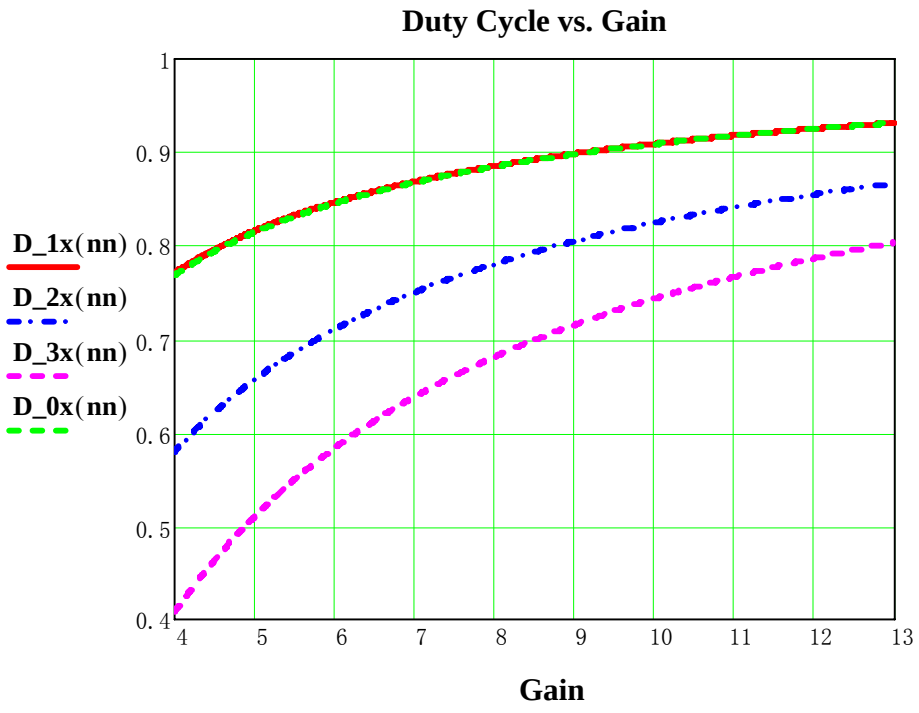

Fig.5.2 Duty Cycle vs. Gain

5.3. Theoretical Efficiency Analysis

When driving a LED string using a single Boost converter, the output voltage will increase with the number of LEDs in series. LEDs are current-driven devices and the preferred driving method is to directly regulate the driving current, this eliminates changes in current due to variations in forward voltage. Since the current is regulated, the output power will go up with the number of LEDs in series. Assume Boost converter operates in CCM. According to V_{in},

V_{out} and output current, the peak inductor current I_p and the valley current I_v can be solved, as shown in (5.1).

$$\begin{cases} I_p = \dfrac{2I_oL_of_sV_o^2 + V_oV_{in}^2 - V_{in}^3}{2L_oV_{in}V_of_s} \\ I_v = \dfrac{2I_oL_of_sV_o^2 - V_oV_{in}^2 + V_{in}^3}{2L_oV_{in}V_of_s} \end{cases} \tag{5.1}$$

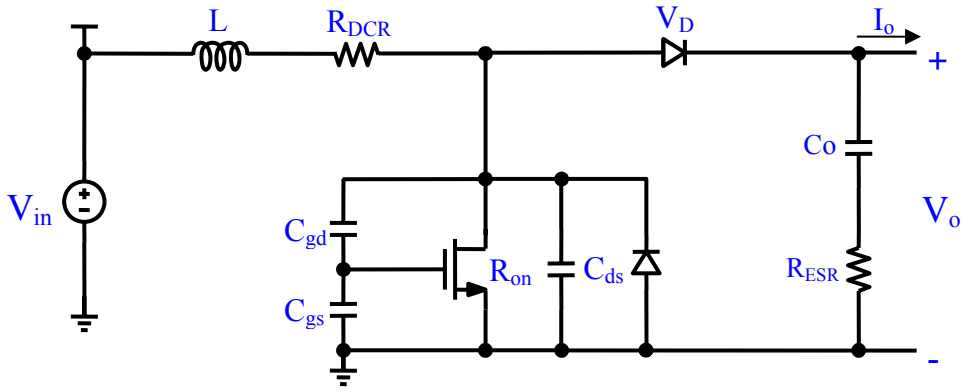

Fig.5.3 Power Stage of Boost Converter

Similar to a Buck converter, we can also classify the loss of the Boost converter into conduction loss and switching loss according the current obtained in (5.1). The loss breakdown of a single Boost converter is shown in Table 5.3 In order to see the variation trends of the losses with the output voltage, Fig.5.4 plots the curves of conduction loss and switching loss versus the output voltage. When the output voltage is increasing and the load current is regulated to be a constant, both of conduction loss and switching loss increase. However, switching loss increases much faster and becomes dominant at high output voltage.

Table 5.3 Loss breakdown of Boost Converter

Loss	Category	Boost Converter
Conduction Loss	On-Resistance	$P_{ron}=(V_o-V_{in})(I_p^2+I_pI_v+I_v^2)R_{on}/3V_o$
	Diode	$P_D=V_DI_o$
	DCR + ESR	$P_{DCR}=(I_p^2+I_pI_v+I_v^2)R_{DCR}/3$ $P_{esr}=(V_{in}(I_p^2+I_pI_v+I_v^2)/3V_o-I_o^2)R_{esr}$
Switching Loss	Turn-on	$P_{Turn\text{-}on}=\frac{1}{2}V_oI_vt_{on}f_s$
	Turn-off	$P_{Turn\text{-}off}=\frac{1}{2}V_oI_pt_{off}f_s$
	Coss charging	$P_{Coss}=\frac{1}{2}(\frac{4}{3}C_{oss})V_o^2f_s$
	Gate Driver	$P_{dr}=C_{iss}V_{gs}^2f_s$
	Reverse Recovery	$P_{rr}=V_oQ_{rr}f_s$

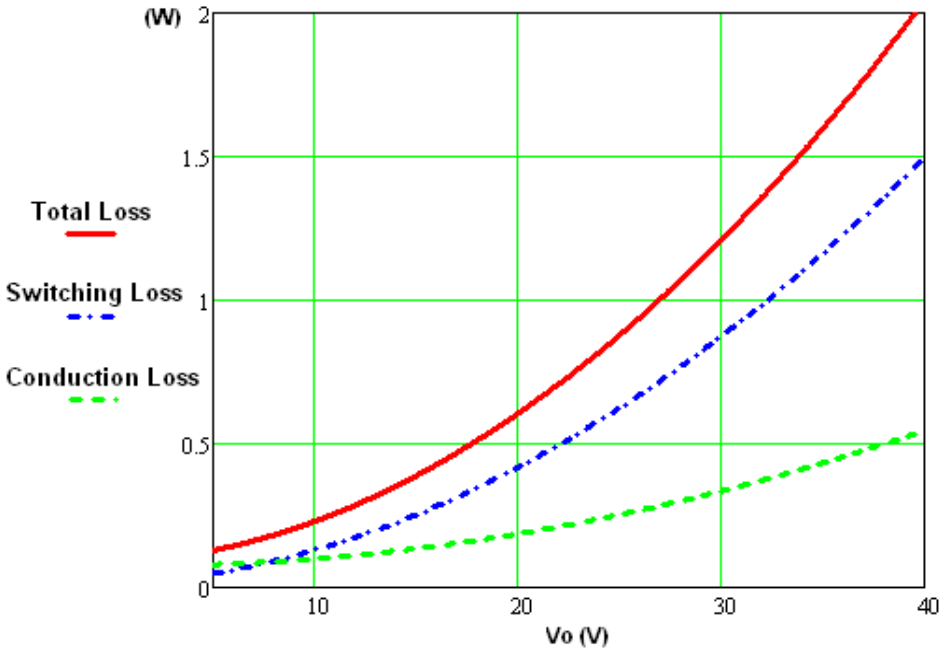

Fig.5.4 Loss vs. Output Voltage (Boost Converter)

As a contrast, the multi-modes charge pump also needs to be analyzed in order to see the trend of losses versus the output voltage. Using the similar methodology shown in Chapter 4, the equations of charging and discharging current through flying capacitors can be derived. Based on the equations, the RMS, peak and valley value of charging and discharging current are calculated, which are denoted as I_{Ch_RMS}, I_{Ch_p}, I_{Ch_v}, I_{Dis_RMS}, I_{Dis_p} and I_{Dis_v} respectively. Table 5.4 shows the loss breakdown of a 3x mode charge pump. For a fair comparison, assume the charge pump and Boost converter are outputting the same power. The calculated switching loss and conduction loss versus output voltage are plotted in Fig.5.5. It can be seen that the dominant loss in the charge pump is conduction loss and does not change with output voltage since the LED current is regulated instead of the output voltage. The switching loss is increasing, but much slower than that in a Boost converter.

Table 5.4 Loss breakdown of 3x mode Charge Pump

Loss	Category	3x Charge Pump
Conduction Loss	On-Resistance	$P_{ron}=I_{Ch\_rms}^{2}4R_{on}+I_{Dis\_rms}^{2}3R_{on}$
	ESR	$P_{esr}=(I_{Ch\_rms}^{2}+I_{Dis\_rms}^{2})2R_{esr}+I_{Co\_rms}^{2}R_{esr}$
Switching Loss	Turn-on	$P_{Turn\text{-}on}=\frac{1}{18}(4I_{Ch\_p}+6I_{Dis\_p})V_o t_{on} f_s$
	Turn-off	$P_{Turn\text{-}off}=\frac{1}{18}(4I_{Ch\_v}+6I_{Dis\_v})V_o t_{off} f_s$
	Coss charging	$P_{Coss}=\frac{1}{2}(\frac{4}{3}C_{oss})(\frac{16V_o^{2}}{9})f_s$
	Gate Driver	$P_{dr}=7C_{iss}V_{gs}^{2}f_s$

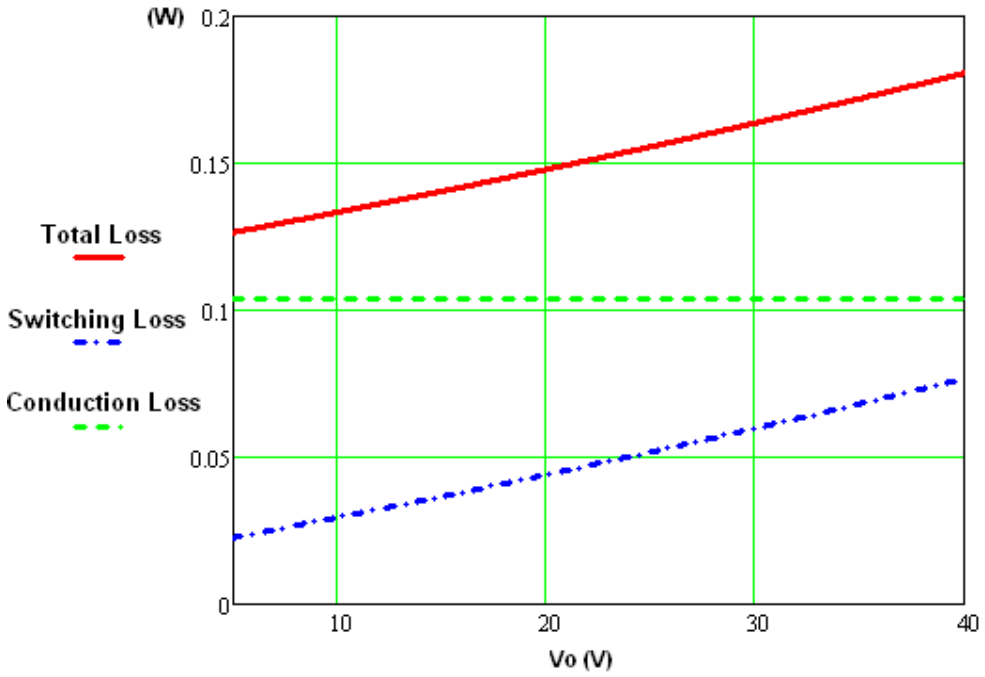

Fig.5.5. Loss vs. Output Voltage (3x Mode Charge Pump)

Due to different characteristics of a Boost converter and charge pump, the cascading solution can benefit the overall efficiency. It utilizes the low-switching loss feature of the charge pump and minimizes the conduction loss by moving it at the low current side. It reduces the switching loss of the Boost converter by moving it to the low voltage side. Besides, same current rating but lower voltage rating device can be used by the Boost converter to further reduce the switching loss and conduction loss. A Boost converter paired with a charge pump having small transistors with a lower current rating can be implemented.

Fig.5.6 shows the comparisons of efficiency among different combinations of multi-modes charge pump and Boost converter when driving a LEDs string from a minimum battery

voltage. It can be seen that Boost converter with 3x mode charge pump has the highest efficiency at high output voltage while Boost converter with 2x mode charge pump is the best for medium output voltage. Boost converter with 1x mode charge pump has a comparable efficiency to single Boost converter at low output voltage. By adjusting the modes of charge pump according to the output voltage requirement, a best efficiency curve can be achieved when driving different numbers of LEDs, as shown in the gray line. Compared with single Boost converter, the maximum efficiency improvement is 10% at 40V output (10-11 LEDs).

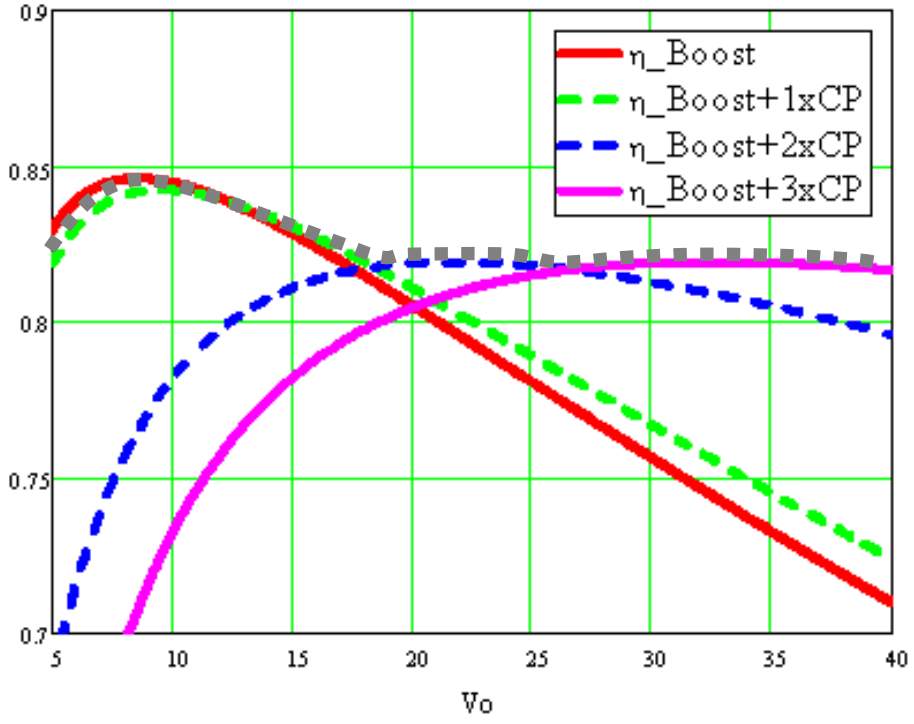

Fig.5.6. Efficiency vs. Output voltage @Vin=2.7V, Io=125mA.

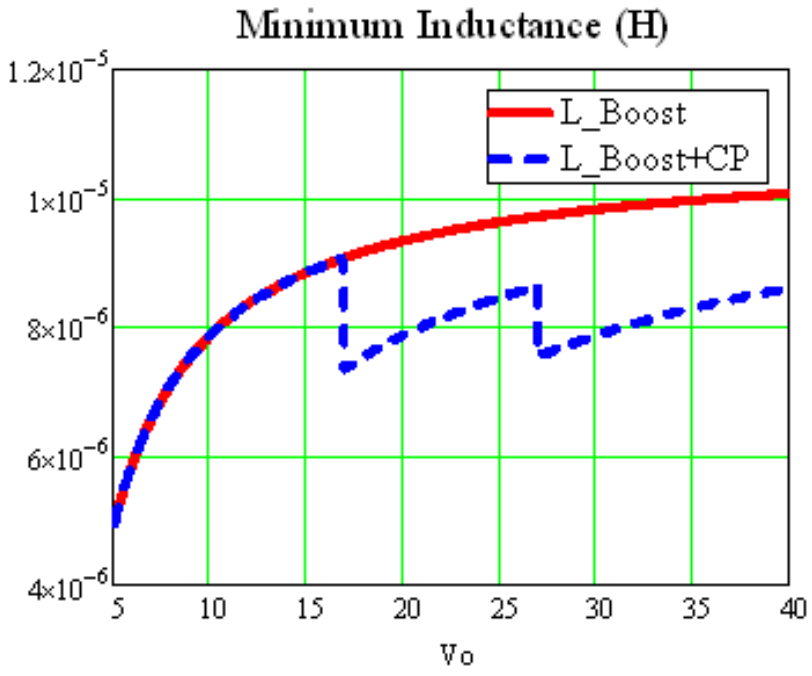

Fig.5.7. Minimum Inductance vs. Vo @Vin=2.7V, Io=125mA

On the other hand, the inductor value can be reduced to achieve the same ripple requirement by cascading a multi-modes charge pump with a Boost converter. For a given input voltage, the inductor ripple current is decided by the duty cycle and inductor value. From Fig.5.2, the required duty cycle of a Boost converter cascading with a multi-modes charge pump is less than that of a single Boost converter, thus the minimum inductance can be reduced. Fig.5.7 shows that the minimum inductance is reduced by 15% due to the existence of the charge pump. With reduced duty cycle and inductance, the transient response will also be benefited by the two-stage cascaded solution.

5.4. Experiment Verifications

To verify the performance of proposed solution, a prototype is built to generate up to 40V from a single lithium battery voltage (2.7-5.5V), as shown in Fig.5.8. The circuit parameters are shown in Table 5.5. A string of twelve white power LEDs will be the load of designed high gain step-up converter. Each LED has a typical 3.6V forward voltage and 120mA DC forward current. An efficiency comparison between a single high-voltage (60V) Boost converter and a low-voltage (30V) Boost converter cascaded with multi-modes charge pump are performed.

Fig.5.9 shows the node voltages in designed cascaded converter. It can be seen that the output voltage reaches 30V while the input voltage is 3.5V. The multi-modes charge pump operates at 3x mode. Fig.5.9 (a) shows the node voltages of flying capacitor Cf1 while Fig.5.9 (b) shows node voltages of flying capacitor Cf2. Fig.5.9 (c) shows measured PWM signals in the Boost converter and the Charge Pump. The Boost converter operates at 1MHz with 70.49% duty cycle while the Charge Pump operates at 500 kHz with 50% duty cycle.

For generating an output voltage above 20V from a 2.7V input, the duty cycle of a single Boost converter needs to always stay above 90%. The duty cycle is 96% when the output voltage is 38V. The duty cycle of designed cascaded converter is much better, which always below 90%. The duty cycle is only 84% when the output voltage is 39V. The tested duty cycle variation with output voltage is shown in Fig.5.10.

Fig.5.11 shows the efficiency variation with the output voltage for a single Boost converter and a Boost converter cascaded with a multi-modes charge pump. The efficiency of a single

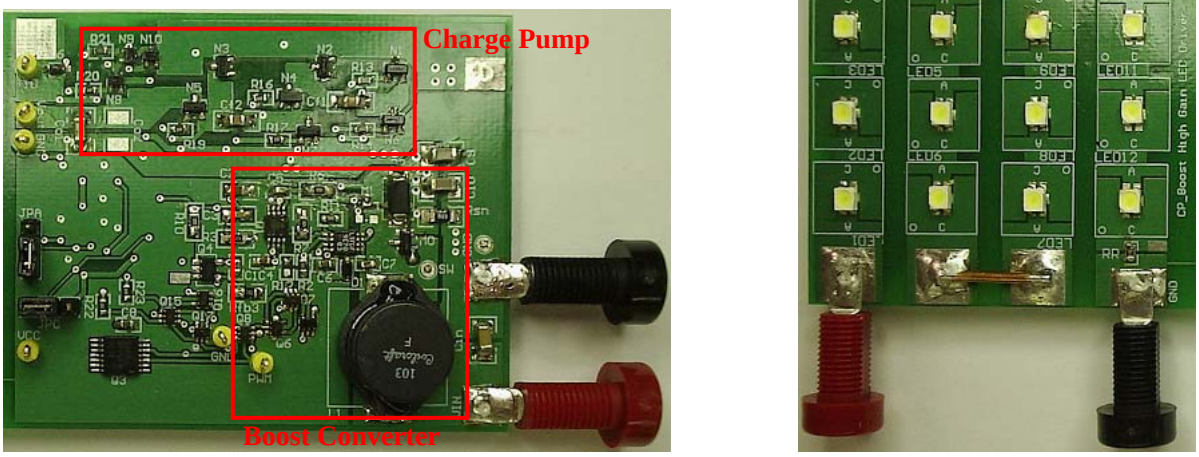

(a) High Gain Boost LED Driver (b) White LED String

Fig.5.8. Designed High Voltage Gain Transformerless LED driver.

Table 5.5 Primary Parameters of Circuit under Test

Charge Pump Based Boost Converter						**Single Boost Converter**			
	MOSFETs	**f_s**	**C_f/L_o**	**C_o**		**MOSFET**	**f_s**	**L_o**	**C_o**
Charge Pump	IRLML2060 (60V, 1A)	500kHz	1μF	2.2uF		Si3458BDV (60V/3.6A)	1MHz	10μH	2.2uF
Boost	Si2306BDS (30V/3.5A)	1MHz	10μH	2.2uF					

Boost converter drops when driving more than 4 LEDs and is only 72.5% when generating a 38V driving voltage. Using a multi-mode charge pump, the efficiency can be improved by increasing the conversion mode when the number of LEDs increases. It can be seen that the efficiency curve is almost flat when the generated driving voltage is from 20V to 40V. Therefore, significant improvement can be achieved when driving more than 7 LEDs. The

efficiency is 83% when driving 11 LEDs, which is 10.5% improvement comparing with the single Boost converter. One drawback is that the mode transition between 1x and 2x mode happens around 17V since the Boost stage using 30V device, so the efficiency is lower than the single Boost converter around that point.

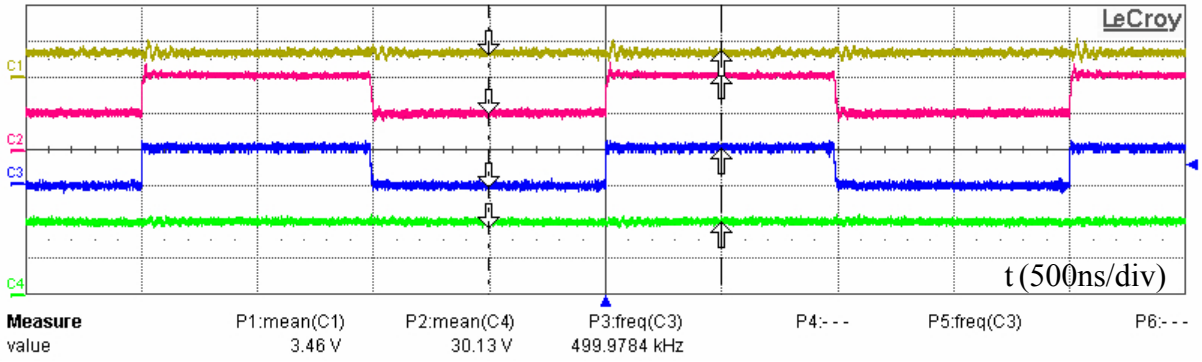

CH1: V_{in} (5V/div); CH2: V_{Cf1+} (10V/div); CH3: V_{Cf1-} (10V/div); CH4: V_o (15V/div)

(a) Node Voltages of Flying Capacitor Cf1

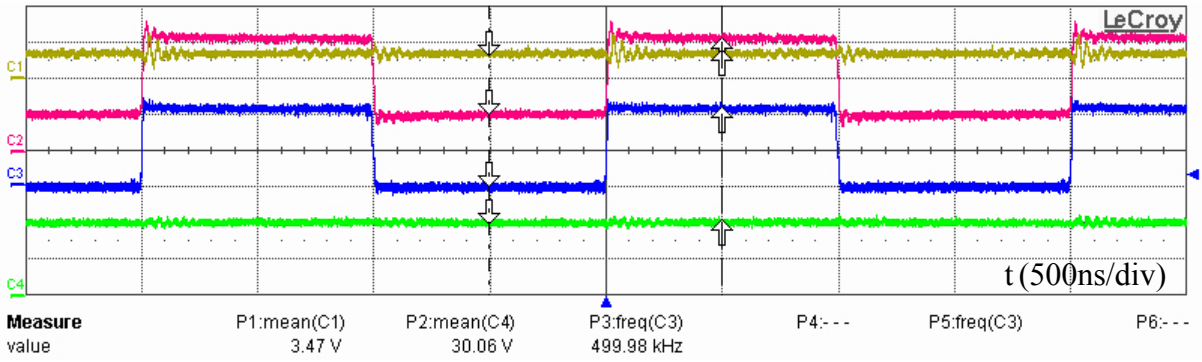

CH1: V_{in} (5V/div); CH2: V_{Cf2+} (10V/div); CH3: V_{Cf2-} (10V/div); CH4: V_o (15V/div)

(b) Node Voltages of Flying Capacitor Cf2

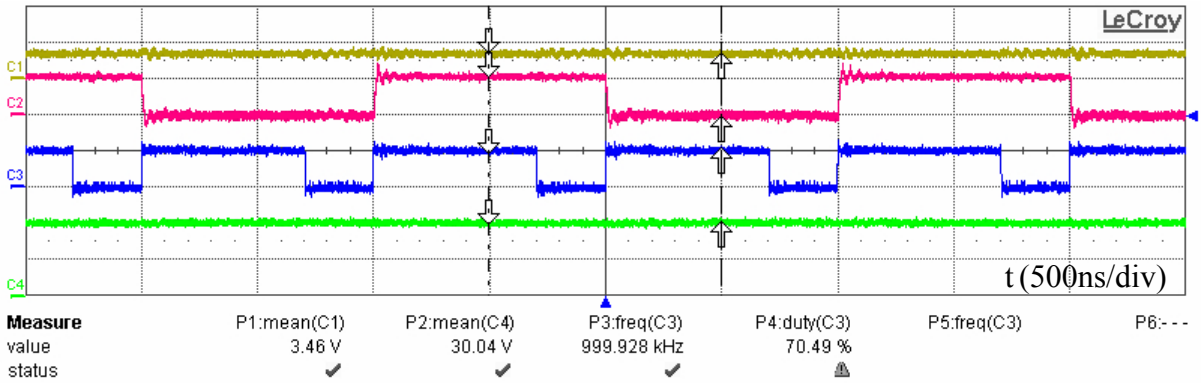

CH1: V_{in} (5V/div); CH2: V_{PWM_CP} (5V/div); CH3: V_{PWM_BOOST} (5V/div); CH4: V_o (15V/div)

(c) PWM Signals of Boost Converter and Charge Pump Converter

Fig.5.9. Node Voltages in Designed Boost LED Driver (V_{in}=3.5V, V_o=30V, I_{out}=120mA)

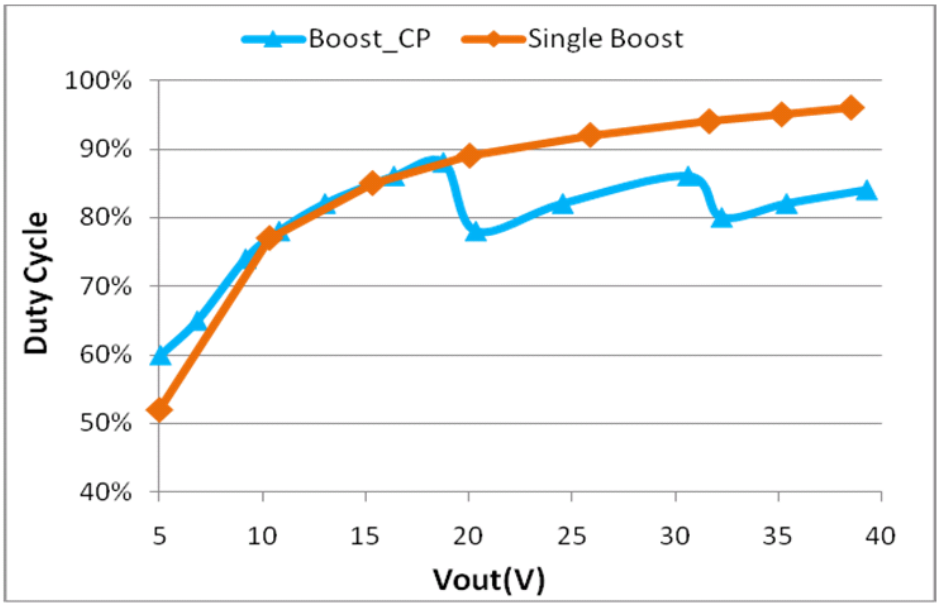

Fig.5.10. Duty Cycle vs. Output Voltage (V_{in}=2.7V, I_{out}=120mA)

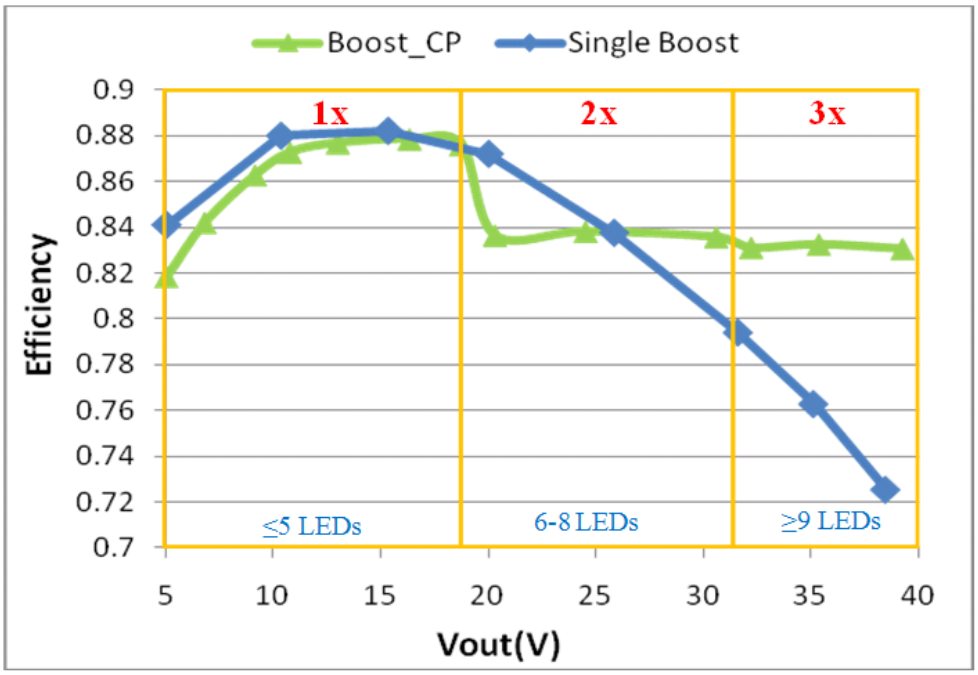

Fig.5.11. Efficiency Comparison between two High Voltage Gain LED Drivers.

(V_{in}=2.7V, I_{out}=120mA)

5.5. Summary

A high voltage gain step-up DC-DC converter is proposed for LED backlighting applications. A multi-modes step-up charge-pump is cascaded with a Boost converter to achieve a high voltage gain. The charge-pump is unregulated and can switches between 1x, 2x, and 3x modes according to the output requirement. The LED current is regulated by the Boost converter. The charge pump is located at the low current side therefore can have very high efficiency. The Boost converter is moved to the low voltage side and operates at a lower

duty cycle comparing with the single stage solution, thus the efficiency is improved. Without using transformers, the proposed solution can achieve high voltage gain as well as high overall efficiency. Theoretical efficiency derivations and experiment results have been given to verify the proposed solution.

Chapter 6. Conclusions and Future Work

6.1. Conclusions

In low power portable applications, charge pump regulators are considered as an ideal solution for their compact sizes and low cost. However, traditional charge pumps are not very efficient for battery powered applications because of the wide input voltage variation and output voltage regulation. In addition, the power rating of charge pump is very limited due to its huge conduction loss at high output current.

For automotive system, telecommunication systems and industry applications, the input voltage varies much wider than in portable applications. A power supply that can operate under a very wide input voltage range is a must for these applications. The most popular non-isolated topology of wide input DC-DC converter, Buck regulator, usually shows a low efficiency at high input voltage. In addition, high input-to-output step-down ratio creates significant challenges for the PWM controller design due to extremely narrow PWM pulses.

Similarly, converters that are required to generate a wide output voltage range also have the issues of low efficiency and extreme duty cycle at high output voltage, such as the LED

driver which drives a long LED string. A Boost converter is the preferred solution to drive LEDs in series in order to avoid current mismatch between different LEDs. However, it has difficulty in generating a very high voltage gain and the efficiency is also degraded at high output voltage.

It is the purpose of this work to develop high efficiency charge pump based DC-DC converters with wide input and output range.

The contributions of this work include:

1) Proposed a multi-modes regulated charge pump with improved efficiency over wide input and load range for portable applications. By alternating the switch network, it can realize 2x, 1.5x, and 1.33x conversion modes over a wide input range (2.7-4.5V). During each mode, the output voltage is regulated by a controlled current source. The regulated charge pump is designed for a very wide load range (10mA to 500mA).

A hybrid control scheme is proposed and analyzed to achieve a high efficiency over a wide load range. When the load current decreases to light load condition, device segmentation control is used; when the load current further decreases, pulse skipping modulation is used in addition to device segmentation. By using proposed hybrid control scheme, the gate driver and switching loss at light load can be greatly reduced, and improves the light load efficiency.

Due to the hybrid control scheme, the small signal model and stability analysis for the multi-modes charge pump are derived to provide a reference for compensator and ensure the

stability over wide input range and load range.

2) Proposed the structure of charge-pump based Buck converter for wide input range applications. The first stage is a multi-modes charge-pump and the second stage is a synchronous buck converter. The charge-pump is unregulated and adaptively switches between 1x, 0.5x, and 0.33x modes according to input voltage. It does the rough voltage conversion while buck converter does the fine voltage regulation.

Theoretical efficiency analysis and comparisons between multi-modes charge-pump and synchronous Buck are given. As they exhibit different efficiency tendencies within the same input range, it is proved that the total efficiency is improved by combining them, especially at high input voltage.

Evaluate the control benefits of multi-modes charge pump based Buck converter with wide input range. The small signal model of charge pump-based Buck converter at voltage and current mode are derived. The gain, bandwidth, and phase margin are improved compared with that of single Buck converter. The output filter size can also be reduced.

3) Proposed a high gain transformerless converter for LED backlight applications by extending the concept of the charge-pump based Buck converters.

As a conclusion, charge pump based DC-DC converter is a good solution for wide input/output range applications. A Multi-modes charge pump can be used solely for portable applications and achieve a performance comparable with inductor-based converters.

Meanwhile, by combining with inductor-based PWM DC-DC converters, it also provides a possible solution for applications having a wide conversion ratio to improve the overall performance.

6.2. Future Work

Charge pump itself has poor regulation ability, but can have some advantages when combined with PWM DC-DC converters. More future work can be done towards this direction.

1) In specific applications that require both step-up and step-down functions and have a very wide conversion gain range, a multi-modes charge pump can also be combined with Buck-Boost converter for efficiency optimization.

2) The structures of step-up multi-modes charge pump and step-down multi-modes charge pump are symmetrical. Similarly, the structures of Buck converter and Boost converter are symmetrical as well. Therefore, the multi-modes charge pump based DC-DC converter can also be considered a possible solution for bidirectional converters that require a very wide conversion ratio.

References

[1][Online] Available: http://www.apple.com/ipad/

[2]Maksimovic, D.; Dhar, S.; “Switched-Capacitor DC-DC Converters for Low-power On-Chip Applications,” 1999 IEEE 30th Annual Power Electronics Specialists Conference, PESC 99, Vol.1, Page(s):54-59, Aug 1999.

[3]Mathieu Renaud, Yves Gagnon, “Inductorless versus Inductor-Based Integrated Switching Regulators: Bill Of Material, Efficiency, Noise, and Reliability Comparisons” Intégration Dolphin Inc.

[4]Lingyin Zhao, Jinrong Qian, “DC-DC Power Conversions and System Design Considerations for Battery Operated System”, Texas Instruments. [Online]Available: http://focus.ti.com/download/trng/docs/seminar/Topic%206%20-%20DC-DC%20Power%20Conversion%20and%20System%20Design%20Considerations%20for%20Battery%20Operated%20System.pdf.

[5]Thiele, G.; Bayer, E.; “Current Mode Charge Pump: Topology, Modeling and Control”, 2004 IEEE 35th Annual Power Electronics Specialists Conference, PESC 2004, Vol.5, Page(s): 3812-3817, Jun 2004.

[6]Bayer, E; Schmeller, H, “A High Efficiency Single-Cell Cascaded Charge Pump Topology-the competitive alternative to inductive boost converters”, 2001 IEEE 32nd

Annual Power Electronics Specialists Conference, PESC 2001, Vol. 1, Page(s): 290-295, Jun 2001.

[7]Favrat, P.; Deval, P.; Declercq, M.J.; “A High-Efficiency CMOS Voltage Doubler,” IEEE Journal of Solid-State Circuits, Vol.33, Issue 3, Page(s):410-416, Mar 1998.

[8]Jae-Youl Lee, Sung-Eun Kim, et al, “A Regulated Charge Pump with Small Ripple Voltage and Fast Start-Up”, IEEE JOURNAL OF SOLID-STATE CIRCUITS, Vol.41, Issue 2, Page(s):425-432, Feb 2006.

[9]Michael D. Seeman, and Seth R. Sanders, “Analysis and Optimization of Switched-Capacitor DC–DC Converters”, IEEE TRANSACTIONS ON POWER ELECTRONICS, Vol.23, Issue 2, Page(s):841-851, Mar 2008.

[10]Lifang Liu; Zhiliang Chen; “Analysis and Design of Makowski Charge-Pump Cell”, 6th International Conference On ASIC, ASICON 2005, Vol.1, Page(s):497-502, Oct. 2005.

[11]Wonseok Lim; Byungcho Choi; Yonghan Kang; “Control Design and Closed-Loop Analysis of a Switched-Capacitor DC-to-DC Converter”, 2001 IEEE 32nd Annual Power Electronics Specialists Conference, PESC 2001, Vol. 3, Page(s):1295-1300, Jun 2001.

[12]I. Oota, N. Hara, and F. Ueno, “A general method for deriving output resistances of serial fixed type switched-capacitor power supplies,” 2000 IEEE International Symposium on Circuits and Systems, ISCAS2000, Vol.3, Page(s):503-506, May 2000.

[13]Brigitte Kormann, “High-Efficiency, Regulated Charge Pumps for High-Current

Applications", Unitrode Design Seminar, 2001.

[14]B. Robert Gregoire, "A Compact Switched-Capacitor Regulated Charge Pump Power Supply", IEEE JOURNAL OF SOLID-STATE CIRCUITS, Vol. 41, NO. 8, Page(s): 1944-1953, Aug 2006.

[15]Liyu Yang, Rong Guo,"Inductor-less switching power supplies", Project Report for RF Micro Devices, Aug 2008.

[16]Application Note 1845, "Choosing the Right DC-DC Converter for Automotive Applications", Maxim Semiconductor Corporation, [Online] Available: http://www.maxim-ic.com/app-notes/index.mvp/id/1845.

[17]Bob Bell, David Pace, "Buck Regulator Topologies for Wide Input/Output Voltage Differentials", National Semiconductor Corporation, [Online] Available: http://www.national.com/vcm/national3/en_US/resources/power_designer/national_power_designer111.pdf

[18]MAX5033 Datasheet, Maxim Semiconductor Corporation, [Online] Available: http://datasheets.maxim-ic.com/en/ds/MAX5033.pdf

[19]MAX15031 Datasheet, Maxim Semiconductor Corporation, [Online] Available: http://datasheets.maxim-ic.com/en/ds/MAX15031.pdf

[20]Application Notes AN-1214, "LM3354/5 Evaluation Board", National Semiconductor Corporation, [Online] Available: http://www.national.com/an/AN/AN-1214.pdf

[21][Online] Available: http://www.coilcraft.com/smpower.cfm

[22]Charge pump IC with slim outline from National Semiconductor. [Online] Available: http://www.national.com/analog/power

[23]E.Bayer, H.Schmeller, G.Sporer, “Charge Pumps Become Differentiated”, Proc. of Wireless Symposium Portable by Design, Feb 2000. [Online] Available: Http://www.huret.com/archivesx/PBD-2000/Texas-Instrument-2000.pdf.

[24][Online] Available: http://www.mpoweruk.com/performance.htm.

[25][Online] Available: http://powerelectronics.com/power_management/led_drivers/.

[26]Baderna, D.; Cabrini, A.; Torelli, G.; Pasotti, M.; “Efficiency Comparison between Doubler and Dickson Charge Pumps,” IEEE International Symposium on Circuits and Systems, ISCAS 2005, Vol. 2, Page(s):1891-1894, May 2005.

[27]J. S. Brugler, “Theoretical performance of voltage multiplier circuits,” IEEE J. Solid-State Circuits, Vol. 6, No. 3, Page(s):132-135, Jun 1971.

[28]J.-T. Wu and K.-L. Chang, “MOS charge pumps for low-voltage operation,” IEEE J. Solid-State Circuits, Vol. 33, No. 4, Page(s):592-597, Apr 1998.

[29]Erich Bayer, Hans Schmeller, “Charge Pump with ACTIVE CYCLE Regulation-Closing the Gap between Linear- and Skip Modes”, 2000 IEEE 31st Annual Power Electronics Specialists Conference, PESC 2000, Vol.3, Page(s): 1497-1502, Jun 2000.

[30]Soldera, J., Vilas Boas, A., Olmos, A., “A Low Ripple Fully Integrated Charge Pump

Regulator”, 16th Symposium on Integrated Circuits and Systems Design, SBCCI 2003, Page(s): 177-180, Sept. 2003.

[31]Brigitte Kormann, Jim Pelfrey, “Simple Design of an Ultra-Low-Ripple DC/DC Boost Converter with TPS60100 Charge Pump”, Texas Instruments Analog Applications Journal, Literature No. SLYT015, Page(s):15-18, May 2000.

[32]Brigitte Kormann, “TPS6010x/TPS6011x Charge Pump”, Texas Instruments Application Report, Literature No. SLVA070A, Dec 1999.

[33]Thomas Schaffner, “Additional Negative Output with TPS601xx”, Texas Instruments Design Idea Page, Literature No. SLVA098, Mar 2001.

[34]Application Note AN-113, “A Simple Model for DC/DC Charge Pumps”, Analogic Tech, [Online] Available: http://www.eetasia.com/STATIC/PDF/200806/EEOL_2008 JUN26_ POW_ACC_AN_02.pdf?SOURCES=DOWNLOAD.

[35]Ping Luo, Zhaoji Li, Bo Zhang, “Analysis of PSM mode in switching converter and its improved mode”, 2005 International Conference on Communications, Circuits and Systems, Vol.2, Page(s): 1385-1389, May 2005.

[36]Chi-Chang Wang, Jiin-Chuan Wu, “Efficiency improvement in charge pump circuits”, IEEE Journal of Solid-State Circuits, Vol.32, Issue 6, Page(s):852-860, Jun 1997.

[37]Musunuri, S., Chapman, P.L “Improvement of Light-Load Efficiency Using Width-Switching Scheme for CMOS Transistors”, IEEE Power Electronics Letters,

Vol.3, Issue 3, Page(s):105-110, Sept 2005.

[38]Michael D. Mulligan, Bill Broach, Thomas H. Lee, “A 3MHz Low-Voltage Buck Converter with Improved Light Load Efficiency”, IEEE International Solid-State Circuits Conference, ISSCC 2007, Page(s): 528-620, Feb 2007.

[39]Michael D. Mulligan, Bill Broach, Thomas H. Lee, “A Constant-Frequency Method for Improving Light-Load Efficiency in Synchronous Buck Converters”, IEEE Power Electronics Letters, Vol. 3, No.1, Pages(s): 24-29, Mar 2005.

[40]Siyuan Zhou, Gabriel A. Rincon-Mora, “A High Efficiency, Soft Switching DC-DC Converter with Adaptive Current-Ripple Control for Portable Application”, IEEE Transactions on Circuits and Systems-II: Express Briefs, Vol.53, No.4, Page(s): 319-323, Apr 2006.

[41]Biranchinath Sahu, Gabriel A. Rincon-Mora, “An accurate Low-Voltage, CMOS Switching Power Supply With Adaptive On-Time Pulse-Frequency Modulation (PFM) Control”, IEEE Transactions on Circuits and Systems-I: Regular Papers, Vol.54, No.2, Page(s): 312-321, Feb 2007.

[42]Jaber A. Abu Qahouq, Lilly Huang, “Analysis and Design of Voltage Regulator with Improved Light Load Efficiency”, 2006 IEEE International Conference on Acoustics, Speech and Signal Processing, ICASSP 2006, Vol. 3, Page(s): 1152-1155, May 2006.

[43]H. Visairo-Cruz, P. Kumar, “Dual Voltage Input Reconfigurable VR for Improving

Light-Load Efficiency", 6th International Caribbean Conference on Devices, Circuits and Systems, Page(s): 237-242, Apr 2006.

[44]Michele H. Lim, J.D.van Wyk, Zhenxian Liang, "Effect of Geometry Variation of LTCC Distributed Air-Gap Filter Inductor on Light Load Efficiency of DC-DC Converters", IEEE 41st Industry Applications Annual Meeting, IAS 2006, Vol.4, Page(s): 1884-1890, Oct 2006.

[45]Xunwei Zhou, Mauro Donati, Luca Amoroso, Fred C. Lee, "Improve Light Load Efficiency of Synchronous Rectifier Buck Converter", IEEE 14th Applied Power Electronics Conference and Exposition, APEC 1999, Vol.1, Page(s): 295-302, Mar 1999.

[46]Xunwei Zhou, Mauro Donati, Luca Amoroso, Fred C. Lee, "Improved Light-Load Efficiency for Synchronous Rectifier Voltage Regulator Module", IEEE Transactions on Power Electronics, Vol. 15, No. 5, Page(s): 826-834, Sep 2000.

[47]Williams, R.K.; Grabowski, W.; Cowell, A.; Darwish, M.; Berwick, J.; "The Dual-Gate W-Switched Power MOSFET: A New Concept for Improving Light Load Efficiency in DC/DC Converters", IEEE International Symposium on Power Semiconductor Devices and IC's, ISPSD 97, Page(s): 193-196, May 1997.

[48]Hong-Wei Huang, Chieh-Ching Chien, Ke-Hong Chen, Sy-Yen Kuo, "Highly Efficient Tri-Mode Control of Buck Converters with Load Sensing Technique", 2006 IEEE 37th Power Electronics Specialists Conference, PESC 2006, Page(s): 1-4, Jun 2006.

[49]Biranchinath Sahu, Gabriel A. Rincon-Mora, “A High Efficiency, Dual-Mode, Dynamic Buck-Boost Power Supply IC for Portable Applications”, 18th International Conference on VLSI Design, Page(s): 858-861, Jan 2005.

[50]A. M. Sodagar, K. Najafi, K. D. Wise and M. Ghovanloo, "Fully-Integrated CMOS Power Regulator for Telemetry-Powered Implantable Biomedical Microsystems," 2006 IEEE Custom Integrated Circuits Conference, CICC’06, Page(s): 659-662, Sept 2006.

[51]Robert W. Erickson, Dragan Maksimovic, “Fundamental of Power Electronics”, Springer, 2nd edition, ISBN: 0792372700, January 2001.

[52]De Lima, J.A.; Pimenta, W.A. “A gm-C Ramp Generator for Voltage Feedforward Control of DC-DC Switching Regulators”, IEEE International Symposium on Circuits and Systems, ISCAS 2007, Page(s): 1919-1922, May 2007.

[53]B. Jayant Baliga, “Power Semiconductor Devices”, PWS publishing company, 1st edition, ISBN: 0534940986, May 1995.

[54]Julu Sun; Ming Xu; Lee, F.C.; Yucheng Ying; “High Power Density Voltage Divider and Its Application in Two-Stage Server VR”, IEEE Power Electronics Specialists Conference, PESC 2007, Page(s): 1872-1877, Jun 2007.

[55]Ming Xu; Sun, J.; Lee, F.C.; “Voltage divider and its application in the two-stage power architecture”, Twenty-First Annual IEEE Applied Power Electronics Conference and Exposition, APEC 06, Page(s): 499-505, March 2006.

[56]Application Note, “Improving Efficiency of Synchronous Rectification by Analysis of the MOSFET Power Loss Mechanism”, Infineon Technologies, [Online] Available: http://www.infineon.com/cms/en/corporate/search.html?q=application+note

[57]Fang Zheng Peng; Fan Zhang; Zhaoming Qian, “A magnetic-less DC-DC converter for dual voltage automotive systems” IEEE Transactions on Industry Applications, Vol.39, Issue 2, Page(s): 511-518, Apr 2003.

[58]Yuancheng Ren, Ming Xu, Julu Sun, Lee, F.C., “A Family of High Power Density Unregulated Bus Converters”, IEEE Transactions on Power Electronics, Vol.20, Issue 5, Page(s): 1045-1054, Sep 2005.

[59]Hwu, K.I., Yau, Y.T., “a Simple Resonant Voltage Divider”, Twenty-Fourth Annual IEEE Applied Power Electronics Conference and Exposition, APEC 2009, Page(s): 1115-1120, Feb 2009.

[60]Kisun Lee, Jia Wei, Ming Xu, Lee F.C., “Adaptive Bus Voltage Positioning System for Two Stage Laptop Voltage Regulators”, IEEE Power Electronics Specialists Conference, PESC 2007, Page(s): 2-8, Jun 2007.

[61]Yuancheng Ren, Ming Xu, Kaiwei Yao, Yu Meng, Lee F.C., “Two-Stage approach for 12-V VR”, IEEE Transactions on Power Electronics, Vol. 19, Issue 6, Page(s): 1498-1506, Nov 2004.

[62]Clinton Jensen, “Inductive Based Switching Regulator Circuits Provide High Efficiency

White LED Drives", National Semiconductor Corporation, [Online] Available: http://www.national.com/an/AN/AN-1250.pdf

[63]Application Note 3243, "White-LED Boost Converter vs. Charge Pump", Maxim Semiconductor Corporation, [Online] Available: http://www.maxim-ic.com/app-notes/index.mvp/id/3243

[64]Chris Richardson, "LED Applications and Driving Techniques", National Semiconductor Corporation, [Online] Available: http://www.national.com/onlineseminar/2007/led/national_LEDseminar.pdf

[65]Heinz van der Broeck, Georg Sauerlander, Matthias Wendt, "Power driver topologies and control schemes for LEDs", Twenty-Second Annual IEEE Applied Power Electronics Conference and Exposition, APEC 2007, Page(s): 1319-1325, Mar 2007

[66]M. Rico-Secades, J. Garcia, J. Cardesin, A.J. Calleja, "USING TAPPED-INDUCTOR CONVERTERS AS LED DRIVERS", 41st IEEE Industry Applications Conference, IAS 2006, Page(s): 1794-1800, Oct 2006.

[67]Q. Zhao, F. Tao, and F. C. Lee, "High-efficiency, high step-up dc–dc converters", IEEE Trans. Power Electronics, Vol. 18, Issue 1, Page(s): 65-73, Jan 2003.

[68]L. Huber and M. M. Jovanovic, "A design approach for server power supplies for networking", 15th IEEE Applied Power Electronics Conference and Exposition, APEC 2000, Vol. 2, Page(s): 1163-1169, Feb 2000.

[69]Oded Abutbul, Amir Gherlitz, Yefim Berkovich, “Step-Up Switching-Mode Converter With High Voltage Gain Using a Switched-Capacitor Circuit”, IEEE Transactions on Circuits and Systems I: Fundamental Theory and Applications, Vol. 50, Issue 8, Page(s): 1098-1102, Aug 2003.

[70]Abutbul, O.; Gherlitz, A.; Berkovich, Y.; Ioinovici, A; “Boost Converter with High Voltage Gain Using a Switched Capacitor Circuit”, IEEE International Symposium on Circuits and Systems, ISCAS 2003, Vol.3, Page(s): 296-299, May 2003.

[71]Pilawa-Podgurski, R.C.N.; Giuliano, D.M.; Perreault, D.J., “Merged Two-stage Power Converter Architecture with Soft Charging Switched-Capacitor Energy Transfer”, IEEE Power Electronics Specialists Conference, PESC 2008, Page(s): 4008-4015, June 2008.